

~~CONFIDENTIAL~~Copy 273  
RM L56106Reg# 128  
JAN 16

D024204

TECH LIBRARY KAFB, NM

**NACA**

TECHNICAL

# RESEARCH MEMORANDUM

PRESSURE DISTRIBUTION INDUCED ON A FLAT PLATE BY A  
SUPersonic AND SONIC JET EXHAUST AT A  
FREE-STREAM MACH NUMBER OF 1.80

By Abraham Leiss and Walter E. Bressette

Langley Aeronautical Laboratory  
Langley Field, Va.

CLASSIFIED DOCUMENT

This material contains information affecting the National Defense of the United States within the meaning of the espionage laws, Title 18, U.S.C., Secs. 793 and 794, the transmission or revelation of which in any manner to an unauthorized person is prohibited by law.

*Established and removed*  
**NATIONAL ADVISORY COMMITTEE  
FOR AERONAUTICS**

WASHINGTON

January 10, 1957

~~CONFIDENTIAL~~



0144204

NACA RM 156106

## NATIONAL ADVISORY COMMITTEE FOR AERONAUTICS

## RESEARCH MEMORANDUM

PRESSURE DISTRIBUTION INDUCED ON A FLAT PLATE BY A  
SUPERSONIC AND SONIC JET EXHAUST AT A  
FREE-STREAM MACH NUMBER OF 1.80

By Abraham Leiss and Walter E. Bressette

## SUMMARY

As a continuation of previous research at Mach numbers of 2.02 and 1.39, an experimental investigation was made of the pressures induced on a flat plate by a propulsive jet exhausting from sonic and supersonic nozzles at a free-stream Mach number of 1.80. Measurements of the pressure distribution on a flat-plate wing were made at zero angle of attack for four different locations of the jet exhaust nozzle beneath the wing. Both a choked convergent nozzle and a convergent-divergent nozzle on the nacelle were used. The nozzles were operated at nacelle-exit total-pressure ratios from 2 to 16 and the Reynolds number per foot was approximately  $13 \times 10^6$ .

Two distinct shock waves impinged on the wing surface and greatly altered the pressure distribution at all nozzle positions. Positive incremental normal force resulted on the wing at all positions. Comparisons are presented for two free-stream Mach numbers.

## INTRODUCTION

A series of investigations to determine the effect of a propulsive jet, issuing from the rear of a nacelle into free-stream supersonic flow, on a zero-angle-of-attack flat-plate wing surface has been completed. References 1 and 2 contain the results of the tests at free-stream Mach numbers of 2.02 and 1.39. The data presented herein were obtained for a free-stream Mach number of 1.80 using a cold helium propulsive jet. The results presented in references 1 and 2 show that a propulsive jet issuing from the rear of a nacelle into free-stream supersonic flow produced strong disturbances which were responsible for the formation of shock waves in the free stream, downstream of the jet exit. Induced lift was produced when these shock waves in the external flow impinged upon

an adjacent surface. Mach number comparisons as well as sonic and super-sonic nacelle-exit comparisons are presented in this paper.

The data presented were obtained over a range of nacelle-exit total-pressure ratios from 2 to 16 at a free-stream Mach number of 1.80. The free-stream Reynolds number per foot was approximately  $13 \times 10^6$ . The investigation was conducted in the preflight jet of the Langley Pilotless Aircraft Research Station at Wallops Island, Va.

#### SYMBOLS

A area, sq in.

$\Delta C_N$  incremental normal-force coefficient,  $\frac{N_n - N_f}{q_\infty A_e}$

$C_p$  pressure coefficient,  $\frac{p_w - p_\infty}{q_\infty}$

$$\Delta C_p = C_{p,n} - C_{p,f}$$

$C_T$  gross-thrust coefficient,  $T/q_\infty A_e$

D diameter, in.

H total pressure, lb/sq in.

$H_e/p_\infty$  nacelle-exit total-pressure ratio

M Mach number

N normal force, lb

p static pressure, lb/sq in.

$P_e/p_\infty$  nacelle-exit static-pressure ratio

q dynamic pressure  $\gamma p M^2 / 2$ , lb/sq in.

T gross thrust,  $\gamma p_e M_e^2 A_e + p_e A_e - p_\infty A_e$

x chordwise distance from nacelle exit, in.

- $y$  spanwise distance from nacelle center line, in.  
 $\theta$  exit shock angle, deg  
 $\alpha$  jet shock angle, deg  
 $\gamma$  specific-heat ratio; 1.40 for air, 1.67 for helium

Subscripts:

- b nacelle base  
c combustion chamber  
e nacelle exit  
f propulsive jet off  
n propulsive jet on  
T nozzle throat (for sonic  $T = e$ )  
w wing  
 $\infty$  free stream

APPARATUS

The tests were made in the preflight jet facility (described in ref. 3) of the Langley Pilotless Aircraft Research Station at Wallops Island, Va. A Mach number 1.80, 27- by 27-inch nozzle was used for these tests. A photograph of the nacelle mounted in the test position beneath the flat-surface wing at the exit of the 27- by 27-inch nozzle is shown as figure 1.

A sketch of the nacelle with its principal dimensions is shown in figure 2. The exit areas  $A_e$  of the supersonic and sonic nacelles were 0.567 and 0.407 square inch, respectively. The body of the nacelle had a maximum diameter of 1.12 inches with an overall length of 11.65 inches. A convergent-divergent nozzle providing a supersonic exit was constructed for the nacelle. In addition, a convergent nozzle providing a sonic nacelle exit was installed for one test position. The nacelle was mounted on a hollow support strut which served as a housing for the pressure tubes and helium feed line. The leading edge of the strut was swept back from the nacelle at a  $25^\circ$  angle, while the trailing

edge was swept back at a  $40^{\circ}$  angle. The strut had a hexagonal cross section as shown in figure 2. Figure 3 shows the location of the nacelle with respect to the wing and preflight-jet-nozzle exit. The wing as shown in figures 1 and 3 is described in reference 2.

### INSTRUMENTATION

The internal static pressure and the manifolded total pressure of the nacelle were measured for all tests. The location of these orifices is shown in figure 2. The total drag (nacelle jet off) and the net thrust (nacelle jet on) were measured with a  $\pm 150$ -pound maximum thrust drag balance at position  $I_b$  (fig. 3).

The position of 47 static-pressure orifices (0.06-inch diameter) on the wing are shown in figure 4. The free-stream total pressure and the stream static pressure (1/2 inch up stream from preflight nozzle exit) were the pressures measured on the preflight jet 27- by 27-inch nozzle.

All pressures were recorded by electrical pressure recorders of the strain-gage type. A 10-cps timer correlated all time histories on recording paper. Shadowgraphs, which were photographed at an exposure of approximately 0.003 second, were obtained by using a carbon-arc light source and an opaque-glass screen.

### TESTS AND METHODS

The nacelle was mounted within the Mach number 1.80 rhombus of the preflight jet. The wing was stationary and the nacelle was moved horizontally and vertically between test runs to the four positions shown in figure 3; tests were made at each position. At position  $I_b$ , a sonic nozzle was substituted for the supersonic nacelle-exit nozzle as illustrated in figure 2. At all positions, the nacelle was at an angle of attack and sideslip of  $0^{\circ}$  with respect to both the wing surface and the center line of the test nozzle. The tests were made using a helium propulsive jet, which as shown in reference 4 will yield jet-effect data comparable to a hot jet engine over the range of nacelle-exit static-pressure ratios tested. Although helium has a  $\gamma$  of 1.667 and a typical turbojet with afterburner has a  $\gamma$  of 1.27, the effect of this difference in  $\gamma$  is minor on the wing pressure coefficients at a nacelle-exit static-pressure ratio of 8 or less as shown in reference 4.

The tests were made by first starting the Mach number 1.80 preflight jet and recording jet-off data, then starting the flow of helium and

recording jet-on data. The pressure ratio at the nacelle exit was varied automatically as the helium supply decreased. At position  $I_b$  with free-stream jet on, a high-frequency strain-gage balance was used to measure both the total drag (jet off) and the net thrust (jet on). The gross thrust then was obtained by an algebraic summation of the jet-on and jet-off data. The nacelle-exit static-pressure and the nacelle-exit total-pressure were then computed from the gross thrust. At all test positions  $H_c$  and  $p_c$  were measured inside the nacelle as illustrated in figure 2. From the measured values of  $H_c$  and  $p_c$ , the Mach number in the nacelle chamber was calculated to be approximately 0.30. By using this value of  $M_c$  and assuming one  $\eta$  decrease in pressure between  $H_c$  and  $H_e$ ,  $H_e$  was calculated from the measured values of  $H_c$ . This calculated value of  $H_e$  obtained from the measured values of  $H_c$  is presented in figure 5. Also included in figure 5 is the value of  $H_e/p_\infty$  calculated from the thrust drag measurements at position  $I_b$  (by the method presented in ref. 2) plotted against the measured values of  $H_c/p_\infty$ . Figure 5 indicates that the assumption of one  $\eta$  decrease in pressure from  $H_c$  to  $H_e$  is a valid one and therefore all values of  $H_e/p_\infty$  as used herein were obtained from the measured  $H_c/p_\infty$  values assuming a one  $\eta$  difference. The relationship between nacelle-exit static-pressure ratio and nacelle-exit total-pressure ratio is presented in figure 6. Figure 6 also indicates the range of pressure ratios covered in these tests.

#### ACCURACY

By accounting for the instrument error of 1 percent of full-scale range, the probable error is believed to be within the following limits:

$M$	±0.02
$C_{p,f}$	±0.02
$C_{p,n}$	±0.02
$H_e/p_\infty$	±0.20
$P_e/p_\infty$	±0.03

#### RESULTS AND DISCUSSION

##### Jet-Off Pressure Coefficients

Jet-off pressures were measured at 47 orifices on the wing at each of the four nacelle positions. The jet-off pressure coefficients  $C_{p,f}$

~~CONFIDENTIAL~~

were computed and given in table I for all test positions. Figure 7 shows the variation of jet-off pressure coefficients with orifice location for all test positions. Note that the curves are similar to those that are presented in references 1 and 2 with position  $I_b$  lagging behind  $I_a$  and position  $I_c$  lagging behind  $I_a$  and  $I_b$ . The value of  $C_{p,f}$  as plotted includes all the interference effects on the wing. After the  $C_{p,f}$  rise at  $x/D_T$  of 10.76,  $C_{p,f}$  always has a nearly common value due to the intersection on the wing of the nacelle trailing-wake shock wave (described in ref. 5). However, when the trailing-wake shock intersects the wing downstream of  $x/D_T$  of 10.76, the  $C_{p,f}$  value at  $x/D_T$  of 10.76 is negative as shown in figure 7(c) at position  $I_c$  and, in all positions of figure 7(d). This negative value, which is caused by the expansion over the nacelle boattail, is consistent with the negative values of  $C_{p,f}$  preceding the intersection of the trailing-wake shock wave for the other profiles presented and is unaffected when the intersection of the trailing-wake shock wave is downstream of the wing trailing edge. The nacelle was moved 3 inches toward the trailing edge of the wing to position  $II_b$ . The jet-off pressure coefficients  $C_{p,f}$  for test position  $II_b$  are included in figure 7. At position  $II_b$ , the value of  $C_{p,f}$  at orifice  $x/D_T$  of 6.59, along the nacelle center line, was about the same as  $C_{p,f}$  at position  $I_b$  and not appreciably reduced due to the location of the wing trailing edge as it was in reference 2 at  $M_\infty = 1.39$  for two identical vertical positions. This indicates that the base-pressure effects on the pressure data along the nacelle center line, owing to the location of the wing trailing edge, were not as severe for the Mach number 1.80 tests as they were for the Mach number 1.39 tests of reference 2. Figure 8 illustrates the shock waves originating from the nacelle wake for the four test positions. These were photographed with a shadowgraph screen.

#### Jet-On Pressure Coefficients

Shock waves. - Presented in figure 9 are the shadowgraph pictures for various nacelle-exit total-pressure ratios of the flow field about the nacelle exit for the supersonic propulsive jet at the four test positions. Visible downstream of the nacelle exit, in most of the shadowgraph pictures, are two shock waves that impinge upon the wing surface and then are reflected. The first of these shock waves is known as the exit shock, and the second is called the jet shock. In some publications, the exit shock wave and jet shock wave are referred to as the primary and secondary shock waves, respectively. The effect of these exit and jet shock waves is amply described in references 4 and 6.

Figure 10 illustrates the variation of the exit-shock-wave angles (angle between the point of intersection on the wing of the exit shock wave and the nacelle exit) and jet-shock-wave angle with nacelle-exit total-pressure ratio at test positions  $I_a$ ,  $I_b$ , and  $I_c$  for the supersonic nacelle exit as measured from the shadowgraph pictures. The jet-shock-wave angles at position  $I_a$  are not shown as the shadowgraph pictures were not clear enough to detect them. The nacelle distance from the wing was very small at this position.

It can be shown that an imaginary apex for the jet shock wave, in these tests, originates at the nacelle center line the same distance from the nacelle exit for both positions  $I_b$  and  $I_c$ . This fact is substantiated by the method described in appendix A. Figure 11 presents this computed chordwise distance of the apex of the jet shock as it varies with nacelle-exit total-pressure ratio. This curve shows that varying the nacelle location from position  $I_b$  to  $I_c$  had no effect on the origin of the jet-shock-wave angle for these free-stream Mach number 1.80 tests. Therefore, by a simple conical projection, the apex locations can be used in conjunction with the pressure data presented to determine the intersection of the jet shock wave on surfaces other than a flat plate.

Figure 12 presents the data of the sonic nacelle-exit test at position  $I_b$  and shows the corresponding data of the supersonic nacelle exit for the exit-shock-wave and jet-shock-wave angles and their point of intersection and origin with respect to nacelle-exit total-pressure ratio. The exit-shock-wave angles (fig. 12(a)) decreased with an increase in nacelle-exit Mach number because  $p_e/p_\infty$  is less for the supersonic exit than it was for the sonic exit at a given value of  $H_e/p_\infty$ . As shown in references 4 and 6 the exit-shock-wave angle is primarily a function of  $p_e/p_\infty$ , nozzle geometry, and free-stream Mach number. These angles were obtained by direct measurement of the shadowgraph pictures. The jet-shock-wave angles and jet-shock-wave intersection points on the wing were also obtained from the shadowgraph pictures. Note how these are almost identical (within the accuracy of the data) for both the sonic and supersonic nacelle exits. The location of the apex of the sonic-jet shock wave was computed (as described in appendix A) for the supersonic-jet shock wave. The apex of the sonic- and supersonic-jet shock waves is almost identically located as seen in figure 12(c). These results show that the location of the jet-shock-wave apex is only a function of  $H_e/p_\infty$ .

Figure 13 compares the exit and jet-shock-wave angles for the sonic exit at free-stream Mach numbers of 1.39, 1.80, and 2.00 as a function

of nacelle-exit static-pressure ratio. These curves have an increasing trend with increasing values of  $p_e/p_\infty$  for all Mach numbers, and they increase in angle with a decrease in free-stream Mach number at a common value of  $p_e/p_\infty$ . The jet-shock-wave angle is only a function of the free-stream Mach number.

Nacelle position.- In figure 14, the chordwise variation of jet-on pressure coefficients for all test positions is presented at four spanwise positions as a function of distance from the nacelle exit  $x/D_T$  at a nacelle-exit total-pressure ratio of 7 for all pressure orifices. Tabulated in table II are the experimental jet-on pressure coefficients for individual orifice locations at all test positions for integer values of nacelle-exit total-pressure ratios. As shown in reference 2 for jet-on data, there is a reduction in the maximum positive pressure and a rearward movement of the complete pressure profile as the nacelle is lowered in position as well as a general reduction in pressure at each position as the spanwise distance is increased. Also, as in the jet-off condition, increasing the vertical distance between the nacelle exit and the wing moved the point of intersection of the shock wave toward the trailing edge of the wing.

Figure 15 presents the trend of jet-on pressure coefficients as a variable of total-pressure ratio. It can be concluded, by examining these curves (fig. 15(c), in particular), that the higher the total-pressure ratio, the nearer the intersection of the exit shock wave on the wing is to the exit of the nacelle. Note the direct similarity between position  $I_b$  and  $II_b$ . Since position  $II_b$  was 3 inches closer to the wing trailing edge than position  $I_b$ , similar data for these two positions indicate no wing trailing-edge effects as was found in reference 2 for  $M_\infty = 1.39$ .

Nacelle-exit Mach number.- Figure 16 presents the chordwise variation of jet-on pressure coefficients at test position  $I_b$  for both sonic and supersonic nacelle exits at a nacelle-exit total-pressure ratio of 7. Very little difference in the sonic and supersonic  $C_{p,n}$  profiles are noted for the same nacelle-exit total-pressure ratio. This similarity can be expected because as shown in figure 12(d) the jet shock wave intersects the wing at approximately the same value of  $x/D_T$  for both the sonic and supersonic exits. However, as shown in figure 12(a), the exit-shock-wave angle is greater for the sonic exit than it is for the supersonic exit. Therefore it can be expected that a slight dissimilarity exists downstream of the intersection of the exit shock wave as shown in figure 16 and also as presented in reference 2.

CONFIDENTIAL

For identical nacelle-exit static-pressure ratios, the  $C_{p,n}$  curves are dissimilar downstream of the intersection of the exit shock wave, as illustrated in figure 17. Figure 17(a) presents the chordwise variation of  $C_{p,n}$  along the wing center line at test position  $I_b$  for both sonic and supersonic nacelle exits, at a nacelle-exit static-pressure ratio of 1.96. As can be seen in the pictures presented in figure 17, the jet shock wave from the supersonic exit intersects the wing further downstream than the jet shock wave from the sonic exit while the exit shock wave appears to be similar. Reference 4 shows a theoretical increase in the size of a jet boundary with an increase in nozzle divergence angle at the same values of nacelle-exit static-pressure ratio. Therefore, the supersonic nozzle exit would cause a larger value of  $\theta$  than would the sonic exit (illustrated in fig. 2) at the same values of nacelle-exit static pressure. Since  $D_e/D_b$  is greater for the supersonic exit nacelle than the sonic exit nacelle, the base annulus area might cause a larger  $\theta$  for the supersonic nacelle exit. This larger  $\theta$  for the supersonic nacelle exit is indicated in figure 17(a) by a greater positive pressure rise due to the exit shock wave for the supersonic exit. Figure 17(b) makes the same type of comparison as figure 17(a), except at a nacelle-exit static-pressure ratio of 0.98.

#### Incremental Pressure Coefficients

Nacelle position.— Since all the interference effects of each of the test configurations are included in both jet-off ( $C_{p,f}$ ) and jet-on ( $C_{p,n}$ ) pressure coefficients, incremental pressure coefficients  $\Delta C_p$  have been compiled and are presented in figures 18 through 20. The values of the incremental pressure coefficients were used to indicate the magnitude of the jet effects as obtained for these tests. In table III, the incremental pressure coefficients are presented for all test positions for the complete range of total-pressure ratios tested.

Figure 18 presents the chordwise variation of incremental pressure coefficients at two spanwise stations for positions  $I_a$ ,  $I_b$ , and  $I_c$  at a total-pressure ratio of 7. The result of combining jet-on and jet-off wing-profile pressure coefficients as shown in figure 18 indicates positive incremental pressures immediately downstream of the exit shock wave. This positive  $\Delta C_p$  decreases to negative values then approaches a common negative value for all test positions. Figure 19 presents the chordwise variation of incremental pressure coefficients for test positions  $I_b$  and  $II_b$  at a nacelle-exit total-pressure ratio of 7 along the nacelle center line. These curves are identical even though the  $C_{p,f}$  and  $C_{p,n}$  curves were not correspondingly equal for test

CONFIDENTIAL

positions  $I_b$  and  $II_b$ . This is significant in that it substantiates an earlier statement concerning the elimination of the interference effects accumulated in the jet-on and jet-off tests.

Nacelle-exit Mach number. - Shown in figure 20 are the incremental pressure ratios for both sonic and supersonic nacelle exits. Comparisons are illustrated showing  $H_e/p_\infty$  as a constant (12) for both exits and also  $p_e/p_\infty$  as a constant (1.96) for both exits. For the same nacelle-exit static-pressure ratio of 1.96, both the exit- and jet-shock-wave intersection points are at different values of  $x/D_T$  as indicated by the positive incremental-pressure rises. However, for the same nacelle-exit total-pressure ratio of 12, the first positive pressure rise from the exit shock intersection is still at a different value of  $x/D_T$  and the second incremental pressure rise from the jet shock waves occurs at the same value of  $x/D_T$ .

Normal force. - Since the wing trailing-edge effect and other interferences are all eliminated when  $\Delta C_p$  profiles are computed,  $\Delta C_N$  can be computed for any length flat wing less than  $x/D_T = 11.4$ . Presented in figure 21 are the  $\Delta C_p$  profiles across the flat wing at a nacelle-exit total-pressure ratio of 15. The cross-sectional area was integrated for this nacelle-exit total-pressure ratio as well as the complete range of total-pressure ratios tested and cross plotted. Typical curves, illustrating this method, are presented in figure 22 for  $H_e/p_\infty$  of 8 and 15. Figure 22 and the corresponding curves for other nacelle-exit total-pressure ratios were then integrated and  $\Delta C_N$  was determined.

The incremental normal-force coefficients  $\Delta C_N$  based on  $A_T$  with respect to  $H_e/p_\infty$  for test positions  $I_a$ ,  $I_b$ , and  $I_c$  for both sonic and supersonic nacelle exits are shown in figure 23. At all nacelle test positions, positive incremental lift was obtained, and  $\Delta C_N$  resulted with a positive rise as  $H_e/p_\infty$  increased. Note that at lower nacelle-exit total-pressure ratios, the  $\Delta C_N$  curve tends to level off and remain constant. Also, the farther away the nacelle position is to the wing, the longer this constant level persists. This indicates that the value of  $\Delta C_N$  at each test position remains constant to a higher value of  $H_e/p_\infty$  as the nacelle is moved away from the wing surface.

Free-stream Mach number. - Combining the data of reference 2 with these test data results in figure 24 which compares the incremental pressure coefficients at two free-stream Mach numbers. Shown in this figure is the chordwise variation of incremental pressure coefficients

CONFIDENTIAL

at test position  $I_b$  for both sonic and supersonic nacelle exits at free-stream Mach numbers of 1.39 and 1.80 for  $H_e/p_\infty = 7$ . Note that the exit shock wave moves downstream with an increase in free-stream Mach number (also indicated in fig. 13). The  $\Delta C_p$  maximum due to the exit shock wave decreases in value with an increase in free-stream Mach number. Note also that the values of  $\Delta C_p$  downstream of  $x/D_T > 6$  are about the same for both free-stream Mach numbers.

Presented in figure 25 are the variations of incremental pressure coefficients with nacelle-exit total-pressure ratio at free-stream Mach numbers of 1.39 and 1.80 for three different pressure-orifice locations at test position  $I_b$  for both supersonic and sonic nacelle exits. Figures 25(a) through 25(d) indicated the pressure disturbance due to the exit shock wave. The jet-shock-wave effect is noticed in figures 25(e) and 25(f). Note the simular trend for the sonic and supersonic nacelle-exit data for the same pressure orifice and that the supersonic data lags behind the sonic data for each free-stream Mach number at the same pressure orifice. The exit-shock-wave angle effect for the  $M = 1.80$  tests can be seen in figures 25(c) and 25(d), and the exit-shock-wave-angle effect for the  $M_\infty = 1.39$  tests are indicated in figures 25(a) and 25(b). This was expected since the larger shock-wave angle of the  $M_\infty = 1.39$  data produced the pressure rise on the closer nacelle orifice ( $x/D_T = 2.43$ ,  $y/D_T = 0$ ).

Thrust coefficient.- Figure 26 presents the gross-thrust coefficient  $C_T$ , based on  $A_e$ , as it varies with  $H_e/p_\infty$  for the sonic and supersonic nacelle exits. Figure 27 presents the variation of  $\Delta C_N/C_T$  with respect to  $H_e/p_\infty$  for both sonic and supersonic nacelle exits at test positions  $I_a$ ,  $I_b$ , and  $I_c$ . These values were obtained by dividing the data of figure 23 by the value of  $C_T$  in figure 26. The  $\Delta C_N$  increases for both sonic and supersonic nacelle exits at a much slower rate than  $C_T$  at the lower values of  $H_e/p_\infty$  and at approximately a constant rate for  $H_e/p_\infty > 6$ . Position  $I_a$  (only 1.74  $D_T$  from the wing surface) also follows this trend but not as severely at the lower nacelle-exit total-pressure ratios.

Figure 28 presents the variation of incremental normal force to thrust ratio with nacelle-exit total-pressure ratios at position  $I_b$  for both sonic and supersonic nacelle exits at free-stream Mach numbers of 1.39 and 1.80. The change in free-stream Mach number from 1.80 to 1.39 seems to have little or no effect on  $\Delta C_N/C_T$ .

~~CONFIDENTIAL~~  
CONCLUSIONS

Experimental studies have been made at a free-stream Mach number of 1.80 of a small-scale propulsive jet exhausting from sonic and supersonic nozzles parallel to a flat surface wing. The scope and results of these tests are summarized as follows.

1. Shock waves, formed in the external flow because of the presence of the propulsive jet, impinged on the flat surface and greatly altered the pressure distribution.
2. The jet-shock-wave angle is only a function of free-stream Mach number and its theoretical apex originates at the same distance from the nozzle exit for the same nacelle-exit total-pressure ratio at all test positions.
3. Both the jet-shock-wave and exit-shock-wave angles decrease with an increase in free-stream Mach number at the same values of nacelle-exit total-pressure ratios.
4. Positive incremental normal force on the wing was obtained at all test positions.
5. The incremental normal force increased with increased nacelle-exit total pressure.

Langley Aeronautical Laboratory,  
National Advisory Committee for Aeronautics,  
Langley Field, Va., August 24, 1956.

  
~~CONFIDENTIAL~~

## APPENDIX A

THE METHOD USED TO CALCULATE THE DISTANCE FROM THE NACELLE EXIT  
 TO THE APEX OF THE JET SHOCK WAVE ON THE NACELLE CENTER  
 LINE TO PROVE THAT THIS DISTANCE IS A CONSTANT  
 FOR ALL NACELLE TEST POSITIONS

A geometric layout to the location of the jet shock wave is shown in figure 29. The algebraic solution was determined as follows:

$$\left. \begin{aligned} \frac{y_b}{x_b} &= \tan \alpha = \frac{y_b - y_b}{x_b} \\ x_b &= \frac{y_b - y_b}{\tan \alpha} \end{aligned} \right\} \quad (1)$$

$$\left. \begin{aligned} \frac{y_c}{x_c} &= \tan \alpha = \frac{y_c - y_c}{x_c} \\ x_c &= \frac{y_c - y_c}{\tan \alpha} \end{aligned} \right\} \quad (2)$$

$$x_b = \frac{x_b \tan \alpha - y_b}{\tan \alpha} = x_b - \frac{y_b}{\tan \alpha}$$

$$x_c = x_c - \frac{y_c}{\tan \alpha}$$

As an example, prove that  $x_b = x_c$  at  $H_e/p_\infty = 8$ . Then from figures 3, 10, and 12(d), respectively, the following values are obtained:

$$y_b = 3.48D_T \quad y_c = 4.98D_T$$

$$\alpha_b = \alpha_c = 35.5^\circ$$

$$x_b = 5.84D_T \quad x_c = 7.94D_T$$

Therefore

$$x_b = 5.84D_T - \frac{3.48D_T}{0.713} = 0.96D_T$$

$$x_c = 7.94D_T - \frac{4.98D_T}{0.713} = 0.96D_T$$

Thus

$$x_b = x_c$$

For other nacelle-exit total-pressure ratios, the following values of  $x_b$ ,  $x_c$ ,  $x_b$ , and  $x_c$  may be obtained:

$H_e/p_\infty$	$x_b$	$x_c$	$x_b$	$x_c$
7	5.50	7.60	0.62	0.62
9	6.20	8.30	1.32	1.32
11	6.90	9.00	2.02	2.02
13	7.40	9.50	2.52	2.52
15	7.90	10.00	3.02	3.02

These results are plotted in figure 11.

~~CONFIDENTIAL~~

## REFERENCES

1. Bressette, Walter E.: Investigation of the Jet Effects on a Flat Surface Downstream of the Exit of a Simulated Turbojet Nacelle at a Free-Stream Mach Number of 2.02. NACA RM L54E05a, 1954.
2. Bressette, Walter E., and Leiss, Abraham: Investigation of Jet Effects on a Flat Surface Downstream of the Exit of a Simulated Turbojet Nacelle at a Free-Stream Mach Number of 1.39. NACA RM L55L13, 1956.
3. Faget, Maxime A., Watson, Raymond S., and Bartlett, Walter A., Jr.: Free-Jet Tests of a 6.5-Inch-Diameter Ram-Jet Engine at Mach Numbers of 1.81 and 2.00. NACA RM L50I06, 1951.
4. Bressette, Walter E.: Some Experiments Relating to the Problem of Simulation of Hot Jet Engines in Studies of Jet Effects on Adjacent Surfaces at a Free-Stream Mach Number of 1.80. NACA RM L56E07, 1956.
5. Cortright, Edgar M., Jr., and Kochendorfer, Fred D.: Jet Effects on Flow Over Afterbodies in Supersonic Stream. NACA RM E53H25, 1953.
6. Love, Eugene S., and Grigsby, Carl E.: Some Studies of Axisymmetric Free Jets Exhausting From Sonic and Supersonic Nozzles Into Still Air and Into Supersonic Streams. NACA RM L54L31, 1955.

~~CONFIDENTIAL~~

TABLE I.- VALUES OF JET-OFF PRESSURE COEFFICIENTS FOR  
ALL WING ORIFICE POSITIONS

Orifice ordinates		$C_{p,f}$ at test positions -			Orifice ordinates		$C_{p,f}$ at test position
x/D_T	y/D_T	I_a	I_b	I_c	x/D_T	y/D_T	II_b
10.76	0.00	-0.006	0.002	0.005	6.59	0.00	0.019
9.72	.00	.001	.019	.027	5.55	.00	-.079
8.68	.00	.014	.027	.023	4.51	.00	-.056
7.63	.00	.010	.028	-.075	3.47	.00	-.101
6.59	.00	.018	.035	-.060	2.43	.00	-.079
5.55	.00	.023	-.095	-.092	1.39	.00	-.055
4.51	.00	.039	-.065	-.069	.35	.00	-.037
3.47	.00	.039	-.103	-.025	-.69	.00	-.003
2.43	.00	-.117	-.087	-.012	-1.73	.00	.008
1.39	.00	-.087	-.047	0	-2.77	.00	.065
.35	.00	-.095	-.016	.009	-3.82	.00	.035
-.69	.00	-.030	0	.009	-4.86	.00	0
10.76	1.40	-.002	.005	.009	6.59	1.40	-.055
9.72	1.40	.018	.023	.032	5.55	1.40	-.077
8.68	1.40	.020	.034	-.068	4.51	1.40	-.063
7.63	1.40	.019	.037	-.064	3.47	1.40	-.105
6.59	1.40	.010	-.040	-.067	2.43	1.40	-.053
5.55	1.40	.018	-.109	-.104	1.39	1.40	-.058
4.51	1.40	.031	-.081	-.062	.35	1.40	-.037
3.47	1.40	-.119	-.117	-.027	-.69	1.40	0
2.43	1.40	-.119	-.068	-.012	-1.73	1.40	.017
1.39	1.40	-.097	-.038	.011	-2.77	1.40	.042
.35	1.40	-.097	-.012	.010	-3.82	1.40	0
-.69	1.40	-.030	0	.010	-4.86	1.40	0
10.76	4.17	.008	.018	-.042	6.59	4.17	-.079
9.72	4.17	.024	.031	-.060	5.55	4.17	-.132
8.68	4.17	.020	-.078	-.061	4.51	4.17	-.048
7.63	4.17	-.031	-.064	-.070	3.47	4.17	-.031
6.59	4.17	-.089	-.115	-.061	2.43	4.17	-.032
5.55	4.17	-.099	-.094	-.054	1.39	4.17	-.026
4.51	4.17	-.097	-.057	-.027	.35	4.17	.005
3.47	4.17	-.052	-.034	-.007	-.69	4.17	.026
2.43	4.17	-.020	-.010	0	-1.73	4.17	0
1.39	4.17	-.020	-.007	0	-2.77	4.17	0
.35	4.17	-.020	-.007	0	-3.82	4.17	0
10.76	6.94	-.078	-.085	-.084	6.59	6.94	-.048
9.72	6.94	-.075	-.071	-.047	5.55	6.94	-.023
8.68	6.94	-.055	-.033	-.022	4.51	6.94	-.016
7.63	6.94	-.032	-.034	-.019	3.47	6.94	.026
6.59	6.94	-.047	-.036	-.016	2.43	6.94	.008
5.55	6.94	-.050	-.035	-.024	1.39	6.94	-.001
4.51	6.94	-.045	-.023	-.020	.35	6.94	0
3.47	6.94	-.030	-.010	0	-.69	6.94	0
10.76	11.11	-.057	-.027	-.036	6.59	11.11	.008
9.72	11.11	-.044	-.010	-.021	5.55	11.11	.004
8.68	11.11	-.035	-.006	-.027	4.51	11.11	-.030
7.63	11.11	-.020	-.005	-.021	3.47	11.11	0

TABLE II.— VALUES OF JET-ON PRESSURE COEFFICIENTS FOR ALL WING ORIFICE POSITIONS FOR TOTAL-PRESSURE RATIO'S OF 2 TO 16

(a) Test position I<sub>s</sub> (supersonic exit)

Orifice coordinates		Pressure coefficients for nozzles-exit total-pressure ratio $R_e/R_{\infty}$ of -														
$x/D_T$	$y/D_T$	2	3	4	5	6	7	8	9	10	11	12	13	14	15	16
10.76	0	-0.024	-0.025	-0.025	-0.025	-0.027	-0.027	-0.027	-0.029	-0.029	-0.029	-0.029	-0.027	-0.027	-0.027	-0.022
9.72	0	0	.001	0	.001	.001	0	-.001	-.001	-.002	-.003	-.003	0	0	0	-.006
8.68	0	.001	.001	0	.002	.001	-.001	-.001	0	0	0	0	-.002	-.007	-.011	-.014
7.63	0	-.004	-.004	-.005	-.005	-.005	-.004	-.004	-.004	-.005	-.006	-.013	-.015	-.011	-.014	-.015
6.59	0	-.001	0	.001	.003	.004	.003	.003	.001	0	-.001	.006	.013	.020	.023	.030
5.55	0	.010	-.005	-.002	-.001	-.001	-.003	-.006	-.001	.003	.007	.009	.011	.010	.007	-.004
4.51	0	.004	.011	.008	.009	.008	.005	.007	-.009	.009	.009	.002	-.025	-.026	-.026	-.027
3.47	0	.022	.028	.022	.025	.024	.023	.025	-.009	-.050	-.056	-.056	-.055	-.055	-.055	-.055
2.43	0	.052	.053	.054	.057	0	.005	.008	.013	.017	.023	.031	.036	.040	.044	.044
1.39	0	-.083	-.085	-.082	-.080	-.083	.044	.061	.073	.088	.105	.114	.126	.137	.150	.153
.35	0	-.092	-.091	-.094	-.099	-.093	-.094	-.094	-.094	-.094	-.094	-.094	-.094	-.094	-.094	-.095
-.69	0	-.050	-.050	-.050	-.050	-.050	-.050	-.050	-.050	-.050	-.050	-.050	-.050	-.050	-.050	-.050
10.76	1.40	-.013	-.008	-.013	-.011	-.010	-.010	-.010	-.009	-.009	-.008	-.004	-.007	-.006	-.003	-.007
9.72	1.40	.004	.005	.005	.005	.004	.005	.004	.004	.004	.003	.003	.003	.003	.007	.008
8.68	1.40	.006	.008	.007	.008	.007	.007	.006	.006	.006	.006	.006	.006	.005	.005	.001
7.63	1.40	.001	.003	.003	.004	.003	.005	.004	.005	.005	.005	.005	.003	.003	.015	.019
6.59	1.40	-.007	-.004	-.003	-.002	-.007	-.003	-.006	-.006	-.006	-.004	.001	.003	.006	.010	.013
5.55	1.40	-.016	-.010	-.011	-.008	-.012	-.014	-.012	-.006	-.006	-.006	-.004	-.025	-.070	-.097	-.103
4.51	1.40	-.004	.004	.004	-.004	-.001	.001	0	-.002	-.043	-.043	-.043	-.043	-.047	-.067	-.067
3.47	1.40	.021	.031	.027	.041	.037	.035	.035	-.013	-.014	-.014	-.013	-.010	-.009	-.003	.001
2.43	1.40	.025	.025	-.036	-.048	.015	.022	.034	.043	.050	.058	.064	.071	.078	.081	.086
1.39	1.40	-.094	-.096	-.095	-.094	-.099	-.097	-.095	-.086	-.050	-.016	.044	.074	.090	.098	.103
.35	1.40	-.097	-.097	-.097	-.097	-.097	-.097	-.097	-.097	-.097	-.097	-.097	-.097	-.097	-.097	-.097
-.69	1.40	-.050	-.050	-.050	-.050	-.050	-.050	-.050	-.050	-.050	-.050	-.050	-.050	-.050	-.050	-.050
10.76	4.17	-.013	-.008	-.008	-.007	-.007	-.007	-.007	-.006	-.009	-.011	-.011	-.009	-.006	-.004	-.001
9.72	4.17	.005	.006	.007	.009	.008	.007	.007	.005	.005	.005	.005	.007	.010	.011	.013
8.68	4.17	.008	.008	.006	.007	.005	.001	.002	.004	.004	.004	.004	.006	.025	.041	.048
7.63	4.17	.001	.003	0	-.001	-.002	0	-.004	-.011	-.080	-.083	-.087	-.088	-.090	-.094	-.099
6.59	4.17	-.019	-.014	-.013	-.010	-.010	-.010	-.023	-.026	-.025	-.024	-.022	-.021	-.019	-.017	-.016
5.55	4.17	-.059	-.100	-.100	-.088	-.098	-.096	-.094	-.094	-.094	-.094	0	.001	.003	.005	.006
4.51	4.17	-.095	-.097	-.096	-.093	-.099	-.097	-.099	-.096	-.096	-.092	-.081	-.063	-.057	-.056	-.051
3.47	4.17	-.054	-.054	-.054	-.052	-.053	-.054	-.054	-.054	-.054	-.054	-.054	-.054	-.055	-.055	-.055
2.43	4.17	-.020	-.020	-.020	-.020	-.020	-.020	-.020	-.020	-.020	-.020	-.020	-.020	-.020	-.020	-.020
1.39	4.17	-.020	-.020	-.020	-.020	-.020	-.020	-.020	-.020	-.020	-.020	-.020	-.020	-.020	-.020	-.020
.35	4.17	-.020	-.020	-.020	-.020	-.020	-.020	-.020	-.020	-.020	-.020	-.020	-.020	-.020	-.020	-.020
10.76	6.9%	-.033	-.031	-.030	-.026	-.026	-.028	-.031	-.032	-.032	-.033	-.032	-.032	-.031	-.030	-.030
9.72	6.9%	-.059	-.059	-.058	-.053	-.049	-.058	-.057	-.057	-.059	-.059	-.059	-.059	0	.001	.001
8.68	6.9%	-.034	-.054	-.055	-.053	-.053	-.052	-.052	-.051	-.048	-.044	-.046	-.046	-.046	-.046	.030
7.63	6.9%	-.034	-.054	-.055	-.054	-.054	-.054	-.054	-.054	-.054	-.054	-.054	-.053	-.053	-.053	-.053
6.59	6.9%	-.049	-.049	-.047	-.049	-.049	-.046	-.045	-.046	-.046	-.046	-.045	-.043	-.043	-.042	-.041
5.55	6.9%	-.047	-.047	-.049	-.049	-.049	-.049	-.049	-.048	-.047	-.047	-.047	-.047	-.047	-.047	-.046
4.51	6.9%	-.045	-.045	-.045	-.045	-.045	-.045	-.045	-.045	-.045	-.045	-.045	-.045	-.045	-.045	-.045
3.47	6.9%	-.030	-.030	-.030	-.030	-.030	-.030	-.030	-.030	-.030	-.030	-.030	-.030	-.030	-.030	-.030
10.76	11.11	-.037	-.041	-.058	-.059	-.044	-.042	-.039	-.037	-.037	-.037	-.037	-.038	-.040	-.041	-.041
9.72	11.11	-.025	-.028	-.027	-.026	-.025	-.025	-.025	-.026	-.027	-.026	-.027	-.029	-.030	-.034	-.046
8.68	11.11	-.015	-.018	-.017	-.015	-.023	-.021	-.017	-.016	-.016	-.015	-.016	-.018	-.021	-.025	-.028
7.63	11.11	-.020	-.020	-.020	-.020	-.020	-.020	-.020	-.020	-.020	-.020	-.020	-.020	-.020	-.020	-.020
Re/ $R_{\infty}$		.33	.49	.69	.82	.98	1.15	1.31	1.48	1.64	1.80	1.96	2.13	2.29	2.46	2.62

REF ID: A64702  
CONFIDENTIAL

TABLE II.- VALUES OF JET-ON PRESSURE COEFFICIENTS FOR ALL WING ORIFICE POSITIONS FOR TOTAL-PRESSURE RATIOS OF 2 TO 16 - Continued

(b) Test position  $I_b$  (supersonic exit)

Orifice coordinates		Pressure coefficients for nozzle-exit total-pressure ratio $H_e/H_a$ of -														
x/D <sub>w</sub>	y/D <sub>w</sub>	2	3	4	5	6	7	8	9	10	11	12	13	14	15	16
10.76	0	-0.010	-0.009	-0.009	-0.008	-0.008	-0.008	-0.008	-0.008	-0.010	-0.015	-0.019	-0.020	-0.019	-0.016	
9.72	0	.005	.005	.005	.005	.005	.005	.005	.005	.005	.005	.004	.005	.010	.015	.020
8.68	0	.007	.009	.009	.009	.010	.008	.006	.005	.007	.012	.017	.020	.022	.023	.025
7.65	0	.007	.007	.007	.008	.005	.001	.003	.005	.009	.009	.004	.007	.017	.020	.025
6.59	0	.014	.017	.019	.011	.015	.018	.018	.011	.023	.027	.028	.030	.030	.030	.031
5.55	0	.006	.003	.016	.022	.022	.010	.010	.009	.006	.005	.004	.004	.002	.001	0
4.51	0	.005	.004	.005	.005	.010	.005	.015	.022	.030	.057	.043	.038	.031	.026	.018
3.47	0	.101	.101	.101	.101	.101	.101	.101	.101	.101	.101	.098	.080	.051	.035	.024
2.43	0	.087	.087	.087	.087	.087	.088	.087	.087	.088	.088	.088	.088	.088	.089	.089
1.39	0	.048	.048	.048	.047	.049	.048	.048	.048	.048	.049	.049	.049	.049	.048	.048
.35	0	.016	.015	.016	.016	.017	.017	.016	.017	.017	.018	.018	.019	.019	.019	.019
-.69	0	0	0	0	0	0	0	0	0	0	0	0	0	0	0	0
10.76	1.40	-.007	-.005	-.006	-.004	-.005	-.003	-.005	-.005	-.007	-.008	-.013	-.016	-.014	-.014	-.008
9.72	1.40	.010	.009	.009	.009	.009	.010	.010	.007	.001	.005	.007	.013	.018	.025	.027
8.68	1.40	.015	.015	.015	.015	.015	.014	.010	.012	.015	.019	.023	.026	.027	.029	.030
7.65	1.40	.012	.013	.015	.015	.008	.009	.013	.014	.013	.015	.015	.019	.021	.021	.022
6.59	1.40	.005	.007	.009	.010	.010	.010	.008	.008	.024	.025	.026	.026	.026	.026	.026
5.55	1.40	.014	0	.011	.018	.019	.018	.018	.015	.012	.009	.007	.005	.002	0	.004
4.51	1.40	.038	.037	.032	.032	.030	.030	.030	.030	.030	.040	.046	.052	.056	.060	.065
3.47	1.40	-.119	-.119	-.118	-.117	-.118	-.118	-.117	-.116	-.117	-.116	-.117	-.117	-.116	-.116	-.115
2.43	1.40	-.067	-.067	-.068	-.067	-.069	-.069	-.068	-.067	-.068	-.068	-.068	-.069	-.068	-.068	-.069
1.39	1.40	-.036	-.036	-.037	-.037	-.039	-.036	-.037	-.036	-.036	-.037	-.039	-.038	-.038	-.038	-.038
.35	1.40	-.012	-.012	-.012	-.012	-.012	-.012	-.012	-.012	-.012	-.012	-.012	-.012	-.012	-.012	-.012
-.69	1.40	0	0	0	0	0	0	0	0	0	0	0	0	0	0	0
10.76	4.17	.008	.002	.002	.002	.001	0	.002	0	.003	.003	.005	.006	.006	.005	.005
9.72	4.17	.011	.015	.016	.014	.011	.013	.013	.015	.015	.016	.020	.020	.021	.021	.021
8.68	4.17	.008	.009	.009	.011	.013	.015	.010	.004	.011	.014	.013	.011	.009	.008	.008
7.65	4.17	.017	.011	.013	.010	.010	.008	.002	.002	.005	.009	.012	.015	.018	.018	.018
6.59	4.17	.111	.111	.111	.111	.111	.110	.109	.107	.091	.090	.017	.018	.020	.020	.020
5.55	4.17	.094	.095	.095	.095	.095	.095	.095	.095	.094	.095	.094	.094	.093	.093	.093
4.51	4.17	.059	.058	.058	.058	.057	.057	.057	.057	.056	.056	.056	.056	.056	.056	.056
3.47	4.17	-.035	-.034	-.035	-.034	-.035	-.035	-.034	-.034	-.034	-.034	-.034	-.035	-.034	-.035	-.035
2.43	4.17	-.017	-.016	-.016	-.016	-.016	-.016	-.016	-.016	-.016	-.016	-.016	-.016	-.016	-.016	-.016
1.39	4.17	-.007	-.007	-.007	-.007	-.007	-.007	-.007	-.007	-.007	-.007	-.007	-.007	-.007	-.007	-.007
.35	4.17	-.007	-.007	-.007	-.007	-.007	-.007	-.007	-.007	-.007	-.007	-.007	-.007	-.007	-.007	-.007
10.76	6.94	-.020	-.076	-.070	-.050	-.055	.025	.025	.020	.017	.004	.002	.005	.006	.006	.005
9.72	6.94	-.070	-.070	-.070	-.070	-.070	-.070	-.070	-.070	-.067	-.067	-.067	-.068	.068	.066	.066
8.68	6.94	-.033	-.033	-.034	-.033	-.033	-.032	-.031	-.032	-.032	-.032	-.031	-.032	.032	.031	.030
7.65	6.94	-.036	-.036	-.035	-.035	-.036	-.035	-.035	-.035	-.034	-.034	-.034	-.034	.034	.034	.034
6.59	6.94	-.036	-.035	-.035	-.035	-.036	-.035	-.035	-.035	-.035	-.035	-.035	-.035	.034	.034	.034
5.55	6.94	-.033	-.033	-.033	-.033	-.034	-.033	-.033	-.033	-.034	-.034	-.034	-.034	.034	.034	.034
4.51	6.94	-.025	-.025	-.025	-.025	-.025	-.025	-.025	-.025	-.025	-.025	-.025	-.025	.025	.025	.025
3.47	6.94	-.010	-.010	-.010	-.010	-.010	-.010	-.010	-.010	-.010	-.010	-.010	-.010	.010	.010	.010
10.76	11.11	-.005	-.005	-.006	-.006	-.006	-.006	-.006	-.006	-.006	-.006	-.006	-.006	.006	.006	.005
9.72	11.11	-.007	-.007	-.009	-.006	-.006	-.005	-.005	-.005	-.010	-.015	-.017	-.019	-.018	-.018	-.018
8.68	11.11	.001	.001	-.002	0	-.001	.001	.001	.001	-.005	-.005	-.005	-.005	-.005	-.005	-.005
7.65	11.11	-.005	-.005	-.005	-.005	-.005	-.005	-.005	-.005	-.005	-.005	-.005	-.005	-.005	-.005	-.005
$x/D_w$		.53	.49	.69	.82	.98	1.15	1.31	1.48	1.64	1.80	1.96	2.13	2.29	2.46	2.62

TABLE II.- VALUES OF JET-ON PRESSURE COEFFICIENTS FOR ALL WING ORIFICES  
POSITIONS FOR TOTAL-PRESSURE RATIOS OF 2 TO 16 - Continued

(c) Test position  $I_0$  (supersonic exit)

Orifice coordinates		Pressure coefficients for nozzle-exit total-pressure ratio $H_e/H_\infty$ of -														
$x/D_T$	$y/D_T$	2	3	4	5	6	7	8	9	10	11	12	13	14	15	16
10.76	0	-0.007	-0.010	-0.010	-0.009	-0.008	-0.009	-0.015	-0.012	-0.012	-0.004	0	0.003	0.003	0.003	0.003
9.72	0	.010	.007	.007	.008	.006	.005	.006	.006	.006	-.042	-.044	-.045	-.046	-.046	-.046
8.68	0	.008	.013	.011	.010	.013	.013	.012	-.010	-.020	-.022	-.023	-.023	-.023	-.023	-.023
7.65	0	.006	.015	.018	.021	.022	.005	-.004	-.003	-.002	0	.001	.003	.003	.004	.003
6.59	0	-.061	-.061	-.061	-.056	-.007	.009	.020	.027	.031	.036	.040	.043	.045	.046	.048
5.55	0	-.093	-.092	-.092	-.091	-.090	-.091	-.091	-.090	-.091	-.090	-.090	-.089	-.088	-.088	-.088
4.51	0	-.068	-.068	-.068	-.068	-.068	-.068	-.068	-.068	-.068	-.068	-.068	-.069	-.068	-.069	-.069
3.47	0	-.025	-.024	-.024	-.024	-.023	-.024	-.024	-.024	-.024	-.024	-.024	-.024	-.024	-.025	-.025
2.43	0	-.010	-.011	-.011	-.011	-.010	-.011	-.011	-.012	-.011	-.012	-.013	-.013	-.014	-.014	-.014
1.39	0	.001	0	0	.001	0	0	0	0	0	0	0	0	0	0	0
.35	0	.013	.014	.014	.015	.016	.015	.017	.017	.016	.015	.015	.015	.014	.014	.014
-.69	0	.009	.009	.009	.009	.009	.009	.009	.009	.009	.009	.009	.009	.009	.009	.009
10.76	1.40	-.008	-.006	-.005	-.005	-.004	-.003	-.008	-.007	-.006	-.006	-.002	-.003	-.004	-.001	-.007
9.72	1.40	.009	.012	.013	.012	.009	.008	.009	.011	.010	.011	.014	.018	.019	.010	.010
8.68	1.40	.012	.019	.013	.015	.020	.018	.009	.011	.012	.012	.012	.013	.013	.012	.012
7.65	1.40	.010	.026	.026	.029	0	-.001	.003	.006	.009	.011	.012	.015	.015	.016	.017
6.59	1.40	-.063	-.068	-.066	-.063	-.061	-.042	.003	.014	.020	.022	.023	.020	.021	.023	.024
5.55	1.40	-.115	-.110	-.104	-.104	-.103	-.103	-.104	-.103	-.103	-.103	-.103	-.103	-.104	-.105	-.104
4.51	1.40	-.060	-.061	-.062	-.060	-.062	-.061	-.061	-.061	-.061	-.062	-.062	-.062	-.063	-.062	-.062
3.47	1.40	-.025	-.026	-.026	-.027	-.026	-.027	-.027	-.027	-.027	-.027	-.027	-.028	-.027	-.028	-.028
2.43	1.40	-.011	-.014	-.013	-.013	-.013	-.013	-.012	-.013	-.014	-.013	-.013	-.013	-.014	-.014	-.014
1.39	1.40	.014	.011	.011	.012	.013	.013	.010	.012	.011	.015	.011	.015	.011	.010	.010
.35	1.40	.010	.010	.010	.010	.010	.010	.010	.010	.010	.010	.010	.010	.010	.010	.010
-.69	1.40	.010	.010	.010	.010	.010	.010	.010	.010	.010	.010	.010	.010	.010	.010	.010
10.76	4.17	-.001	-.004	-.003	-.003	-.002	-.001	-.003	-.003	-.001	-.003	-.033	-.032	-.032	-.033	-.031
9.72	4.17	.025	.022	.022	.023	.023	.019	0	.001	.003	.003	.006	.009	.010	.009	.008
8.68	4.17	-.032	-.034	-.034	-.034	-.032	-.032	-.032	-.032	-.031	-.032	-.035	.032	.032	.035	.036
7.65	4.17	-.067	-.070	-.069	-.069	-.068	-.067	-.065	-.065	-.066	-.066	-.068	-.067	-.064	-.059	-.058
6.59	4.17	-.062	-.062	-.062	-.062	-.062	-.060	-.061	-.061	-.062	-.062	-.061	-.061	-.061	-.061	-.061
5.55	4.17	-.035	-.036	-.036	-.036	-.035	-.034	-.035	-.035	-.035	-.035	-.034	-.034	-.034	-.034	-.034
4.51	4.17	-.025	-.028	-.028	-.027	-.026	-.026	-.026	-.026	-.026	-.026	-.026	-.026	-.026	-.026	-.026
3.47	4.17	-.004	-.007	-.007	-.005	-.005	0	0	0	0	0	0	0	0	0	0
2.43	4.17	0	0	0	0	0	0	0	0	0	0	0	0	0	0	0
1.39	4.17	0	0	0	0	0	0	0	0	0	0	0	0	0	0	0
.35	4.17	0	0	0	0	0	0	0	0	0	0	0	0	0	0	0
10.76	6.94	-.080	-.082	-.082	-.082	-.081	-.081	-.081	-.081	-.080	-.079	-.070	-.074	-.040	-.086	-.012
9.72	6.94	-.046	-.047	-.045	-.044	-.045	-.045	-.045	-.045	-.045	-.046	-.046	-.047	-.046	-.047	-.047
8.68	6.94	-.023	-.023	-.022	-.022	-.022	-.022	-.021	-.021	-.022	-.021	-.022	-.021	-.022	-.023	-.023
7.65	6.94	-.017	-.016	-.015	-.015	-.015	-.015	-.015	-.014	-.014	-.015	-.015	-.014	-.014	-.015	-.015
6.59	6.94	-.018	-.017	-.016	-.016	-.016	-.016	-.017	-.017	-.016	-.015	-.015	-.015	-.016	-.016	-.016
5.55	6.94	-.018	-.021	-.021	-.021	-.020	-.020	-.020	-.021	-.020	-.020	-.021	-.021	-.022	-.023	-.023
4.51	6.94	-.020	-.020	-.020	-.020	-.020	0	0	0	0	0	0	0	0	0	0
3.47	6.94	0	0	0	0	0	0	0	0	0	0	0	0	0	0	0
10.76	11.11	-.015	-.017	-.016	-.015	-.015	-.014	-.018	-.013	-.015	-.019	-.022	-.025	-.028	-.030	-.032
9.72	11.11	.003	0	.001	.001	.002	.003	.005	.006	.005	.003	-.002	-.003	-.008	-.011	-.013
8.68	11.11	-.005	-.005	-.004	-.004	-.005	-.005	-.004	0	-.002	-.007	-.010	-.013	-.017	-.019	-.019
7.65	11.11	-.021	-.021	-.021	-.021	-.021	-.021	-.021	-.021	-.021	-.021	-.021	-.021	-.021	-.021	-.021
$P_e/P_\infty$		.33	.49	.69	.82	.96	1.15	1.31	1.48	1.64	1.80	1.96	2.13	2.29	2.46	2.62

TABLE II.- VALUES OF JET-ON PRESSURE COEFFICIENTS FOR ALL WING ORIFICES  
POSITIONS FOR TOTAL-PRESSURE RATIOS OF 2 TO 16 - Continued

(a) Test position II<sub>b</sub> (supersonic exit)

TABLE II.- VALUES OF JET-ON PRESSURE COEFFICIENTS FOR ALL WING ORIFICES  
POSITIONS FOR TOTAL-PRESSURE RATIOS OF 2 TO 16 - Concluded

(e) Fast Position  $I_0$  (sonic exit)

Orifice coordinates		Pressure coefficients for nacelle-exit total-pressure ratio $R_e/R_\infty$ of -															
x/D <sub>T</sub>	y/D <sub>T</sub>	2	3	4	5	6	7	8	9	10	11	12	13	14	15	16	
10.76	0	-0.011	-0.019	-0.010	-0.011	-0.010	-0.011	-0.011	-0.010	-0.009	-0.012	-0.015	-0.024	-0.026	-0.024	-0.022	
9.72	0	.004	.006	.005	.004	.003	.004	.004	.003	.004	.009	.006	.001	.003	.011	.016	
8.68	0	.005	.007	.006	.005	.006	.005	.003	.003	.005	.009	.022	.052	.056	.059	.060	
7.65	0	.008	.004	.003	.003	.003	.001	.008	.015	.020	.022	.017	.058	.083	.088	.089	
6.59	0	.010	.013	.012	.009	.020	.005	.020	.005	.059	.060	.061	.061	.062	.062	.063	
5.55	0	.006	.010	.012	.007	.025	.025	.025	.025	.025	.020	.020	.028	.027	.027	.028	
4.51	0	.005	.005	.002	.002	.010	.019	.025	.021	.026	.043	.046	.049	.052	.052	.053	
3.47	0	.102	.101	.102	.101	.101	.100	.097	.094	.090	.060	.100	.124	.130	.142	.149	
2.43	0	.091	.090	.090	.091	.089	.090	.090	.089	.089	.090	.089	.090	.091	.091	.091	
1.39	0	.046	.045	.046	.047	.046	.046	.046	.045	.045	.045	.045	.045	.046	.046	.046	
.35	0	.018	.017	.019	.019	.018	.018	.018	.017	.017	.018	.018	.018	.019	.019	.020	
-.69	0	0	0	0	0	0	0	0	0	0	0	0	0	0	0	0	
10.76	1.40	-.009	-.007	-.006	-.009	-.008	-.008	-.008	-.007	-.007	-.011	-.016	-.021	-.020	-.017	-.013	
9.72	1.40	.006	.007	.007	.006	.006	.007	.007	.006	.005	0	.006	.012	.020	.027	.027	
8.68	1.40	.011	.013	.011	.011	.010	0	.008	.008	.015	.021	.028	.036	.039	.039	.040	
7.65	1.40	.008	.011	.010	.008	.007	.013	.019	.024	.025	.035	.071	.074	.076	.077	.078	
6.59	1.40	.001	.004	.002	.004	.013	.006	.042	.041	.041	.041	.042	.039	.042	.043	.044	
5.55	1.40	-.013	-.003	-.006	-.038	-.034	-.032	-.032	-.027	-.027	-.024	-.022	.021	.020	.019	.018	
4.51	1.40	-.084	-.085	-.080	-.066	.021	.030	.036	.041	.047	.051	.055	.059	.061	.064	.065	
3.47	1.40	-.118	-.118	-.119	-.118	-.118	-.117	-.116	-.116	-.115	-.114	.090	.015	.050	.060	.112	
2.43	1.40	-.066	-.067	-.068	-.068	-.067	-.067	-.067	-.068	-.068	-.067	-.068	.069	.069	.070	.070	
1.39	1.40	-.037	-.036	-.037	-.037	-.036	-.036	-.035	-.036	-.036	-.036	-.036	.035	.037	.038	.038	
.35	1.40	-.012	-.012	-.012	-.012	-.012	-.012	-.012	-.012	-.012	-.012	-.012	.012	.012	.012	.012	
-.69	1.40	0	0	0	0	0	0	0	0	0	0	0	0	0	0	0	
10.76	4.17	-.005	-.008	-.002	-.004	-.003	-.008	-.006	-.003	-.003	.005	.006	.010	.007	.010	.006	-.074
9.72	4.17	.008	.010	.009	.009	.005	.009	.019	.005	.026	.048	.033	.034	.035	.034	.034	-.074
8.68	4.17	-.004	-.009	-.006	-.005	-.006	-.008	-.032	-.031	-.030	-.030	-.039	.047	.048	.048	.049	
7.65	4.17	-.006	-.005	-.005	-.009	-.004	-.004	.003	.004	.005	.007	.007	.006	.007	.006	.007	
6.59	4.17	-.109	-.108	-.109	-.112	-.105	-.070	-.012	.012	.021	.027	.032	.036	.039	.040	.042	
5.55	4.17	-.100	-.100	-.100	-.100	-.100	-.100	-.100	-.100	-.100	-.100	-.100	-.099	-.093	.048	-.022	
4.51	4.17	-.098	-.097	-.098	-.098	-.096	-.057	-.056	-.056	-.056	-.056	-.057	-.056	-.056	-.057	-.057	
3.47	4.17	-.056	-.056	-.054	-.055	-.054	-.035	-.034	-.034	-.034	-.034	-.034	-.034	-.035	-.034	-.034	
2.43	4.17	-.020	-.019	-.019	-.019	-.019	-.010	-.010	-.010	-.010	-.010	-.010	-.010	-.010	-.010	-.010	
1.39	4.17	-.007	-.007	-.007	-.007	-.007	-.007	-.007	-.007	-.007	-.007	-.007	-.007	-.007	-.007	-.007	
.35	4.17	-.007	-.007	-.007	-.007	-.007	-.007	-.007	-.007	-.007	-.007	-.007	-.007	-.007	-.007	-.007	
10.76	6.94	-.071	-.073	-.067	-.046	-.032	-.029	-.020	-.017	-.015	-.014	-.013	-.012	-.011	-.011	-.011	
9.72	6.94	-.074	-.074	-.074	-.075	-.074	-.074	-.059	-.058	-.058	0	.016	.022	.027	.030	.032	
8.68	6.94	-.052	-.032	-.032	-.032	-.032	-.031	-.031	-.031	-.030	-.030	-.029	-.026	-.026	-.026	-.026	
7.65	6.94	-.037	-.055	-.057	-.057	-.055	-.056	-.054	-.054	-.054	-.054	-.054	-.053	-.053	-.054	-.055	
6.59	6.94	-.059	-.057	-.058	-.058	-.057	-.057	-.056	-.056	-.056	-.056	-.056	-.055	-.056	-.056	-.055	
5.55	6.94	-.036	-.033	-.036	-.036	-.035	-.035	-.034	-.034	-.033	-.033	-.033	-.033	-.034	-.034	-.034	
4.51	6.94	-.028	-.028	-.028	-.028	-.028	-.028	-.028	-.028	-.028	-.028	-.028	-.028	-.028	-.028	-.028	
3.47	6.94	-.010	-.010	-.010	-.010	-.010	-.010	-.010	-.010	-.010	-.010	-.010	-.010	-.010	-.010	-.010	
10.76	11.11	-.027	-.027	-.021	-.026	-.023	-.023	-.023	-.025	-.025	-.025	-.025	-.023	-.024	-.025	-.026	
9.72	11.11	-.010	-.007	-.010	-.008	-.006	-.005	-.005	-.005	-.005	-.005	-.005	-.006	-.007	-.008	-.010	
8.68	11.11	-.004	-.003	-.003	-.006	-.004	-.004	-.004	-.004	-.004	-.004	-.004	-.005	0	-.004	-.003	
7.65	11.11	-.003	-.003	-.003	-.005	-.005	-.005	-.005	-.005	-.005	-.005	-.005	-.005	-.005	-.005	-.005	
$R_e/R_\infty$		.98	1.47	1.96	2.45	2.94	3.43	3.92	4.41	4.90	5.37	5.86	6.37	6.86	7.35	7.84	

TABLE III.- VALUES OF INCREMENTAL PRESSURE COEFFICIENTS FOR ALL WING ORIFICE POSITIONS FOR TOTAL-PRESSURE RATIOS OF 2 TO 16

(a) Test position  $I_m$  (supersonic exit)

Orifice coordinates		Pressure coefficients for nozzle-exit total-pressure ratio $P_e/P_\infty$ of -																
$x/D_\infty$	$y/D_\infty$	2	3	4	5	6	7	8	9	10	11	12	13	14	15	16		
10.76	0	-0.018	-0.019	-0.019	-0.020	-0.021	-0.021	-0.021	-0.023	-0.023	-0.023	-0.023	-0.003	-0.001	0.002	0.005	0.004	
9.72	0	-0.011	-0.010	-0.011	-0.010	-0.011	-0.011	-0.012	-0.013	-0.013	-0.014	-0.014	-0.011	-0.015	-0.017	-0.011	-0.009	
8.68	0	-0.013	-0.013	-0.014	-0.012	-0.013	-0.013	-0.013	-0.015	-0.015	-0.014	-0.014	-0.012	-0.015	-0.017	-0.017	-0.010	
7.63	0	-0.014	-0.014	-0.013	-0.013	-0.013	-0.014	-0.014	-0.014	-0.015	-0.015	-0.016	-0.016	-0.015	-0.015	-0.016	-0.010	
6.59	0	-0.019	-0.018	-0.017	-0.017	-0.016	-0.016	-0.015	-0.015	-0.016	-0.016	-0.016	-0.016	-0.015	-0.016	-0.016	-0.009	
5.55	0	-0.013	-0.013	-0.012	-0.011	-0.011	-0.011	-0.010	-0.010	-0.010	-0.010	-0.010	-0.010	-0.009	-0.009	-0.009	-0.009	
4.51	0	-0.005	-0.006	-0.005	-0.005	-0.005	-0.005	-0.005	-0.005	-0.005	-0.005	-0.005	-0.005	-0.004	-0.003	-0.003	-0.002	
3.47	0	-0.017	-0.007	-0.018	-0.014	-0.015	-0.016	-0.016	-0.016	-0.016	-0.016	-0.016	-0.016	-0.015	-0.015	-0.015	-0.016	
2.43	0	-.149	.152	.171	.174	.177	.180	.183	.186	.189	.192	.195	.198	.201	.212	.224	.237	.242
1.39	0	.004	.002	.005	.071	.110	.132	.148	.161	.175	.188	.198	.201	.212	.224	.237	.242	.242
.35	0	.003	.004	.001	.004	.006	.001	.001	.001	.001	.001	.001	.001	.001	.001	.001	.001	0
-0.69	0	0	0	0	0	0	0	0	0	0	0	0	0	0	0	0	0	
10.76	1.40	-0.011	-0.005	-0.011	-0.009	-0.008	-0.008	-0.008	-0.007	-0.007	-0.006	-0.006	-0.002	-0.005	-0.004	-0.003	-0.005	
9.72	1.40	-0.014	-0.013	-0.015	-0.013	-0.014	-0.013	-0.014	-0.014	-0.014	-0.015	-0.015	-0.011	-0.015	-0.016	-0.016	-0.016	
8.68	1.40	-0.018	-0.018	-0.013	-0.012	-0.013	-0.013	-0.013	-0.016	-0.014	-0.013	-0.014	-0.017	-0.016	-0.016	-0.016	-0.016	
7.63	1.40	-0.013	.016	.016	.019	.019	.016	.008	.006	.008	.008	.009	.009	.017	.017	.017	.017	
6.59	1.40	.017	.014	.014	.014	.014	.017	.017	.017	.017	.017	.017	.017	.017	.017	.017	.017	
5.55	1.40	.034	.028	.029	.026	.026	.026	.026	.026	.026	.026	.026	.026	.026	.026	.026	.026	
4.51	1.40	.005	.007	.006	.005	.005	.005	.005	.005	.005	.005	.005	.005	.004	.004	.004	.004	
3.47	1.40	.140	.150	.146	.155	.156	.156	.156	.156	.156	.156	.156	.156	.156	.156	.156	.156	
2.43	1.40	.142	.144	.095	.111	.132	.141	.153	.161	.169	.177	.185	.190	.197	.208	.205	.205	
1.39	1.40	.005	.001	.003	.003	.002	0	.002	.009	.047	.103	.141	.187	.193	.193	.193	.193	
.35	1.40	0	0	0	0	0	0	0	0	0	0	0	0	0	0	0	0	
-0.69	1.40	0	0	0	0	0	0	0	0	0	0	0	0	0	0	0	0	
10.76	4.17	-0.021	-0.016	-0.016	-0.015	-0.015	-0.015	-0.015	-0.015	-0.014	-0.014	-0.014	-0.019	-0.017	-0.012	-0.012	-0.009	
9.72	4.17	-0.019	-0.018	-0.016	-0.016	-0.015	-0.016	-0.017	-0.019	-0.018	-0.019	-0.017	-0.014	-0.013	-0.014	-0.014	-0.014	
8.68	4.17	-0.017	-0.017	-0.014	-0.014	-0.013	-0.017	-0.019	-0.018	-0.016	-0.016	-0.016	-0.016	-0.016	-0.016	-0.016	-0.016	
7.63	4.17	.032	.026	.026	.051	.050	.026	.079	.071	.066	.063	.063	.064	.065	.065	.065	.065	
6.59	4.17	.070	.073	.076	.076	.076	.076	.076	.076	.076	.076	.076	.076	.076	.076	.076	.076	
5.55	4.17	.004	.001	.001	.001	.001	.001	.001	.001	.001	.001	.001	.001	.001	.001	.001	.001	
4.51	4.17	.002	0	0	0	0	0	0	0	0	0	0	0	0	0	0	0	
3.47	4.17	.002	0	0	0	0	0	0	0	0	0	0	0	0	0	0	0	
2.43	4.17	0	0	0	0	0	0	0	0	0	0	0	0	0	0	0	0	
1.39	4.17	0	0	0	0	0	0	0	0	0	0	0	0	0	0	0	0	
.35	4.17	0	0	0	0	0	0	0	0	0	0	0	0	0	0	0	0	
-0.69	4.17	0	0	0	0	0	0	0	0	0	0	0	0	0	0	0	0	
10.76	6.94	.045	.047	.048	.052	.052	.050	.047	.046	.046	.045	.046	.046	.047	.048	.048	.048	
9.72	6.94	.006	.006	.007	.012	.022	.022	.027	.048	.046	.046	.046	.046	.047	.047	.047	.047	
8.68	6.94	.003	.003	0	.002	.002	.002	.002	.001	.001	.001	.001	.001	.001	.001	.001	.001	
7.63	6.94	-.002	-.002	0	-.005	-.002	-.002	-.002	-.002	-.002	-.002	-.002	-.002	-.002	-.002	-.002	-.002	
6.59	6.94	-.008	-.008	0	0	0	0	0	0	0	0	0	0	0	0	0	0	
5.55	6.94	.003	.003	.001	.001	.001	.001	.001	.001	.001	.001	.001	.001	.001	.001	.001	.001	
4.51	6.94	0	0	0	0	0	0	0	0	0	0	0	0	0	0	0	0	
3.47	6.94	0	0	0	0	0	0	0	0	0	0	0	0	0	0	0	0	
2.43	6.94	0	0	0	0	0	0	0	0	0	0	0	0	0	0	0	0	
1.39	6.94	0	0	0	0	0	0	0	0	0	0	0	0	0	0	0	0	
.35	6.94	0	0	0	0	0	0	0	0	0	0	0	0	0	0	0	0	
-0.69	6.94	0	0	0	0	0	0	0	0	0	0	0	0	0	0	0	0	
10.76	11.11	.020	.016	.018	.018	.015	.015	.018	.020	.020	.019	.019	.019	.017	.016	.014	.013	
9.72	11.11	.038	.016	.017	.018	.009	.012	.012	.013	.018	.019	.019	.019	.017	.016	.014	.013	
8.68	11.11	.032	.017	.018	.009	0	0	0	0	0	0	0	0	0	0	.012	.011	
7.63	11.11	0	0	0	0	0	0	0	0	0	0	0	0	0	0	0	0	

TABLE III.- VALUES OF INCREMENTAL PRESSURE COEFFICIENTS FOR ALL WING ORIFICE  
POSITIONS FOR TOTAL-PRESSURE RATIO OF 2 TO 16 - Continued

(b) Test position  $I_b$  (supersonic exit)

Orifice coordinates		Pressure coefficients for nozzle-exit total-pressure ratio $\frac{H_e}{H_n}$ or -														
$x/D_n$	$y/D_n$	2	3	4	5	6	7	8	9	10	11	12	13	14	15	16
10.76	0	-0.012	-0.011	-0.011	-0.010	-0.010	-0.010	-0.010	-0.011	-0.012	-0.017	-0.021	-0.022	-0.022	-0.022	-0.022
9.72	0	-0.014	-0.013	-0.013	-0.013	-0.013	-0.013	-0.013	-0.013	-0.013	-0.019	-0.020	-0.020	-0.020	-0.020	-0.020
8.68	0	-0.020	-0.018	-0.018	-0.017	-0.017	-0.019	-0.021	-0.025	-0.020	-0.015	-0.015	-0.015	-0.015	-0.015	-0.015
7.63	0	-0.021	-0.016	-0.016	-0.016	-0.016	-0.016	-0.017	-0.017	-0.017	-0.019	-0.019	-0.019	-0.019	-0.019	-0.019
6.59	0	-0.021	-0.018	-0.018	-0.016	-0.016	-0.016	-0.017	-0.017	-0.017	-0.019	-0.019	-0.019	-0.019	-0.019	-0.019
5.55	0	.099	.098	.111	.111	.117	.117	.085	.085	.085	.087	.087	.089	.090	.091	.093
4.51	0	0	.001	.001	.001	.001	.001	.001	.001	.001	.001	.001	.001	.001	.001	.001
3.47	0	.002	.002	.002	.002	.002	.002	.002	.002	.002	.002	.002	.002	.002	.002	.002
2.43	0	0	0	0	0	0	0	0	0	0	0	0	0	0	0	0
1.39	0	0	0	0	0	0	0	0	0	0	0	0	0	0	0	0
.35	0	0	0	0	0	0	0	0	0	0	0	0	0	0	0	0
-.69	0	0	0	0	0	0	0	0	0	0	0	0	0	0	0	0
10.76	1.40	-.012	-.010	-.011	-.009	-.010	-.010	-.010	-.010	-.012	-.015	-.020	-.021	-.019	-.019	-.013
9.72	1.40	-.013	-.014	-.014	-.014	-.013	-.013	-.015	-.016	-.022	-.020	-.016	-.016	-.005	0	.004
8.68	1.40	-.019	-.019	-.019	-.019	-.019	-.020	-.020	-.022	-.019	-.015	-.011	-.008	-.007	-.009	-.017
7.63	1.40	-.023	-.024	-.024	-.024	-.024	-.024	-.024	-.024	-.024	-.024	-.024	-.024	-.024	-.024	-.024
6.59	1.40	.047	.047	.049	.050	.050	.050	.048	.049	.048	.045	.045	.044	.044	.045	.045
5.55	1.40	.055	.109	.120	.127	.090	.091	.094	.097	.100	.102	.104	.107	.109	.112	.114
4.51	1.40	-.008	-.008	-.001	.003	.061	.084	.075	.106	.113	.121	.127	.133	.137	.141	.144
3.47	1.40	-.002	-.008	-.001	0	-.001	-.001	0	-.001	0	-.001	0	0	.001	.001	.001
2.43	1.40	.001	.001	0	.001	.001	-.001	0	-.001	0	0	0	0	0	0	0
1.39	1.40	.008	.008	.001	.001	.001	.002	0	.002	.003	.001	-.001	0	0	0	0
.35	1.40	0	0	0	0	0	0	0	0	0	0	0	0	0	0	0
-.69	1.40	0	0	0	0	0	0	0	0	0	0	0	0	0	0	0
10.76	4.17	-.016	-.016	-.016	-.016	-.017	-.018	-.016	-.018	-.015	-.015	-.012	-.012	-.025	-.049	-.071
9.72	4.17	-.020	-.016	-.015	-.017	-.020	-.018	-.016	-.016	-.006	-.015	-.019	-.019	-.061	-.068	-.063
8.68	4.17	.056	.057	.059	.051	.059	.058	.074	.087	.064	.064	.055	.055	.067	.069	.070
7.63	4.17	.053	.053	.051	.054	.054	.056	.056	.059	.074	.076	.079	.080	.083	.083	.083
6.59	4.17	.004	.004	.004	.004	.005	.005	.006	.006	.024	.065	.098	.120	.133	.140	.150
5.55	4.17	0	0	0	0	0	0	0	0	0	0	0	0	0	0	0
4.51	4.17	-.008	0	0	0	0	0	0	0	0	0	0	0	0	0	0
3.47	4.17	-.001	0	0	0	0	0	0	0	0	0	0	0	0	0	0
2.43	4.17	0	0	0	0	0	0	0	0	0	0	0	0	0	0	0
1.39	4.17	0	0	0	0	0	0	0	0	0	0	0	0	0	0	0
.35	4.17	0	0	0	0	0	0	0	0	0	0	0	0	0	0	0
10.76	6.94	.005	.007	.015	.001	.025	.030	.060	.065	.068	.071	.073	.073	.077	.079	.080
9.72	6.94	.003	.001	.001	.001	.001	.001	.001	.004	.017	.022	.046	.063	.077	.087	.087
8.68	6.94	0	0	0	0	0	0	0	0	0	0	0	0	0	0	0
7.63	6.94	-.002	-.002	-.001	-.001	-.002	-.001	-.001	0	0	0	0	0	0	0	0
6.59	6.94	0	0	0	0	0	0	0	0	0	0	0	0	0	0	0
5.55	6.94	0	0	0	0	0	0	0	0	0	0	0	0	0	0	0
4.51	6.94	0	0	0	0	0	0	0	0	0	0	0	0	0	0	0
3.47	6.94	0	0	0	0	0	0	0	0	0	0	0	0	0	0	0
10.76	11.11	.004	.004	.001	.003	.001	.005	.004	.005	0	0	0	0	0	0	0
9.72	11.11	.003	.005	.001	.004	.002	.004	.004	.005	0	0	0	0	0	0	0
8.68	11.11	.007	.007	.004	.006	.005	.007	.002	.008	.005	.005	.004	.004	.003	0	0
7.63	11.11	0	0	0	0	0	0	0	0	0	0	0	0	0	0	0
	$v_e/v_n$	.33	.49	.69	.82	.98	1.15	1.31	1.48	1.64	1.80	1.96	2.13	2.29	2.46	2.62

TABLE III.- VALUES OF INCREMENTAL PRESSURE COEFFICIENTS FOR ALL WING ORIFICE POSITIONS FOR TOTAL-PRESSURE RATIOS OF 2 TO 16 - Continued.

(c) Test position  $I_x$  (supersonic exit)

Orifice coordinates		Pressure coefficients for nozzle-exit total-pressure ratio $\frac{P_0}{P_\infty}$ of -															
$x/D_T$	$y/D_T$	2	3	4	5	6	7	8	9	10	11	12	13	14	15	16	
10.76	0	-0.012	-0.015	-0.015	-0.014	-0.013	-0.014	-0.018	-0.017	-0.017	-0.009	-0.005	-0.002	0	0	0	
9.72	0	-0.017	-0.020	-0.020	-0.019	-0.021	-0.024	-0.022	-0.019	-0.019	-0.021	-0.069	-0.071	-0.072	-0.073	-0.073	
8.68	0	-0.015	-0.010	-0.012	-0.013	-0.010	-0.010	-0.011	-0.013	-0.013	-0.015	-0.045	-0.046	-0.046	-0.045	-0.046	
7.63	0	.061	.090	.093	.096	.097	.070	.071	.072	.073	.073	.076	.076	.076	.079	.080	
6.59	0	-0.001	-0.001	-0.001	0	.004	.053	.051	.060	.067	.091	.096	.100	.103	.105	.106	
5.55	0	-0.001	0	0	.001	.002	.001	.001	.002	.001	.002	.002	.003	.004	.010	.068	
4.51	0	-0.001	.001	.001	.001	.001	.001	.001	.001	.001	.001	.001	.001	0	.001	0	
3.47	0	0	.001	.001	.001	.002	.001	.001	.001	.001	.001	.001	.001	.001	0	0	
2.43	0	.002	.001	.001	.001	.002	.001	.001	0	0	.001	0	-0.001	-0.001	-0.002	-0.002	
1.39	0	.001	0	0	0	.006	.007	.006	.008	.008	.007	.006	.006	-0.002	-0.003	-0.003	
.35	0	.004	.005	.005	.006	.006	.007	.006	.008	.008	.007	.006	.005	.005	.005	.005	
-.69	0	0	0	0	0	0	0	0	0	0	0	0	0	0	0	0	
10.76	1.40	-0.017	-0.015	-0.014	-0.014	-0.013	-0.014	-0.017	-0.016	-0.015	-0.011	-0.007	-0.006	-0.005	-0.008	-0.013	
9.72	1.40	.023	-.020	-.019	-.020	-.023	-.024	-.025	-.021	-.022	-.031	-.066	-.070	-.071	-.072	-.072	-.072
8.68	1.40	.080	.087	.081	.084	.088	.086	.086	.086	.087	.056	.056	.056	.056	.056	.056	.056
7.63	1.40	.074	.080	.090	.093	.094	.063	.071	.070	.075	.075	.078	.079	.079	.080	.081	
6.59	1.40	.002	-0.001	.001	.002	.006	.023	.023	.064	.061	.078	.089	.092	.097	.098	.100	
5.55	1.40	.001	-.005	0	0	.001	.001	0	.001	.001	.001	.001	.001	0	.001	0	
4.51	1.40	.002	.001	0	0	.002	0	.001	0	.001	0	0	0	0	0	0	
3.47	1.40	.002	-.001	-.001	0	.001	.001	0	0	0	0	0	0	0	0	0	
2.43	1.40	.001	-.002	-.001	-.001	.001	0	0	0	0	0	0	0	0	0	0	
1.39	1.40	.003	0	0	0	.002	0	0	0	0	0	0	0	0	0	0	
.35	1.40	0	0	0	0	0	0	0	0	0	0	0	0	0	0	0	
-.69	1.40	0	0	0	0	0	0	0	0	0	0	0	0	0	0	0	
10.76	4.17	.041	.058	.059	.059	.040	.041	.059	.059	.019	.011	.009	.010	.010	.010	.011	.011
9.72	4.17	.085	.082	.082	.083	.079	.079	.069	.069	.061	.053	.056	.056	.056	.056	.056	.056
8.68	4.17	-.001	-.003	-.003	-.003	.009	.044	.056	.075	.087	.086	.089	.091	.093	.095	.097	
7.63	4.17	.003	0	-.001	-.002	.002	.002	.003	.003	.005	.004	.002	.002	.003	.011	.020	
6.59	4.17	-.001	-.001	-.001	-.001	0	0	0	0	0	0	0	0	0	0	0	
5.55	4.17	.001	-.002	-.002	-.002	0	0	0	0	0	0	0	0	0	0	0	
4.51	4.17	.002	-.002	-.002	-.002	0	0	0	0	0	0	0	0	0	0	0	
3.47	4.17	.003	0	0	0	.001	.002	.001	.001	.001	.001	.001	.002	.002	.001	.001	
2.43	4.17	0	0	0	0	0	0	0	0	0	0	0	0	0	0	0	
1.39	4.17	0	0	0	0	0	0	0	0	0	0	0	0	0	0	0	
.35	4.17	0	0	0	0	0	0	0	0	0	0	0	0	0	0	0	
10.76	6.94	-.004	-.002	-.002	-.002	.005	.005	.005	.005	.005	.004	.003	.014	.050	.044	.058	0
9.72	6.94	-.001	0	0	0	0	0	0	0	0	.001	.001	.001	.001	.001	0	
8.68	6.94	-.001	-.001	0	0	0	0	0	0	0	0	0	0	0	0	0	
7.63	6.94	.002	.003	.004	.005	.004	.004	.004	.005	.005	.004	.004	.003	.004	.005	0	
6.59	6.94	-.002	-.001	0	0	0	0	0	0	0	0	0	0	0	0	0	
5.55	6.94	-.006	.005	.005	.005	.005	.004	.004	.005	.004	.004	.003	.003	.002	0	0	
4.51	6.94	0	0	0	0	0	0	0	0	0	0	0	0	0	0	0	
3.47	6.94	0	0	0	0	0	0	0	0	0	0	0	0	0	0	0	
2.43	6.94	0	0	0	0	0	0	0	0	0	0	0	0	0	0	0	
1.39	6.94	0	0	0	0	0	0	0	0	0	0	0	0	0	0	0	
.35	6.94	0	0	0	0	0	0	0	0	0	0	0	0	0	0	0	
10.76	11.11	.021	.019	.020	.021	.021	.022	.022	.023	.023	.021	.017	.014	.011	.008	.006	0
9.72	11.11	.024	.021	.022	.022	.023	.023	.024	.025	.025	.027	.028	.019	.016	.013	.007	0
8.68	11.11	.024	.021	.022	.022	.023	.023	.024	.025	.025	.026	.027	.020	.017	.014	.012	.004
7.63	11.11	0	0	0	0	0	0	0	0	0	0	0	0	0	0	0	0

$P_0/P_\infty$  .53 .49 .69 .82 .98 1.15 1.31 1.48 1.64 1.80 1.96 2.13 2.29 2.46 2.02

TABLE III.- VALUES OF INCREMENTAL PRESSURE COEFFICIENTS FOR ALL WING ORIFICE  
POSITIONS FOR TOTAL-PRESSURE RATIOS OF 2 TO 16 - Continued

(4) Test position  $\Pi_b$  (supersonic exit)

Orifice ordinates		Pressure coefficients for nozzle-exit total-pressure ratio $R_e/R_m$ of -														
x/D <sub>T</sub>	y/D <sub>T</sub>	2	3	4	5	6	7	8	9	10	11	12	13	14	15	16
6.59	0	-0.017	-0.015	-0.015	-0.018	-0.014	-0.015	-0.021	-0.023	-0.028	-0.060	-0.061	-0.060	-0.060	-0.061	-0.061
5.55	0	.105	.100	.100	.070	.069	.069	.072	.085	.086	.089	.090	.093	.094	.093	.096
4.51	0	0	.001	.001	.006	.060	.076	.085	.095	.102	.107	.114	.118	.123	.127	.131
3.47	0	-.001	0	0	0	0	0	.001	0	.001	.002	.007	.052	.088	-.001	.162
2.43	0	0	0	0	0	0	0	0	0	0	0	0	0	0	0	0
1.39	0	-.001	0	0	0	0	0	0	0	0	0	0	0	0	0	0
.35	0	-.002	-.002	-.001	-.002	-.001	0	0	0	0	0	0	0	0	0	0
-.69	0	0	0	0	0	0	0	0	0	0	0	0	0	0	0	0
-1.73	0	0	0	0	0	0	0	0	0	0	0	0	0	0	0	0
-2.77	0	0	0	0	0	0	0	0	0	0	0	0	0	0	0	0
-3.82	0	0	0	0	0	0	0	0	0	0	0	0	0	0	0	0
-4.86	0	0	0	0	0	0	0	0	0	0	0	0	0	0	0	0
6.59	1.40	.061	.065	.060	.065	.067	.064	.057	.051	.029	.029	.028	.028	.028	.023	.029
5.55	1.40	.105	.110	.098	.095	.093	.090	.092	.094	.099	.106	.105	.107	.111	.111	.118
4.51	1.40	-.004	-.003	-.002	-.010	.073	.093	.107	.116	.124	.132	.138	.143	.149	.154	.156
3.47	1.40	-.006	-.001	-.001	-.001	0	-.001	0	.001	.001	-.001	-.001	0	0	0	-.001
2.43	1.40	-.001	.001	-.001	.002	.003	.003	.004	.005	.004	.005	.003	.002	.001	.001	0
1.39	1.40	.001	0	-.001	0	0	0	0	0	0	0	0	0	0	0	0
.35	1.40	-.003	-.002	-.008	-.003	-.003	-.003	-.003	-.005	-.005	-.005	-.005	-.005	-.005	-.005	-.004
-.69	1.40	0	0	0	0	0	0	0	0	0	0	0	0	0	0	0
-1.73	1.40	0	0	0	0	0	0	0	0	0	0	0	0	0	0	0
-2.77	1.40	0	0	0	0	0	0	0	0	0	0	0	0	0	0	0
-3.82	1.40	0	0	0	0	0	0	0	0	0	0	0	0	0	0	0
-4.86	1.40	0	0	0	0	0	0	0	0	0	0	0	0	0	0	0
6.59	4.17	.003	.012	.000	.013	.014	.014	.020	.014	.072	.100	.112	.119	.126	.130	.132
5.55	4.17	-.004	-.004	-.005	-.004	-.006	-.005	-.005	-.007	-.003	-.005	-.005	-.004	-.005	-.005	-.004
4.51	4.17	-.004	-.004	-.003	-.003	-.004	-.001	-.002	-.001	-.001	.001	.002	-.001	-.001	-.001	-.001
3.47	4.17	-.003	-.002	-.002	-.003	-.003	.003	.004	.004	-.001	.001	.002	-.002	-.002	-.002	-.003
2.43	4.17	-.002	.002	-.001	-.001	0	.001	.001	.001	.001	.001	.001	0	0	0	0
1.39	4.17	-.004	-.005	-.004	-.004	-.005	-.004	-.005	-.004	-.004	-.005	-.004	-.004	-.003	-.003	-.004
.35	4.17	-.002	-.002	-.008	-.002	0	-.001	0	0	0	0	0	0	0	0	0
-.69	4.17	0	0	0	0	0	0	0	0	0	0	0	0	0	0	0
-1.73	4.17	0	0	0	0	0	0	0	0	0	0	0	0	0	0	0
-2.77	4.17	0	0	0	0	0	0	0	0	0	0	0	0	0	0	0
-3.82	4.17	0	0	0	0	0	0	0	0	0	0	0	0	0	0	0
6.59	6.9*	-.005	-.001	-.001	-.001	-.001	-.001	0	0	0	0	0	0	0	0	0
5.55	6.9*	-.001	-.001	-.001	-.001	0	0	0	0	0	0	0	0	0	0	0
4.51	6.9*	-.002	.019	.015	.021	.021	.024	.022	.021	.019	.018	.015	.011	.007	.007	.003
3.47	6.9*	-.005	-.001	0	0	0	.003	.002	.001	0	0	0	0	0	0	0
2.43	6.9*	-.002	0	0	0	0	.002	.001	.002	.001	.002	.005	.010	.002	.007	.017
1.39	6.9*	-.003	0	0	0	0	.004	.005	.004	.003	.003	.002	.002	.003	.003	0
.35	6.9*	0	0	0	0	0	0	0	0	0	0	0	0	0	0	0
-.69	6.9*	0	0	0	0	0	0	0	0	0	0	0	0	0	0	0
6.59	11.11	-.001	.009	.006	.010	.011	.012	.011	.010	.010	.008	.007	.005	.004	.004	.008
5.55	11.11	0	.008	.006	.010	.012	.012	.011	.011	.010	.009	.007	.010	.004	.004	.001
4.51	11.11	0	.011	.005	.009	.011	.011	.011	.010	.008	.007	.006	.004	.002	.002	.001
3.47	11.11	0	0	0	0	0	0	0	0	0	0	0	0	0	0	0
P <sub>e</sub> /P <sub>m</sub>		.35	.49	.69	.82	.98	1.15	1.31	1.46	1.64	1.80	1.96	2.13	2.29	2.46	2.62

TABLE III.- VALUES OF INCREMENTAL PRESSURE COEFFICIENTS FOR ALL WING ORIFICES  
POSITIONS FOR TOTAL-PRESSURE RATIOS OF 2 TO 16 - Concluded

(e) Test position  $I_b$  (sonic exit)

Orifice ordinates		Pressure coefficients for nozzle-exit total-pressure ratio $H_e/p_m$ of -														
$x/D_F$	$y/D_F$	2	3	4	5	6	7	8	9	10	11	12	13	14	15	16
10.76	0	-0.013	-0.021	-0.012	-0.013	-0.012	-0.013	-0.013	-0.012	-0.011	-0.014	-0.017	-0.026	-0.026	-0.026	-0.026
9.72	0	.015	.015	-.014	-.023	-.016	-.015	-.015	-.017	-.023	-.023	-.020	-.016	-.016	-.016	-.016
8.68	0	-.028	-.020	-.021	-.032	-.021	-.022	-.024	-.024	-.024	-.018	-.005	.005	.009	.012	.013
7.63	0	-.026	-.024	-.025	-.021	-.021	-.029	-.020	-.023	-.028	-.026	-.011	-.006	-.113	-.116	-.117
6.59	0	-.025	-.022	-.025	-.014	-.015	-.010	-.015	-.015	-.010	-.004	-.005	-.006	-.007	-.007	-.008
5.55	0	.097	.105	.107	.102	.060	.060	.062	.063	.065	.065	.064	.067	.058	.058	.070
4.51	0	.038	.020	.055	.075	.084	.090	.096	.101	.105	.108	.111	.114	.117	.120	
3.47	0	.001	.008	.001	.008	.002	.003	.006	.005	.005	.005	.005	.005	.005	.005	.005
2.43	0	-.004	-.005	-.005	-.004	-.002	-.003	-.003	-.002	-.002	-.003	-.002	-.003	-.004	-.004	-.004
1.39	0	.001	-.002	-.001	-.001	0	.001	.001	.002	.002	.002	.002	.002	.001	.001	.001
.35	0	-.002	-.001	-.005	-.003	-.002	0	-.002	-.001	-.001	-.002	-.002	-.002	-.002	-.003	-.004
-.69	0	0	0	0	0	0	0	0	0	0	0	0	0	0	0	0
10.76	1.40	-.014	-.018	-.013	-.014	-.013	-.013	-.013	-.012	-.012	-.016	-.021	-.026	-.026	-.026	-.026
9.72	1.40	-.017	-.016	-.016	-.017	-.017	-.016	-.016	-.016	-.016	-.028	-.027	-.025	-.015	-.011	-.009
8.68	1.40	-.028	-.021	-.021	-.023	-.024	-.026	-.026	-.026	-.026	-.019	-.013	-.006	.008	.009	.004
7.63	1.40	-.069	-.026	-.027	-.029	-.030	-.034	-.038	-.033	-.032	-.029	-.028	-.022	-.013	-.113	-.114
6.59	1.40	.041	.044	.042	.044	.055	.058	.068	.068	.061	-.002	-.001	-.001	-.001	-.002	-.002
5.55	1.40	.096	.106	.113	.071	.075	.077	.080	.082	.084	.085	.087	.088	.089	.090	.091
4.51	1.40	-.005	-.002	.001	.007	.102	.111	.117	.122	.128	.132	.136	.140	.142	.145	.146
3.47	1.40	.001	-.001	-.002	-.001	0	.001	.001	.002	.003	.003	.003	.003	.003	.003	.003
2.43	1.40	.002	.001	0	0	.001	.001	0	0	0	0	0	0	0	0	0
1.39	1.40	.001	.002	.008	.001	.001	.002	.003	.002	.002	.002	.002	.003	.001	0	0
.35	1.40	0	0	0	0	0	0	0	0	0	0	0	0	0	0	0
-.69	1.40	0	0	0	0	0	0	0	0	0	0	0	0	0	0	0
10.76	4.17	-.061	-.080	-.080	-.082	-.082	-.082	-.086	-.087	-.087	-.015	-.012	-.008	-.011	-.008	-.008
9.72	4.17	-.024	-.021	-.022	-.026	-.028	-.036	-.036	-.036	-.036	-.059	-.079	-.084	-.085	-.086	-.085
8.68	4.17	.082	.087	.084	.091	.072	.080	.046	.047	.048	.048	.049	.051	.050	.051	.051
7.63	4.17	.068	.059	.059	.055	.060	.063	.069	.068	.069	.071	.071	.070	.071	.071	.071
6.59	4.17	.006	.007	.005	.005	.003	.010	.045	.103	.127	.136	.142	.147	.151	.154	.157
5.55	4.17	-.006	-.006	-.006	-.007	-.006	-.006	-.006	-.006	-.006	-.006	-.006	-.005	.001	.001	.001
4.51	4.17	-.001	0	-.001	-.001	0	0	0	0	0	0	0	0	0	0	0
3.47	4.17	-.002	0	-.001	-.001	0	0	0	0	0	0	0	0	0	0	0
2.43	4.17	0	0	0	0	0	0	0	0	0	0	0	0	0	0	0
1.39	4.17	0	0	0	0	0	0	0	0	0	0	0	0	0	0	0
.35	4.17	0	0	0	0	0	0	0	0	0	0	0	0	0	0	0
-.69	4.17	0	0	0	0	0	0	0	0	0	0	0	0	0	0	0
10.76	6.94	.006	.012	.018	.059	.053	.062	.053	.068	.070	.071	.072	.073	.073	.074	.074
9.72	6.94	-.005	-.003	-.003	-.004	-.003	-.003	0	.012	.012	.012	.012	.011	.011	.011	.011
8.68	6.94	.001	.001	.001	.001	.001	.002	.002	.002	.003	.003	.004	.005	.005	.005	.005
7.63	6.94	-.003	-.001	-.003	-.003	-.001	-.001	0	0	0	0	0	0	0	0	0
6.59	6.94	-.003	-.001	-.002	-.002	-.001	0	0	0	0	0	0	0	0	0	0
5.55	6.94	0	0	0	0	0	0	0	0	0	0	0	0	0	0	0
4.51	6.94	0	0	0	0	0	0	0	0	0	0	0	0	0	0	0
3.47	6.94	0	0	0	0	0	0	0	0	0	0	0	0	0	0	0
10.76	11.11	-.001	.002	0	-.004	.001	.004	.004	.004	.004	.004	.004	.003	.003	.002	.001
9.72	11.11	0	.005	0	-.004	.002	.004	.005	.004	.005	.005	.004	.005	.005	.004	0
8.68	11.11	0	.005	0	-.004	0	.004	.008	.010	.010	.010	.010	.011	.011	.008	.008
7.63	11.11	-.002	0	0	0	0	0	0	0	0	0	0	0	0	0	0
	$p_e/p_m$	.98	1.47	1.96	2.45	2.94	3.43	3.92	4.41	4.90	5.37	5.88	6.37	6.86	7.35	7.84



L-86661

Figure 1.- Photograph of the nacelle mounted beneath the flat-surface wing in the 27- by 27-inch preflight-jet nozzle.

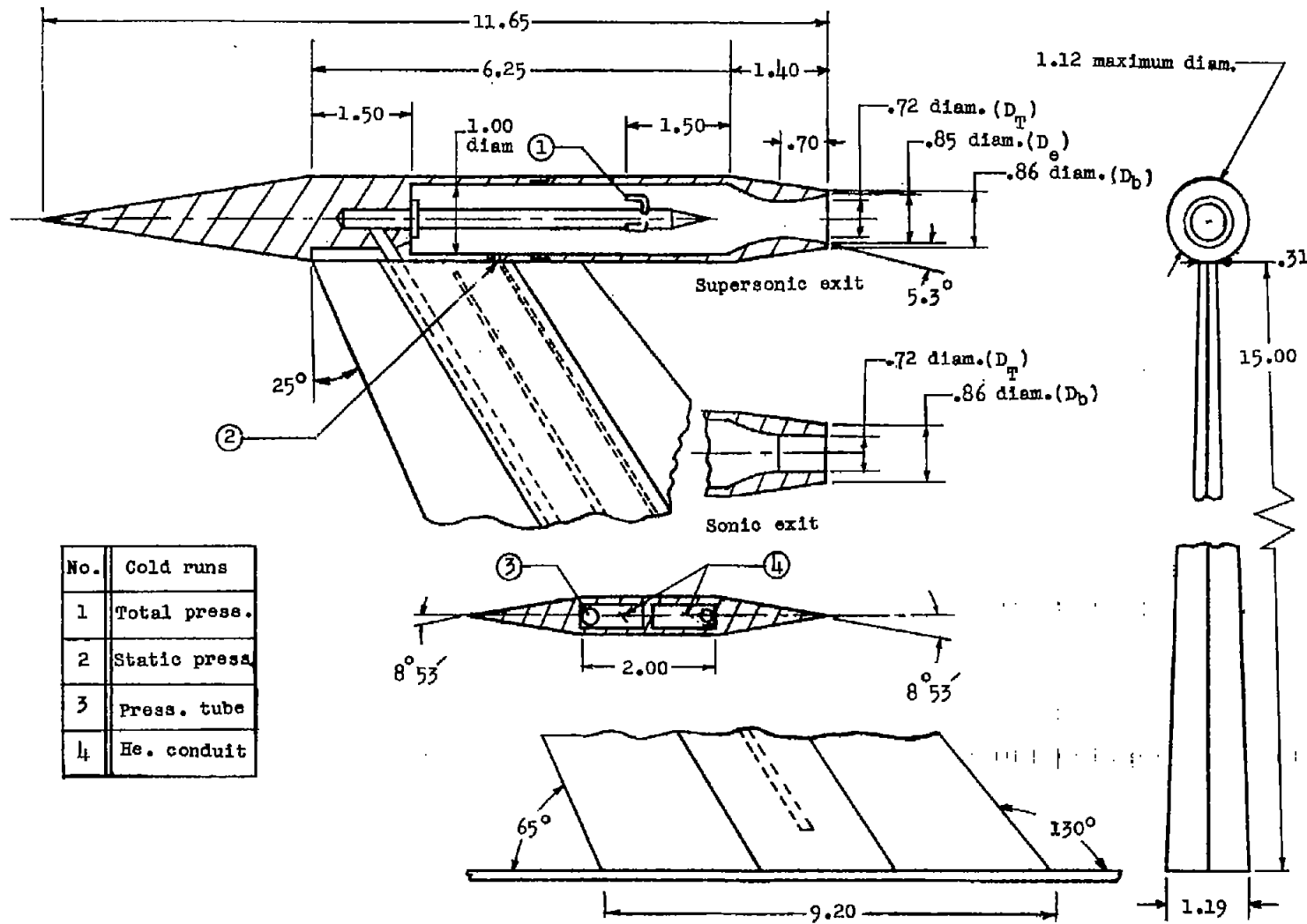


Figure 2.- Schematic diagram of nacelle. All dimensions are in inches.

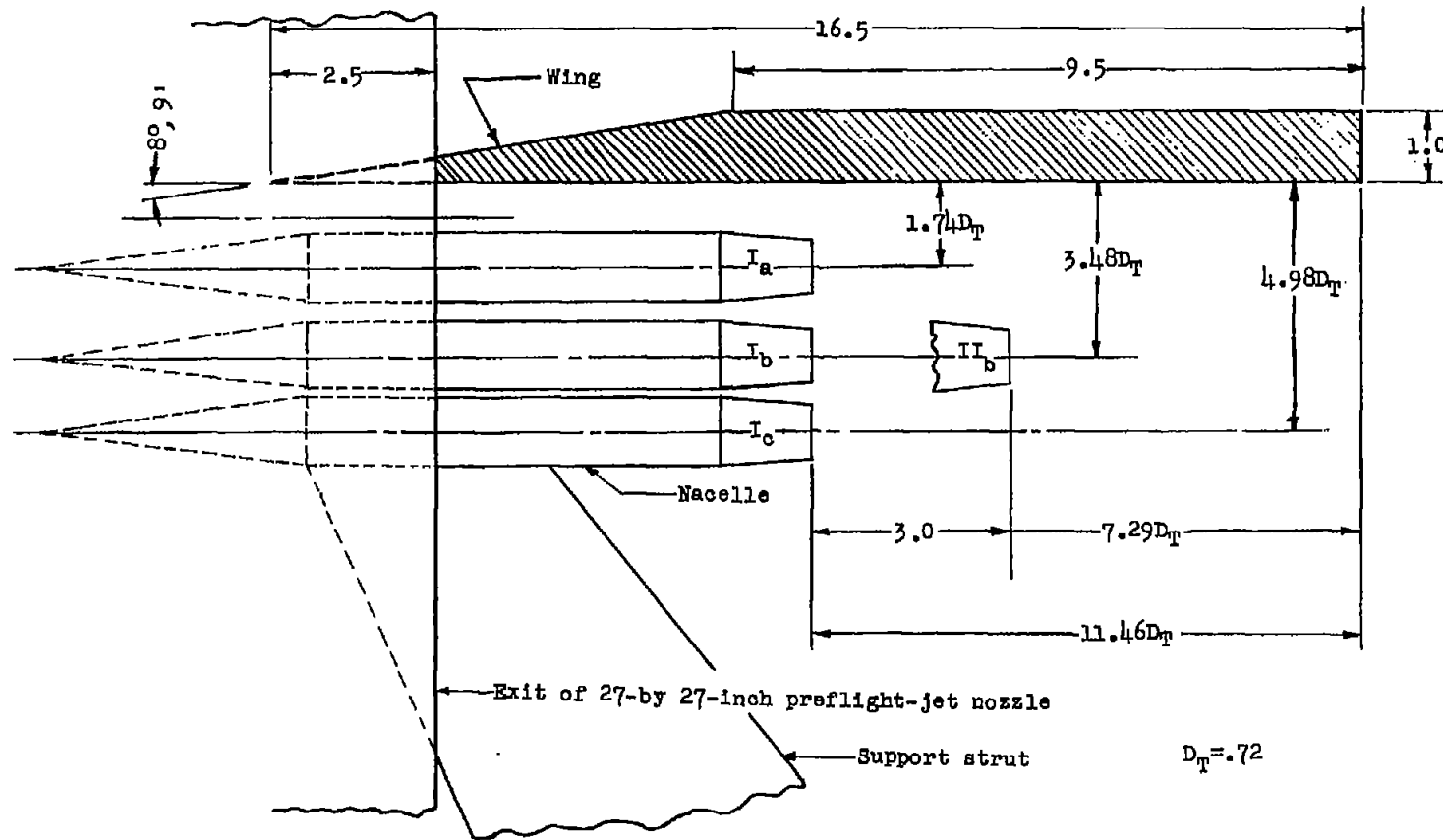


Figure 3.- Arrangement of the nacelle relative to the exit of the 27- by 27-inch preflight-jet nozzle and wing for the four test positions. Dimensions are in inches except as otherwise noted.

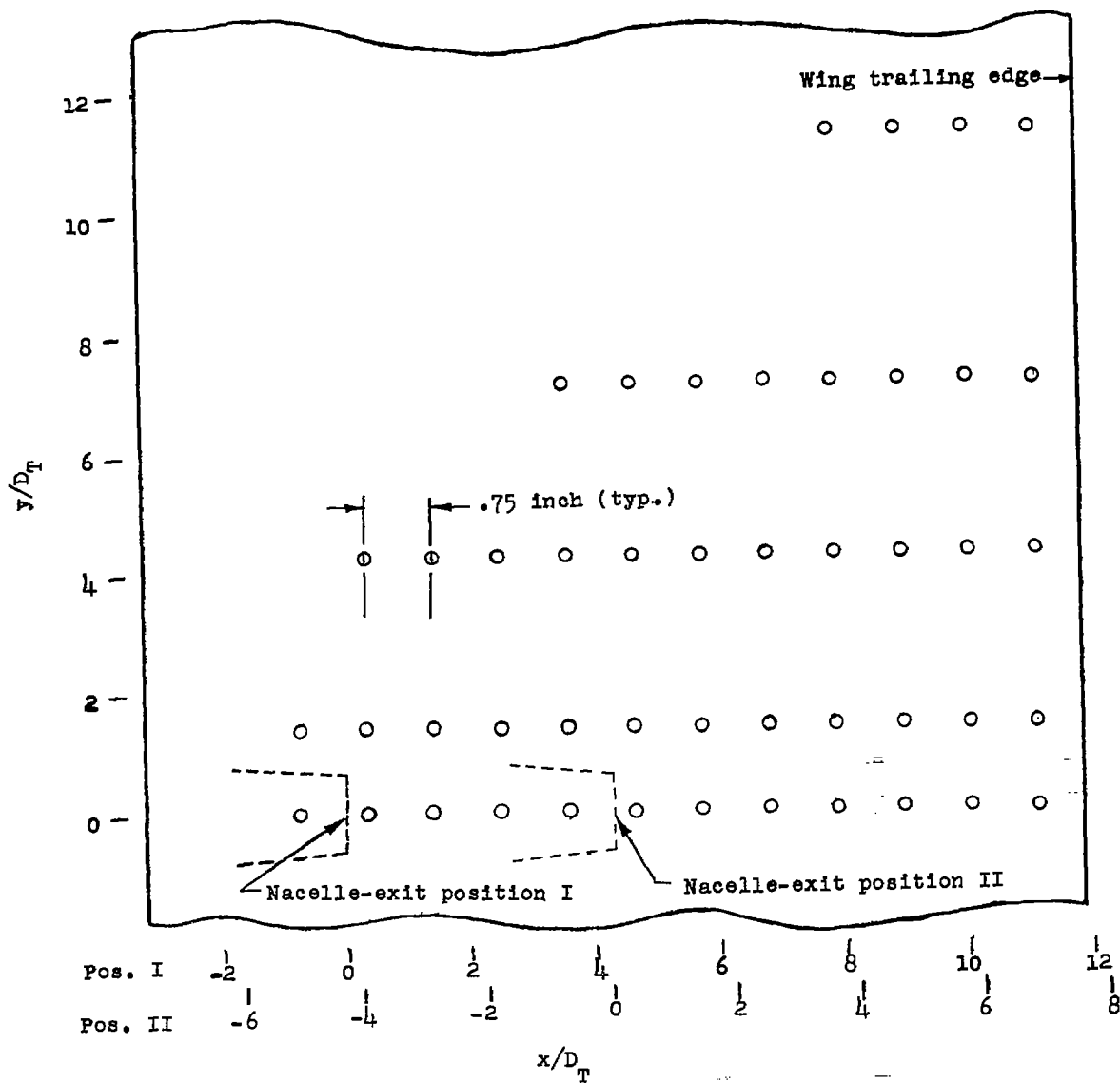


Figure 4.- Location of the wing static-pressure orifices.

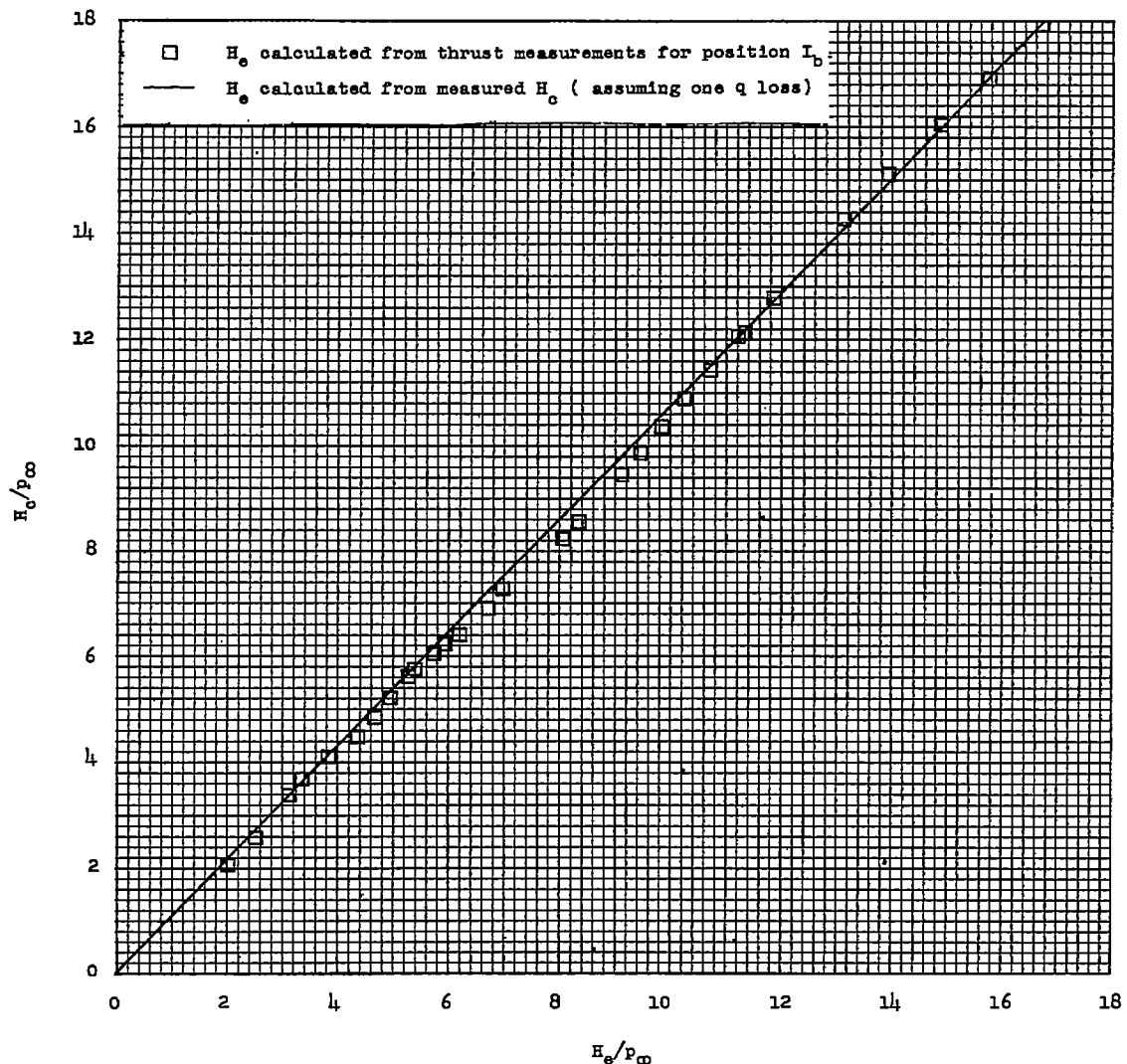


Figure 5.- Variation of nacelle-combustion-chamber total-pressure ratio with nacelle-exit total-pressure ratio for the supersonic nacelle exit.

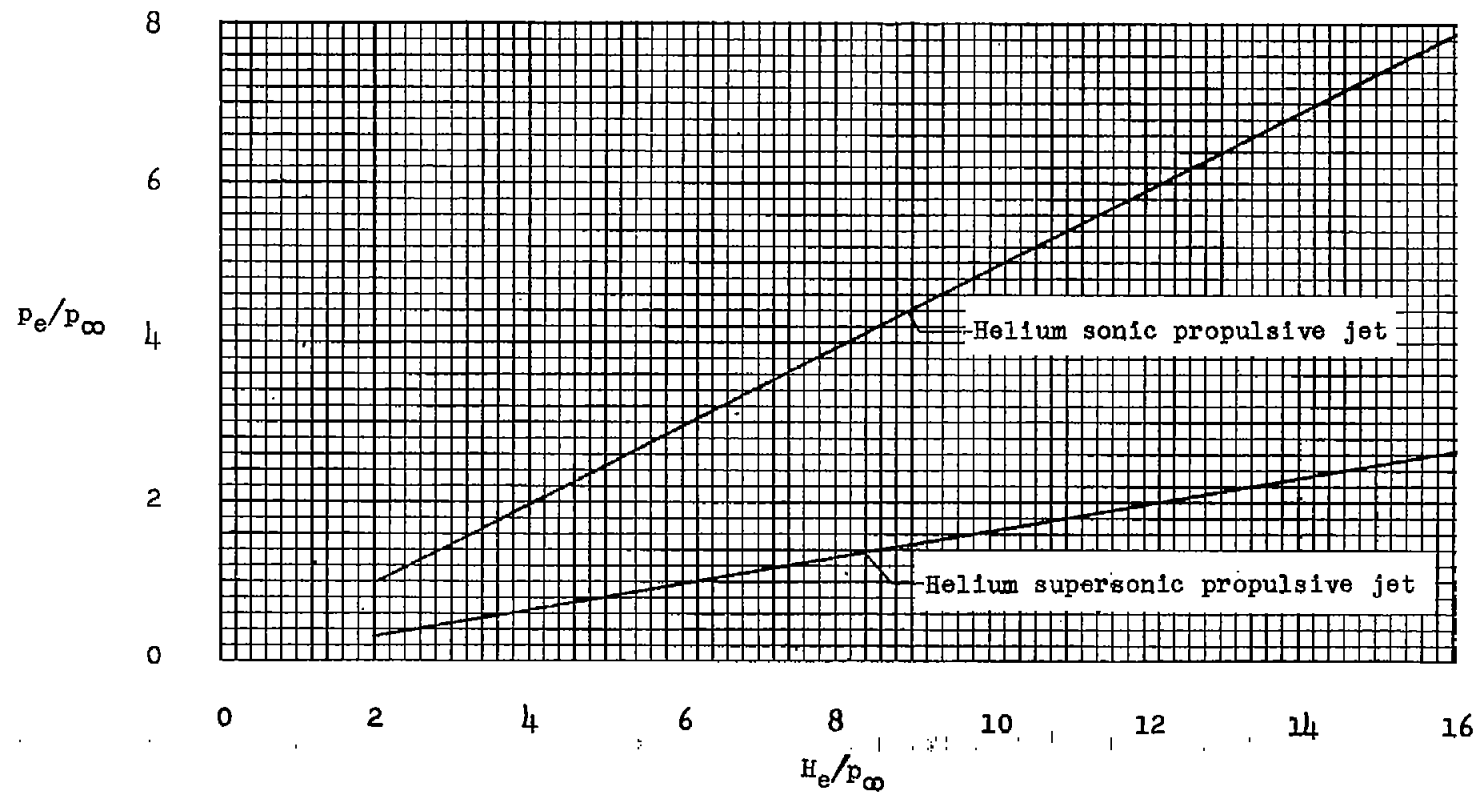
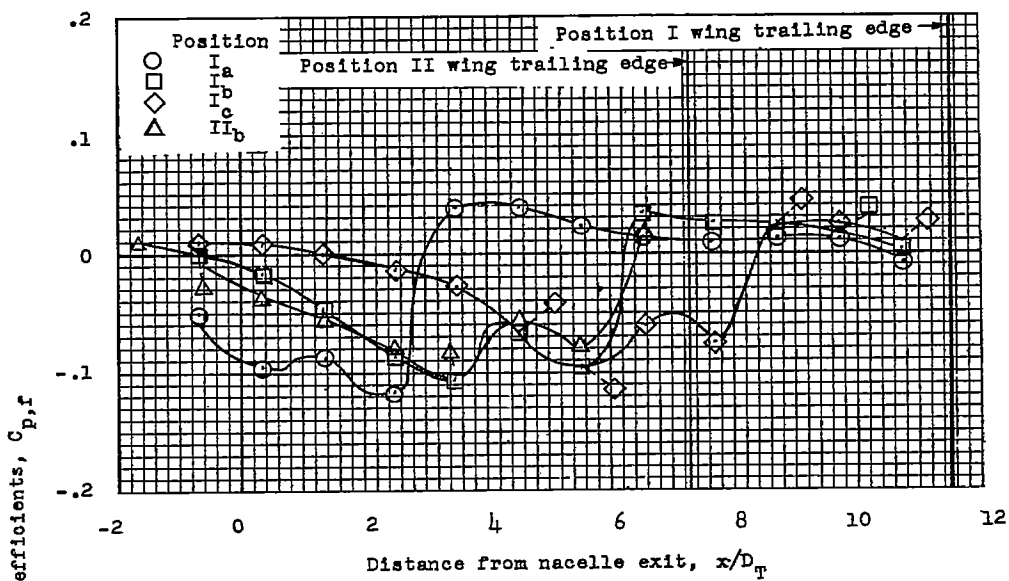


Figure 6.- Variation of static-pressure ratio with total-pressure ratio for both supersonic and sonic propulsive jets.



(a) Along nacelle center line.

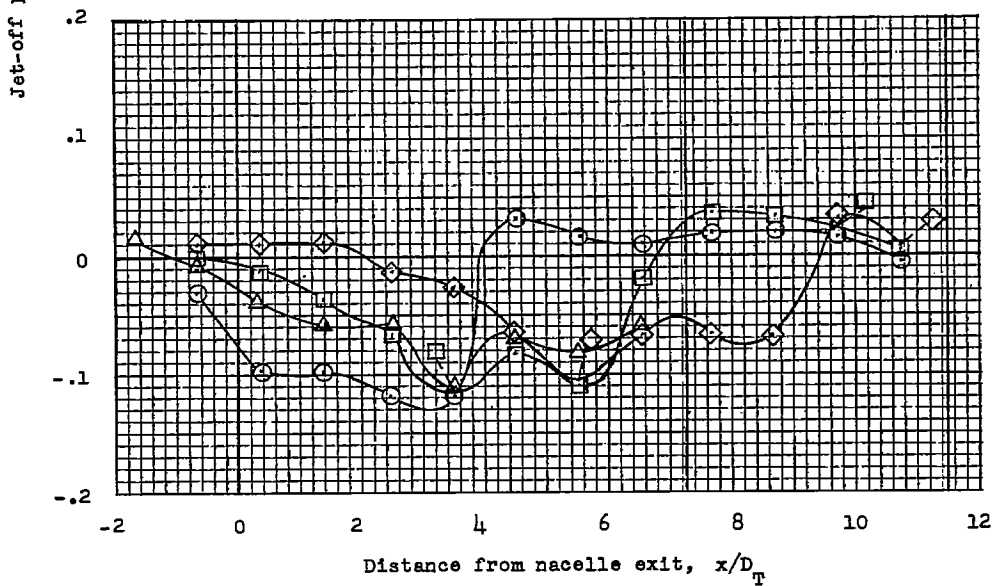
(b) 1.40 $D_T$  spanwise from nacelle center line.

Figure 7.- Chordwise variation of jet-off pressure coefficients for test positions I<sub>a</sub>, I<sub>b</sub>, I<sub>c</sub>, and II<sub>b</sub>.

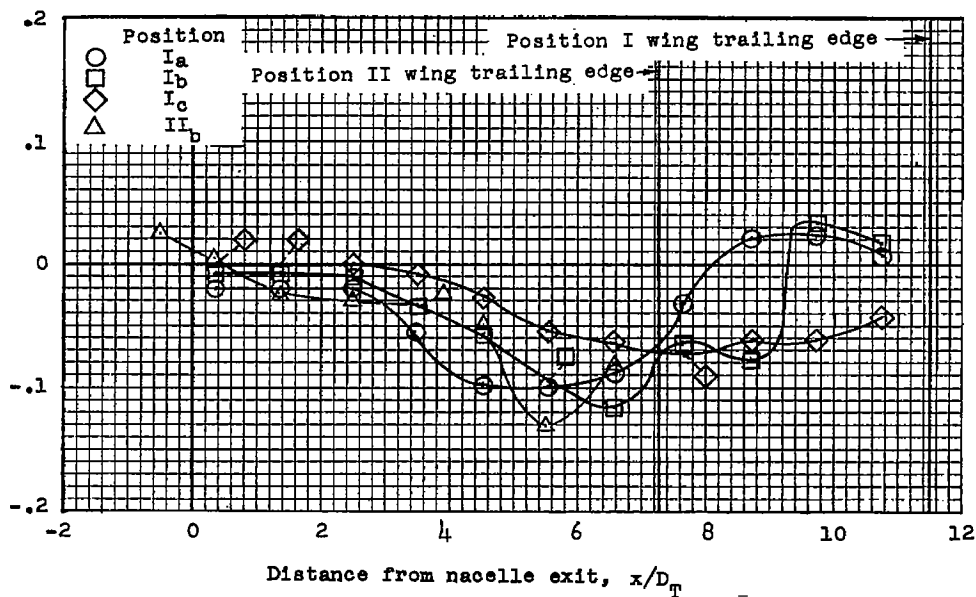
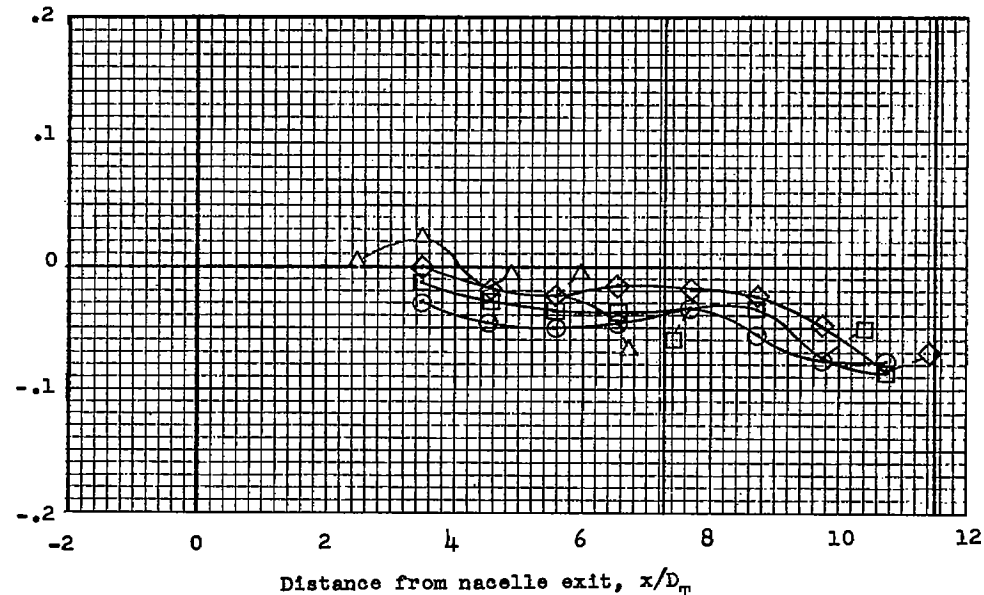
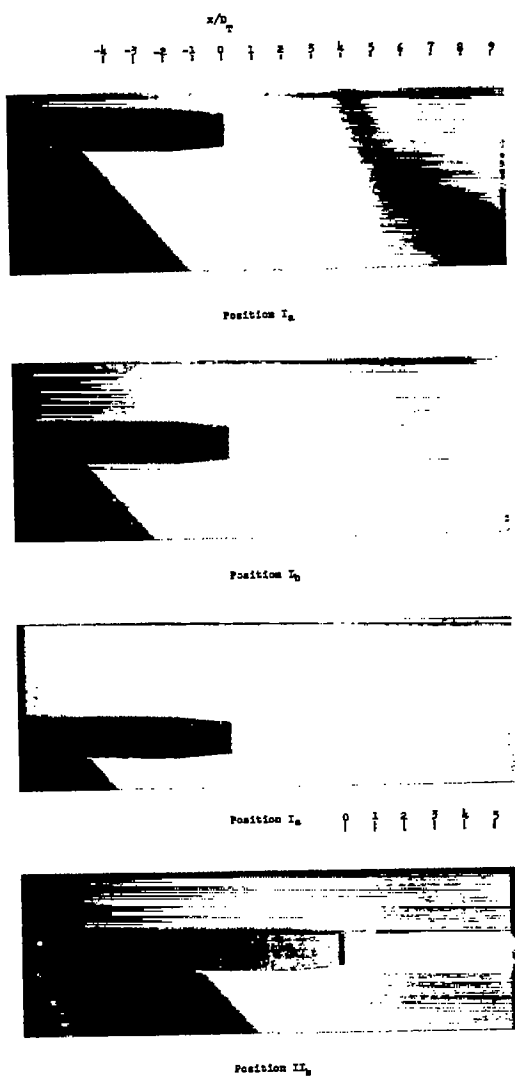
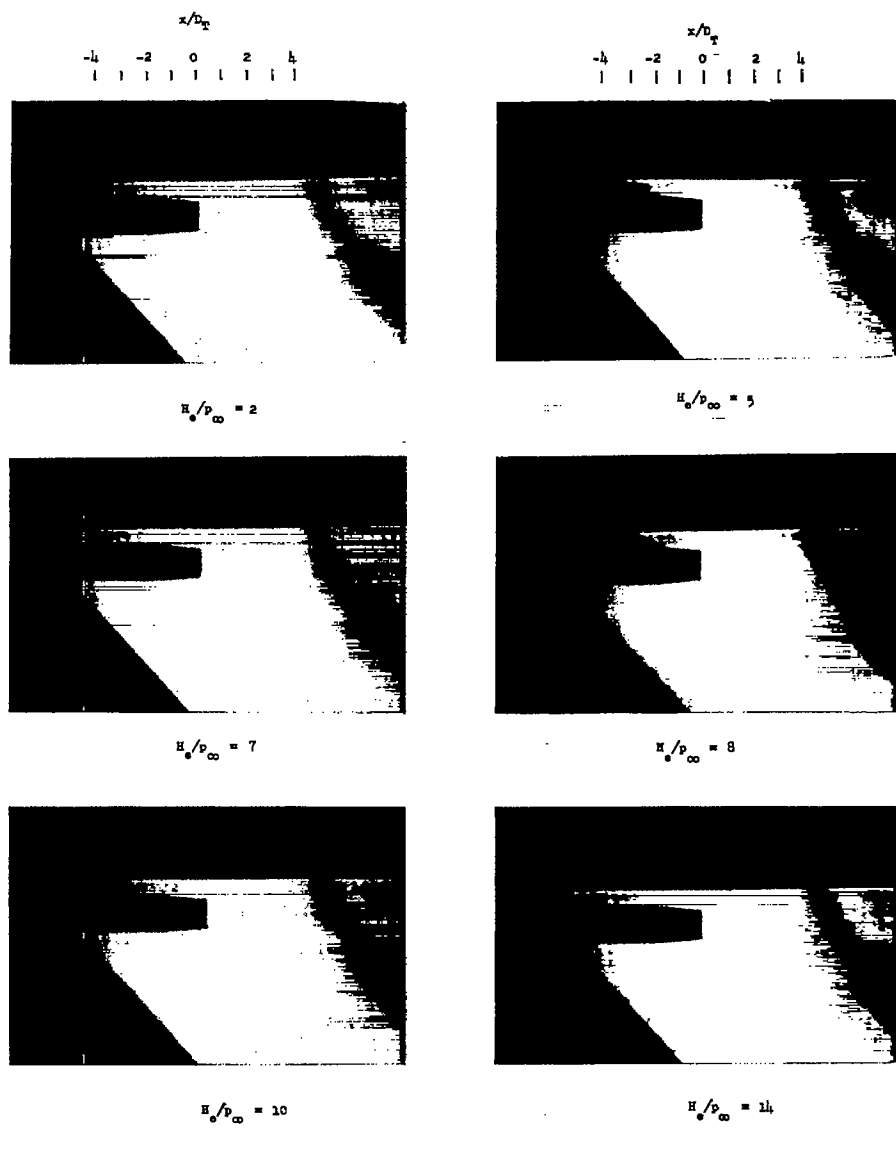
Jet-off pressure coefficient,  $C_{p,f}$ (c)  $4.17D_T$  spanwise from nacelle center line.(d)  $6.94D_T$  spanwise from nacelle center line.

Figure 7.- Concluded.



L-95804

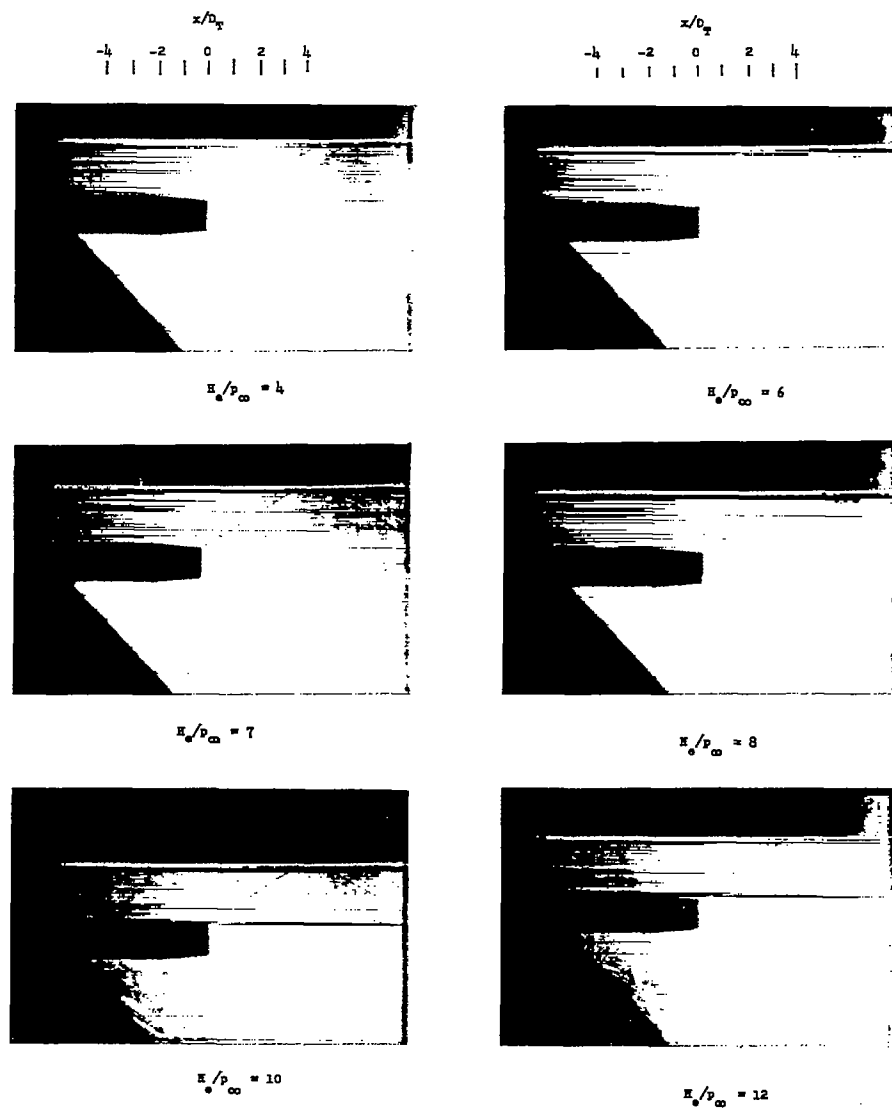
Figure 8.- Shadowgraph pictures of the flow field about the nacelle exit with jet off for test positions I<sub>a</sub>, I<sub>b</sub>, I<sub>c</sub>, and II<sub>b</sub>.

(a) Position I<sub>a</sub>.

L-95805

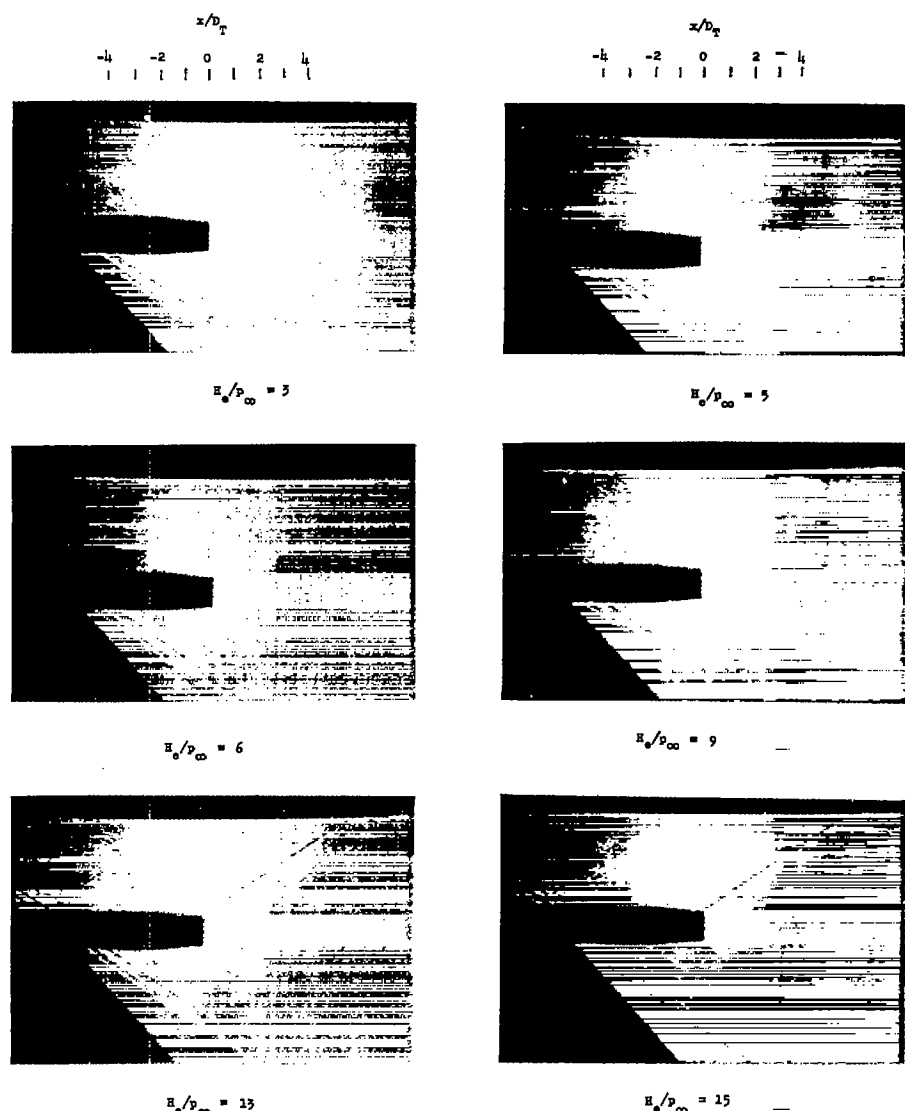
Figure 9.- Shadowgraph pictures of the flow field about the nacelle exit with jet on for test positions I<sub>a</sub>, I<sub>b</sub>, I<sub>c</sub>, and II<sub>b</sub>.

CONFIDENTIAL

(b) Position I<sub>b</sub>.

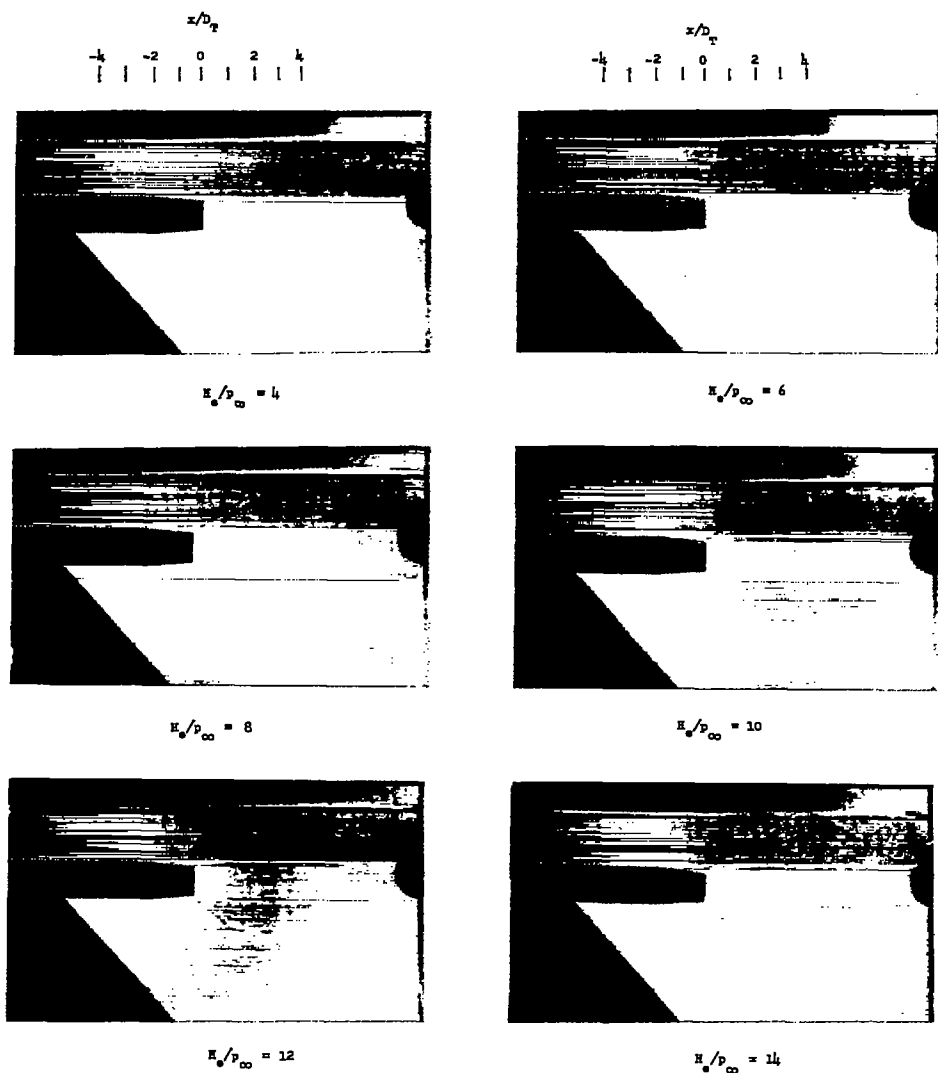
L-95806

Figure 9.- Continued.

(c) Position I<sub>c</sub>.

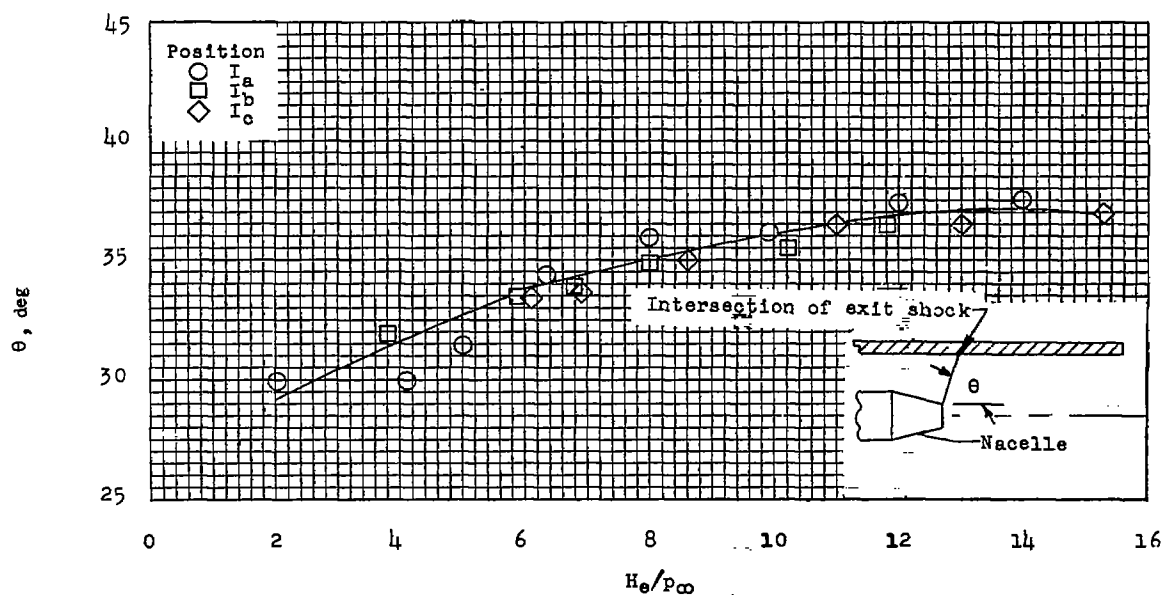
L-95807

Figure 9.- Continued.

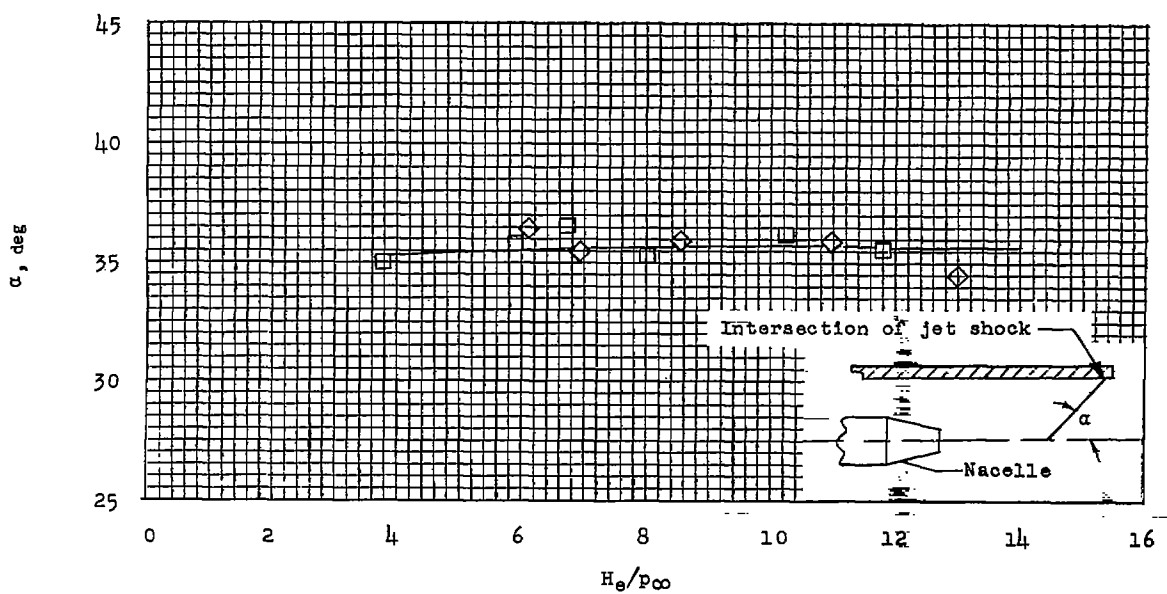
(d) Position II<sub>b</sub>.

L-95808

Figure 9.- Concluded.



(a) Exit-shock-wave angle.



(b) Jet-shock-wave angle.

Figure 10.-- Variation of the angles of inclination from the nacelle center line of the exit and jet shock waves with nacelle-exit total-pressure ratio at test positions  $I_a$ ,  $I_b$ , and  $I_c$  for the supersonic nacelle exit as measured from the shadowgraph pictures.

CONFIDENTIAL

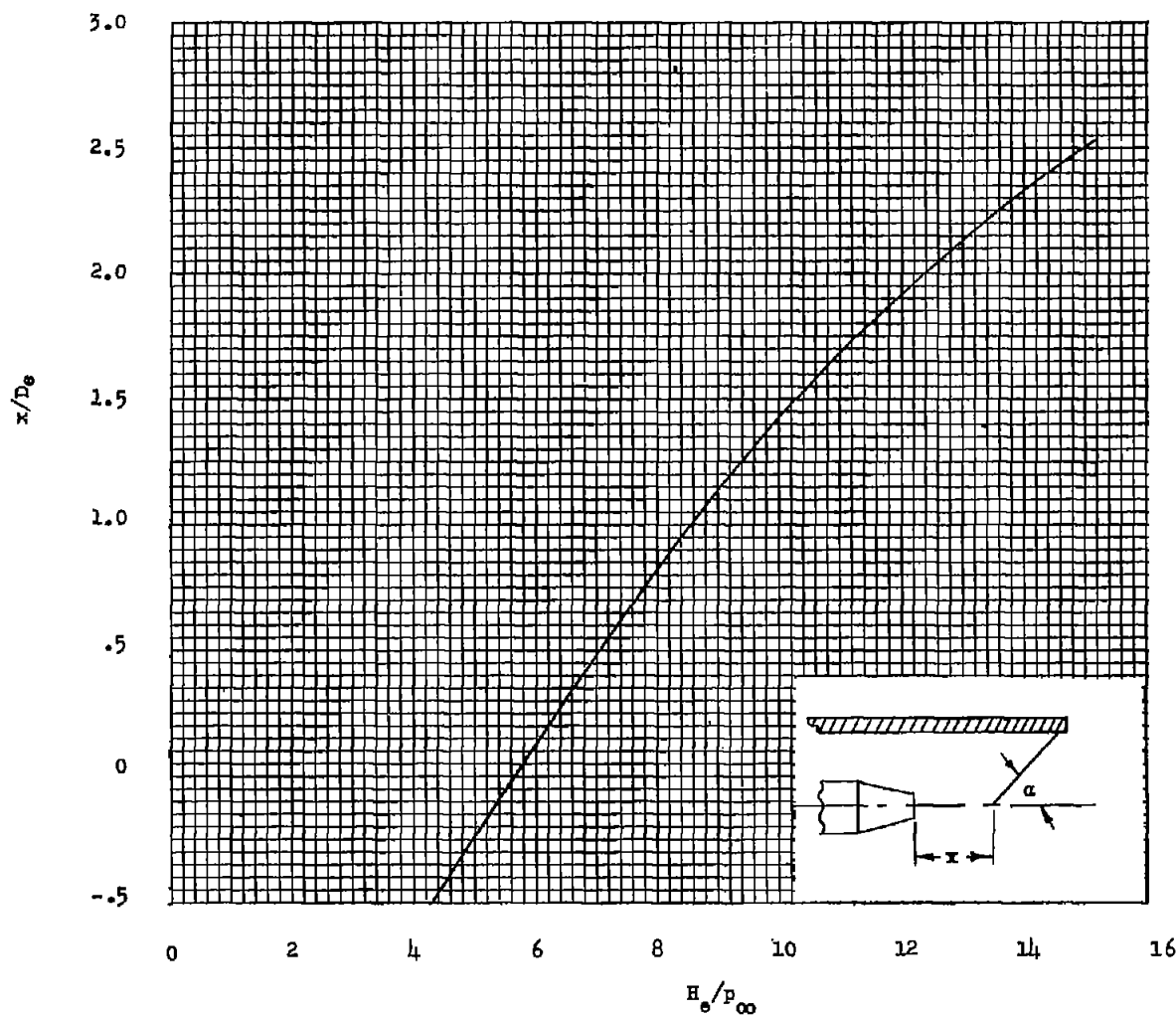


Figure 11.- The calculated chordwise-distance ratio of the apex of the jet shock wave for test positions  $I_b$  and  $I_c$  as it varies with nacelle-exit total-pressure ratio for the supersonic nacelle exit.

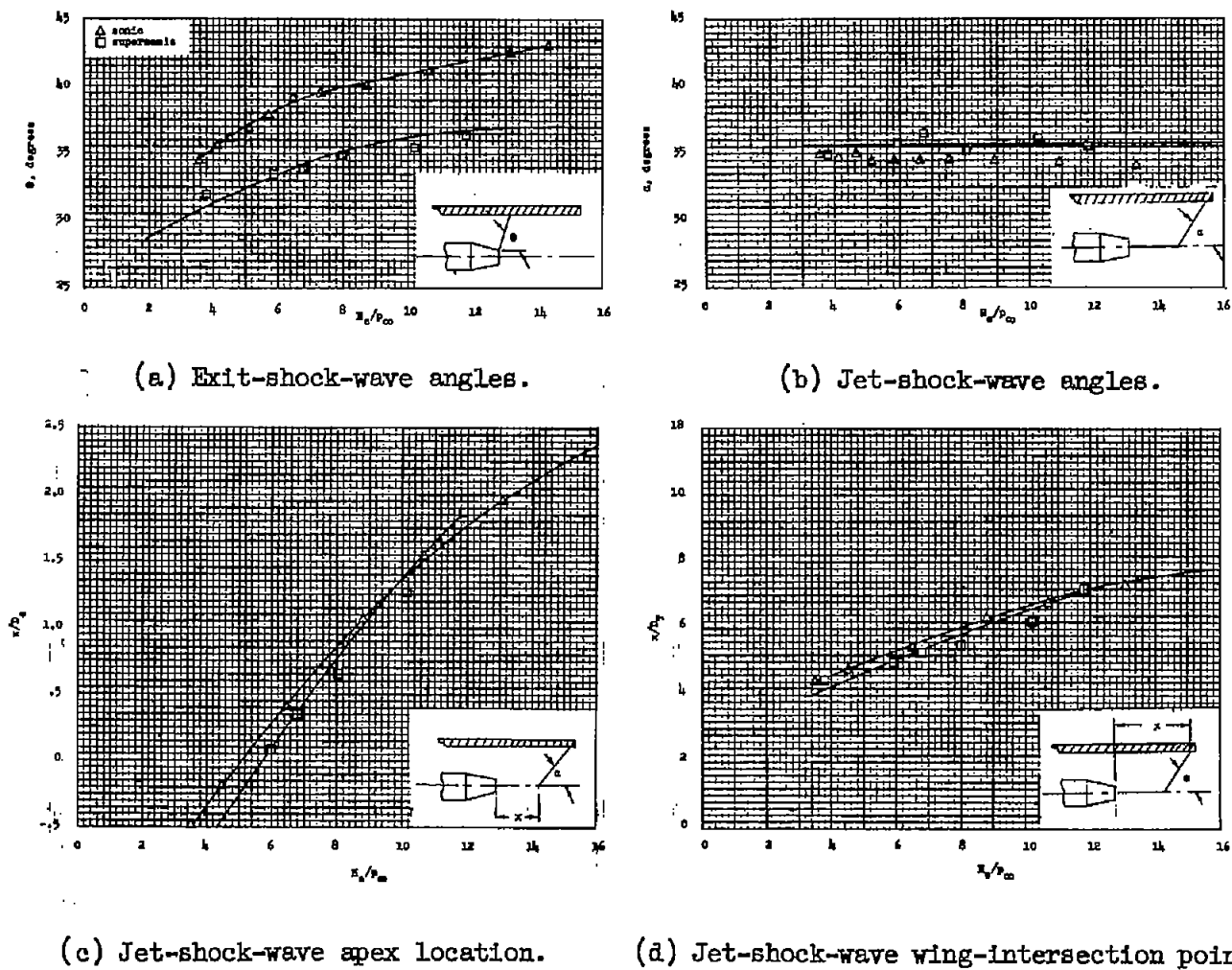


Figure 12.- Variation of  $\theta$ ,  $\alpha$ , jet-shock-wave apex, and wing-intersection point with nacelle-exit total-pressure ratio for the nacelle sonic and supersonic exits at test position  $I_b$ , as measured from the shadowgraph pictures.

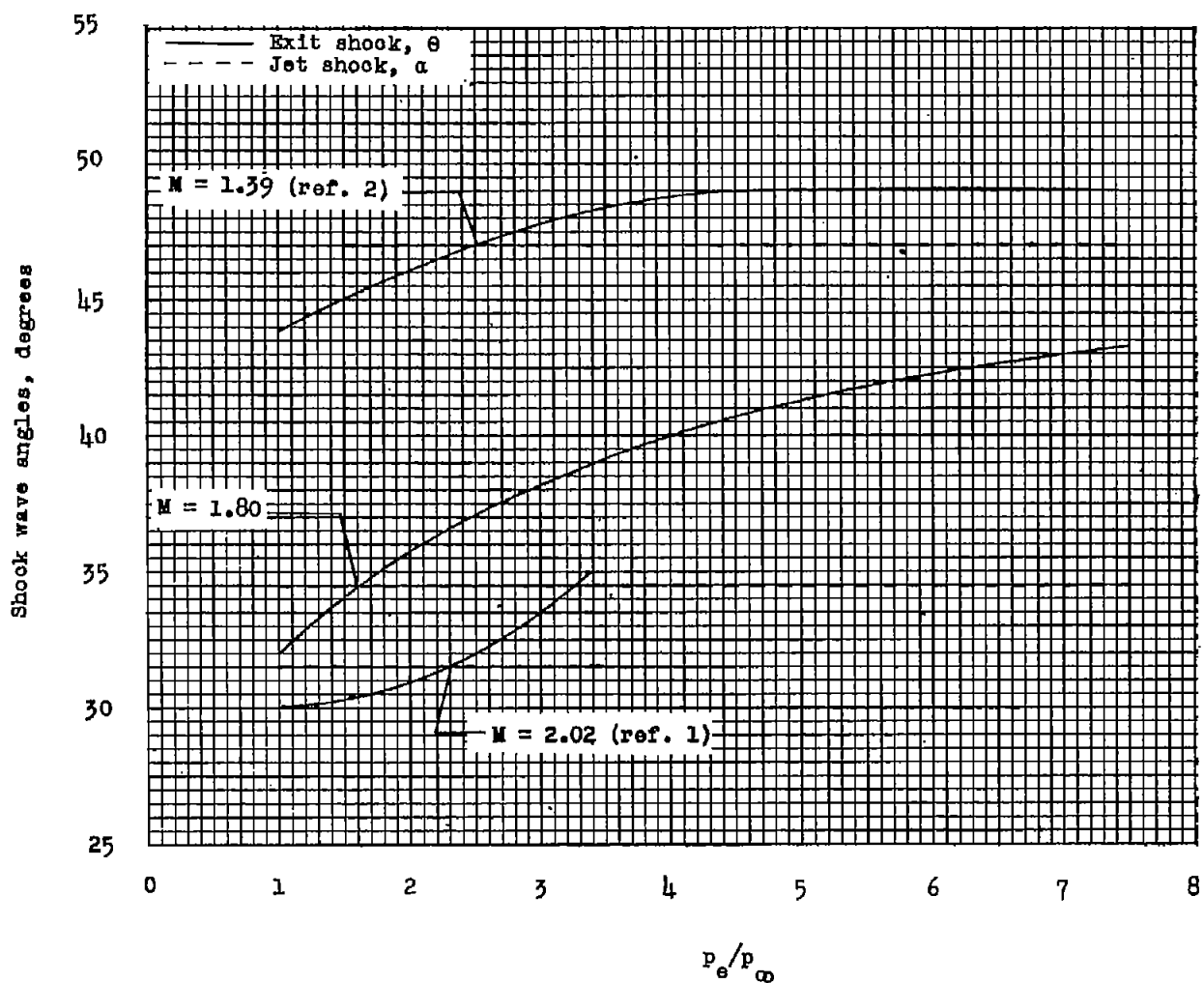
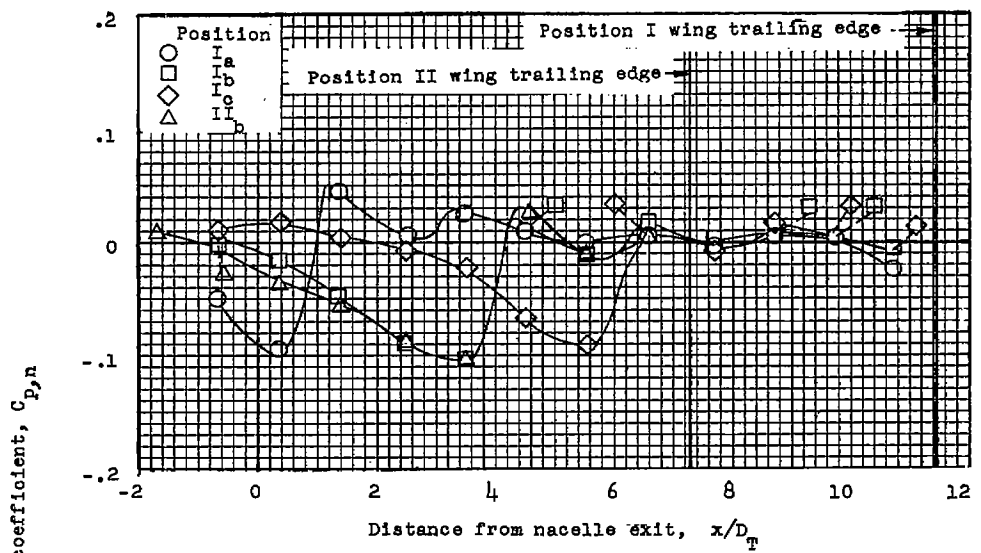


Figure 13.- Variation of exit- and jet-shock-wave angles with nacelle-exit static-pressure ratio for free-stream Mach numbers of 1.39, 1.80, and 2.02 for the nacelle sonic exit.



(a) Along nacelle center line.

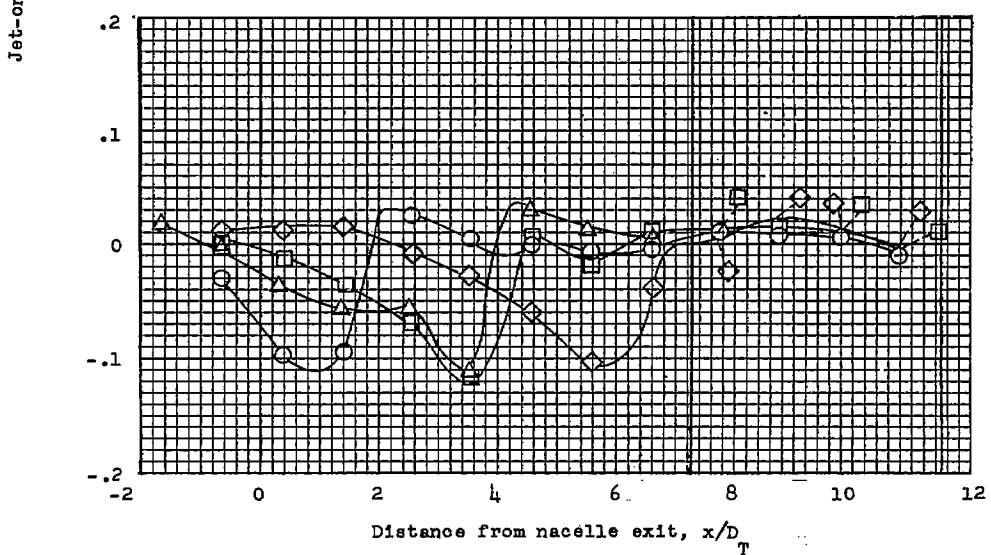
(b)  $1.40D_T$  spanwise from nacelle center line.

Figure 14.- Chordwise variation of jet-on pressure coefficients for test positions  $I_a$ ,  $I_b$ ,  $I_c$ , and  $II_b$  at a supersonic nacelle-exit total-pressure ratio of 7.

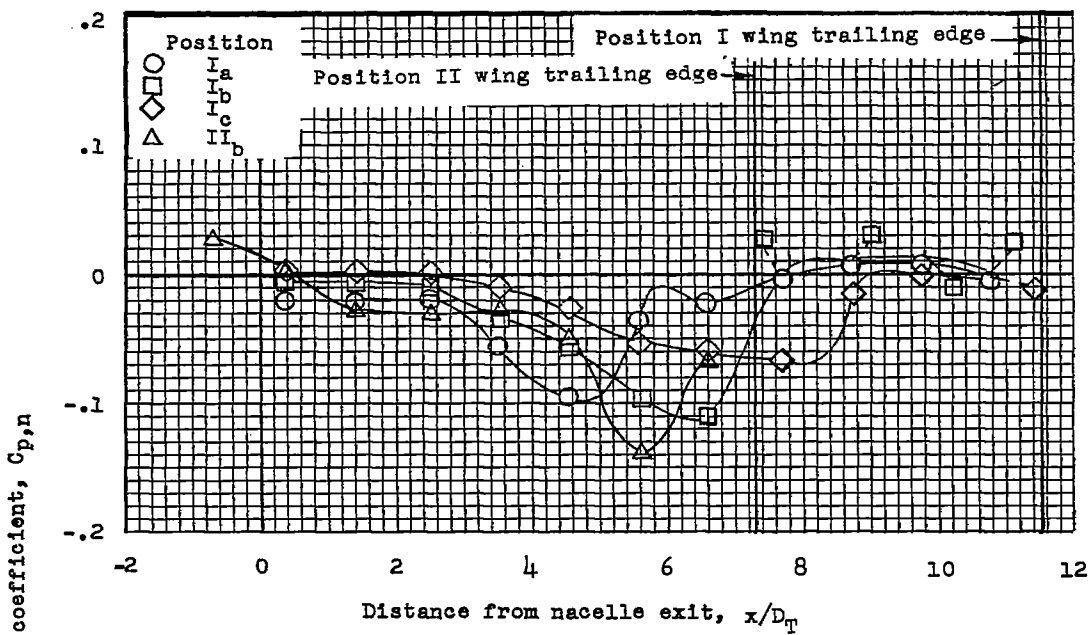
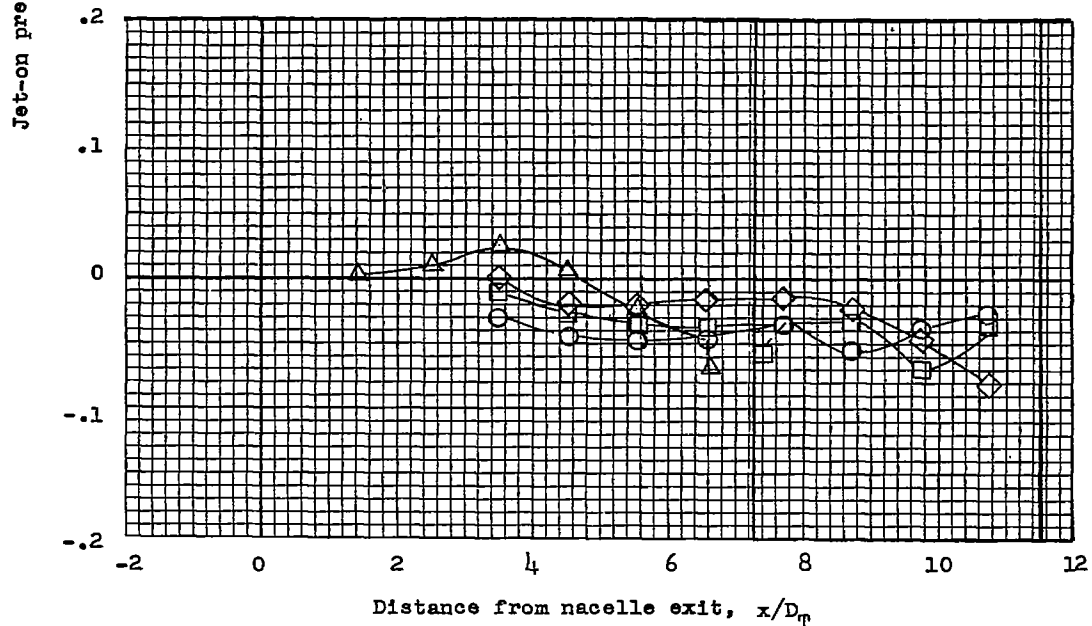
(c)  $4.17D_T$  spanwise from nacelle center line.(d)  $6.94D_T$  spanwise from nacelle center line.

Figure 14.- Concluded.

~~CONFIDENTIAL~~

NACA RM 156106

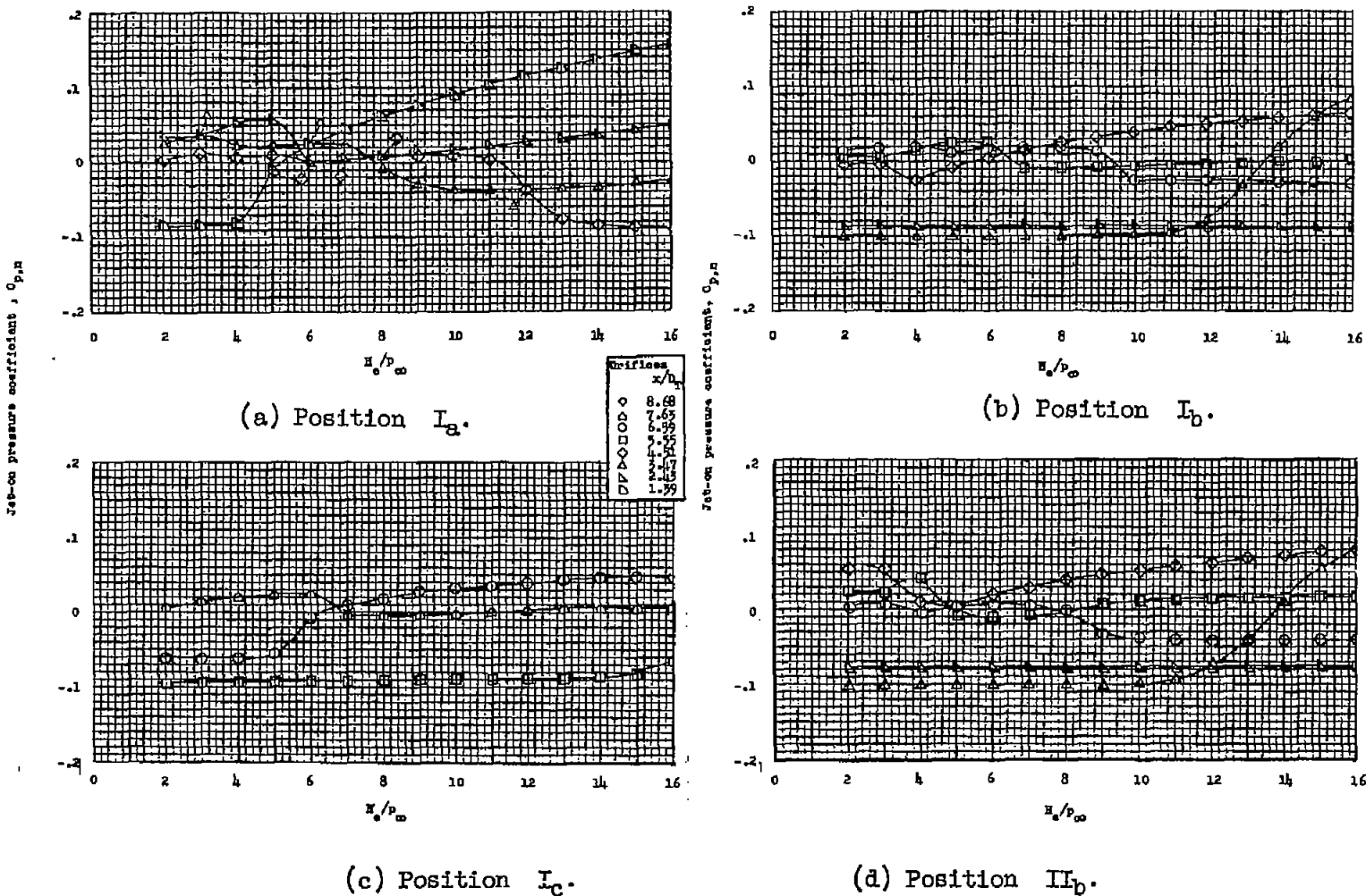
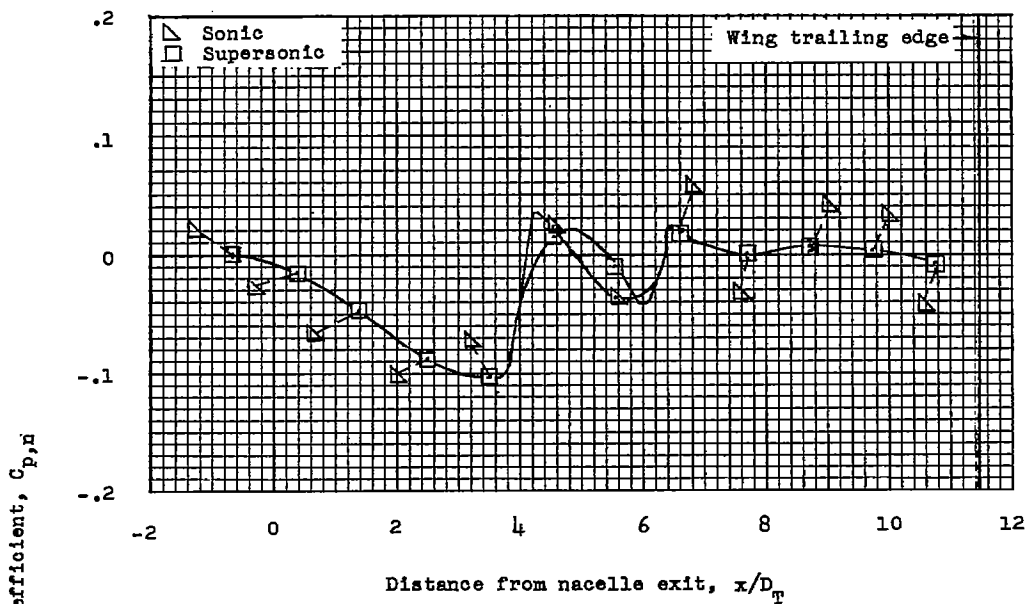


Figure 15.- Variation of jet-on pressure coefficient with total-pressure ratio for various orifices located on the nacelle center line at all test positions.



(a) Along center line.

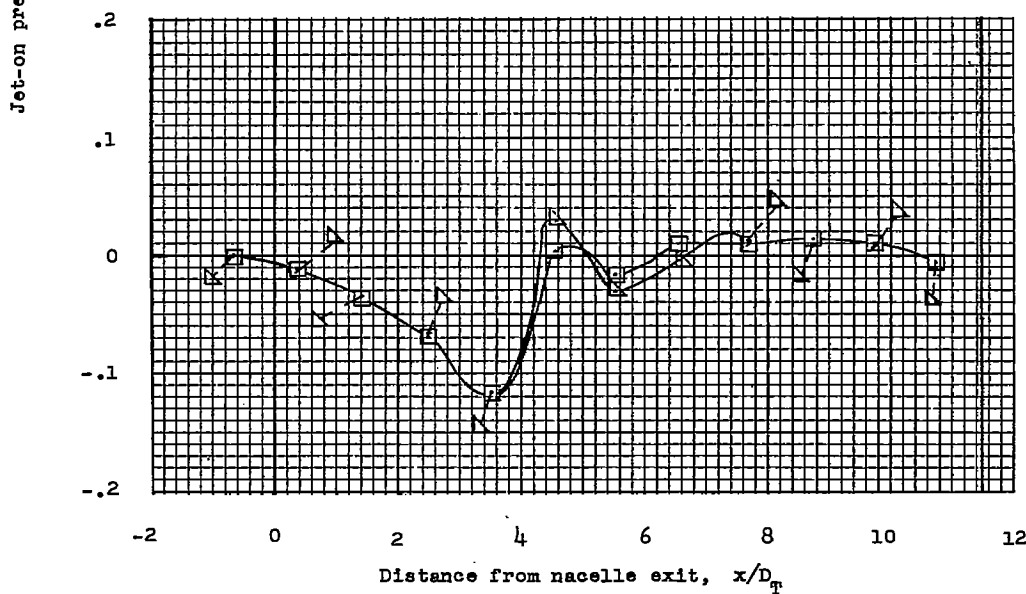
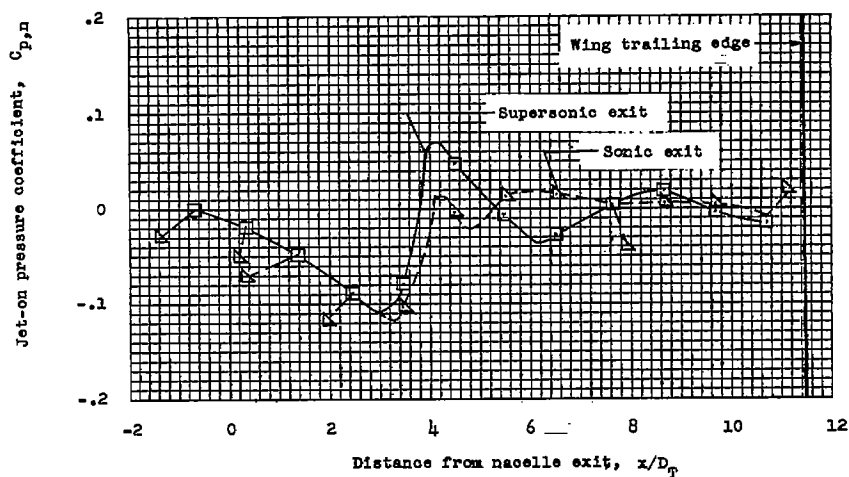
(b)  $1.40D_T$  spanwise from nacelle center line.

Figure 16.- Chordwise variation of jet-on pressure coefficients at test position  $I_b$  for both sonic and supersonic nacelle exit at a nacelle-exit total-pressure ratio of 7.

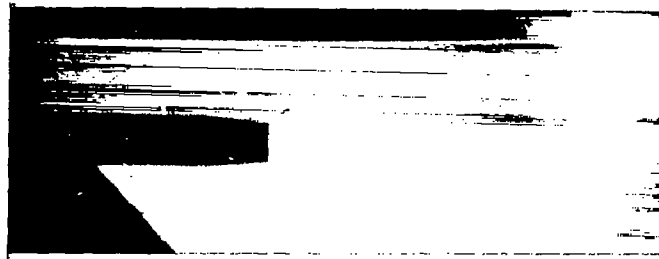
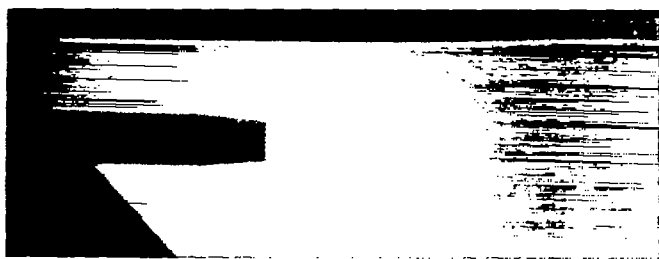
Supersonic nacelle exit,  $H_e/p_\infty = 12$ ,  $M_e = 1.79$ Sonic nacelle exit,  $H_e/p_\infty = 4$ ,  $M_e = 1.0$ 

L-95809

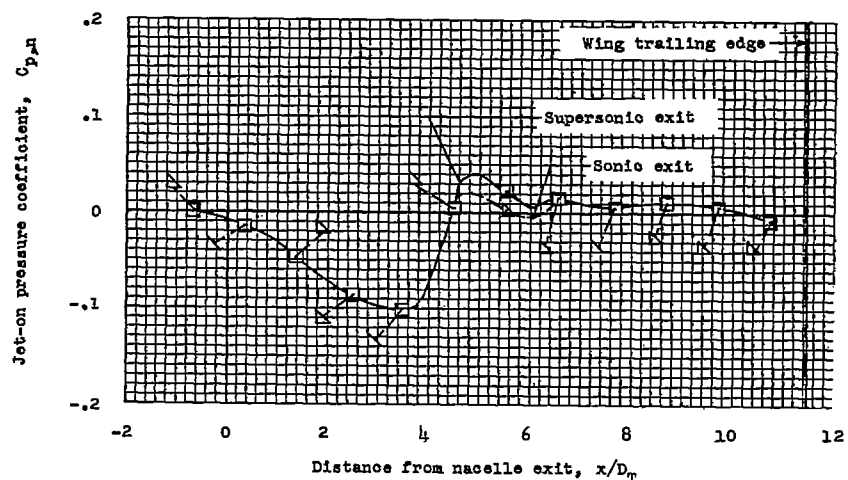


(a) Nacelle-exit static-pressure ratio of 1.96.

Figure 17.- Chordwise variation of jet-on pressure coefficients with shadowgraph pictures at test position  $I_b$  for both sonic and supersonic nacelle exits.

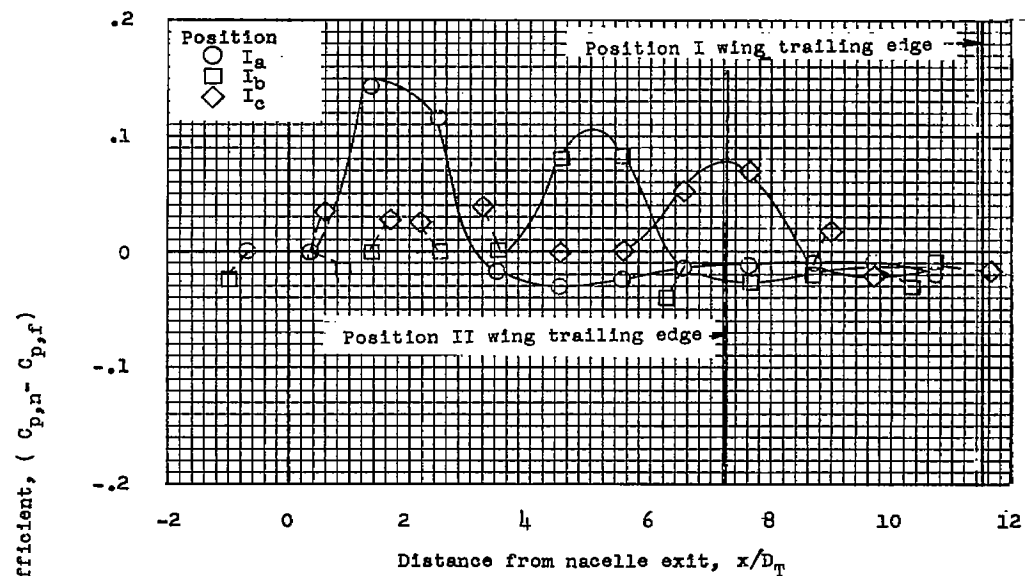
Supersonic nacelle exit,  $H_e/p_\infty = 6$ ,  $M_e = 1.79$ Sonic nacelle exit,  $H_e/p_\infty = 2$ ,  $M_e = 1.0$ 

L-95810



(b) Nacelle-exit static-pressure ratio of 0.98.

Figure 17.- Concluded.



(a) Along nacelle center line.

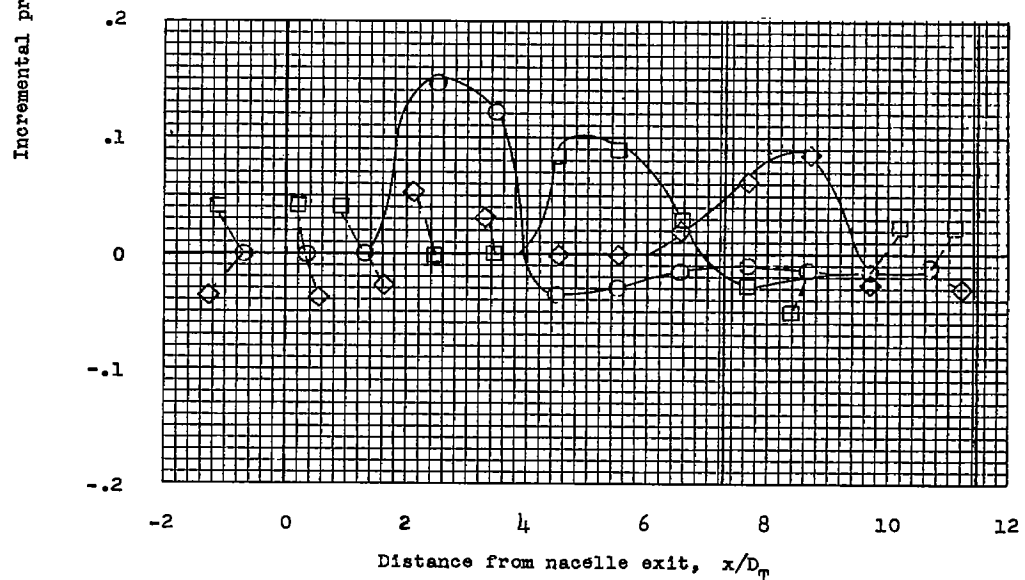
(b)  $1.40D_e$  spanwise from nacelle center line.

Figure 18.- Chordwise variation of incremental pressure coefficient  $p_n - p_f$  at two spanwise stations for positions  $I_a$ ,  $I_b$ , and  $I_c$  at a nacelle-exit total-pressure ratio of 7.

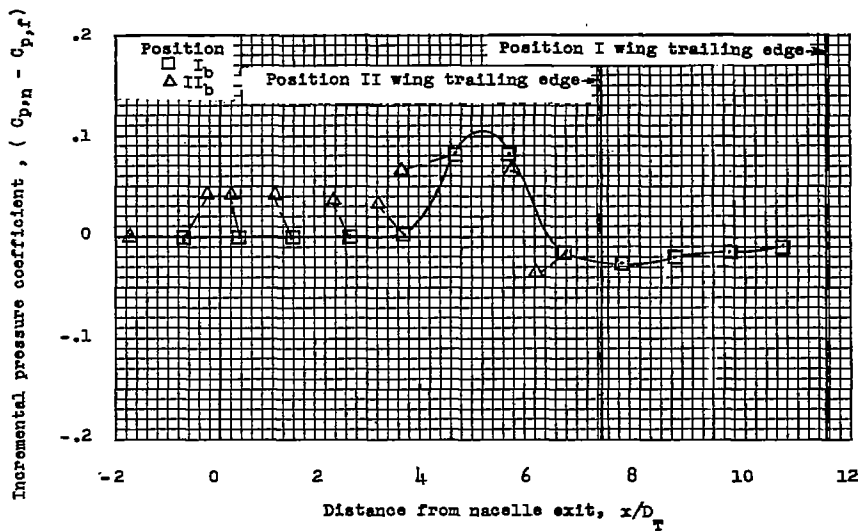


Figure 19.- Chordwise variation of incremental pressure coefficients for test positions  $I_b$  and  $II_b$  at a nacelle-exit total-pressure ratio of 7 along the nacelle center line.

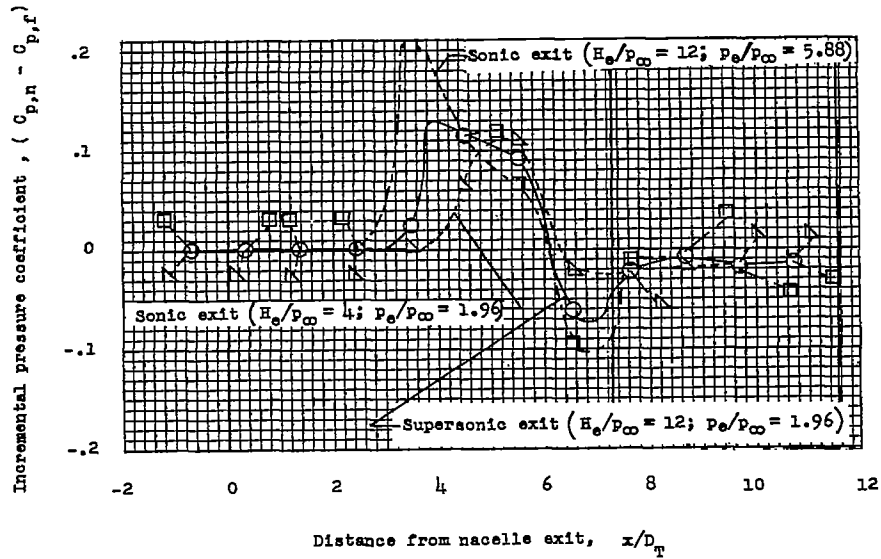


Figure 20.- Chordwise variation of incremental pressure coefficients at test positions  $I_b$  for both sonic and supersonic nacelle exit at a nacelle-exit total-pressure ratio of 12 and a nacelle-exit static-pressure ratio of 1.96.

CONFIDENTIAL

NACA RM 156106

NACA RM 156106

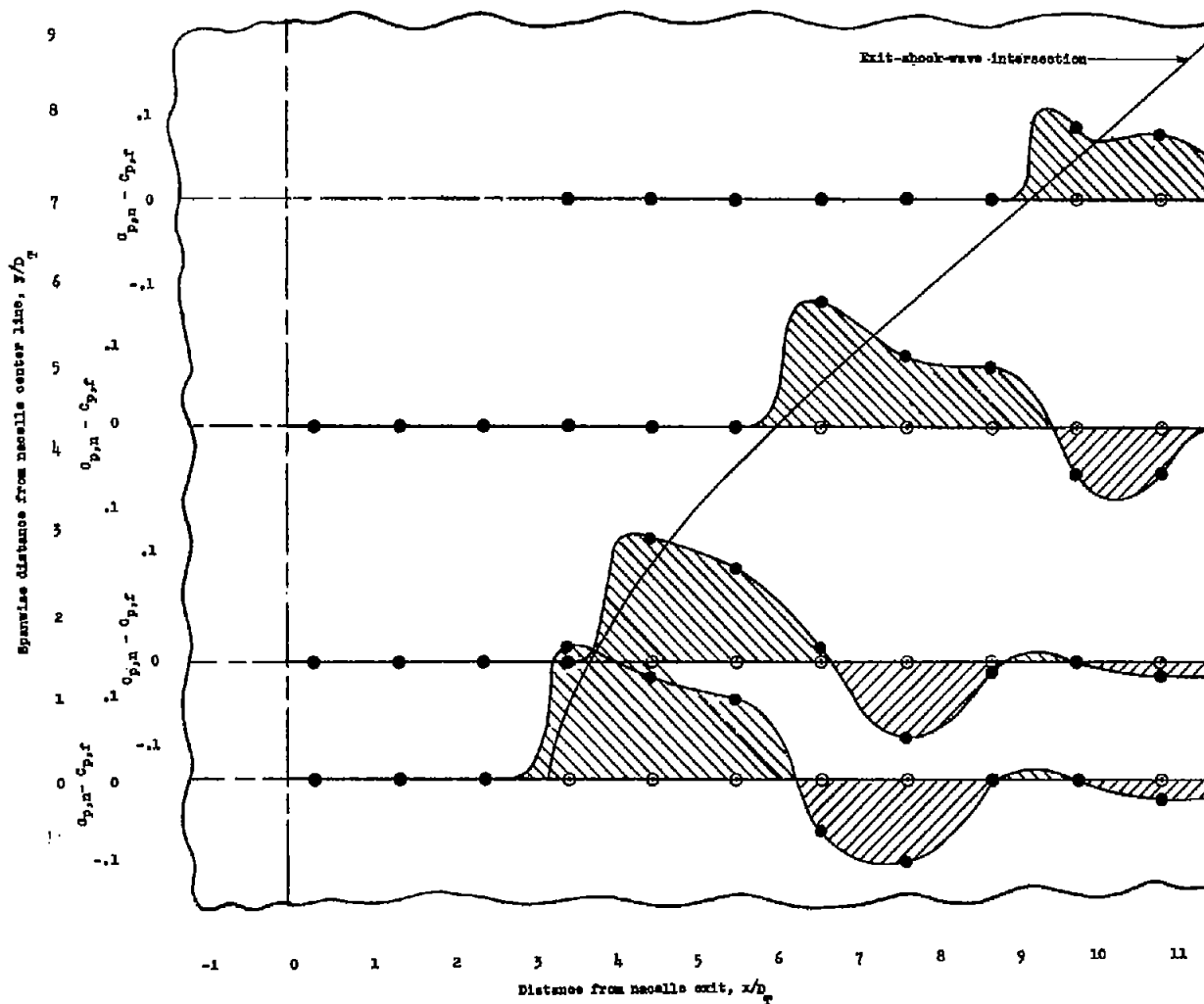


Figure 21.- Incremental-pressure-coefficients profile for a nacelle-exit total-pressure ratio of 15 at position  $I_b$  showing area that was integrated to compute  $\Delta C_n$ .

REPRODUCED BY  
MICRORADAR

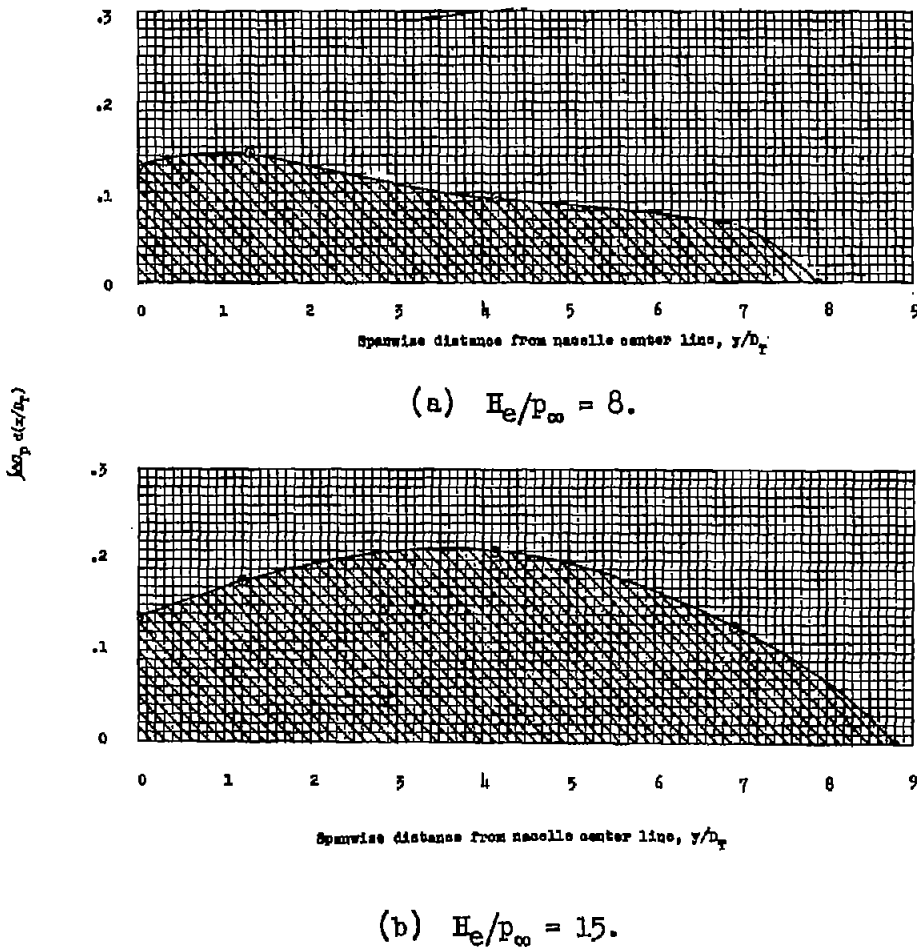


Figure 22.- Variation of a typical  $\Delta C_p d(x/D_T)$  with  $y/D_T$  showing second process of integration in obtaining  $\Delta C_N$  for position  $I_b.$

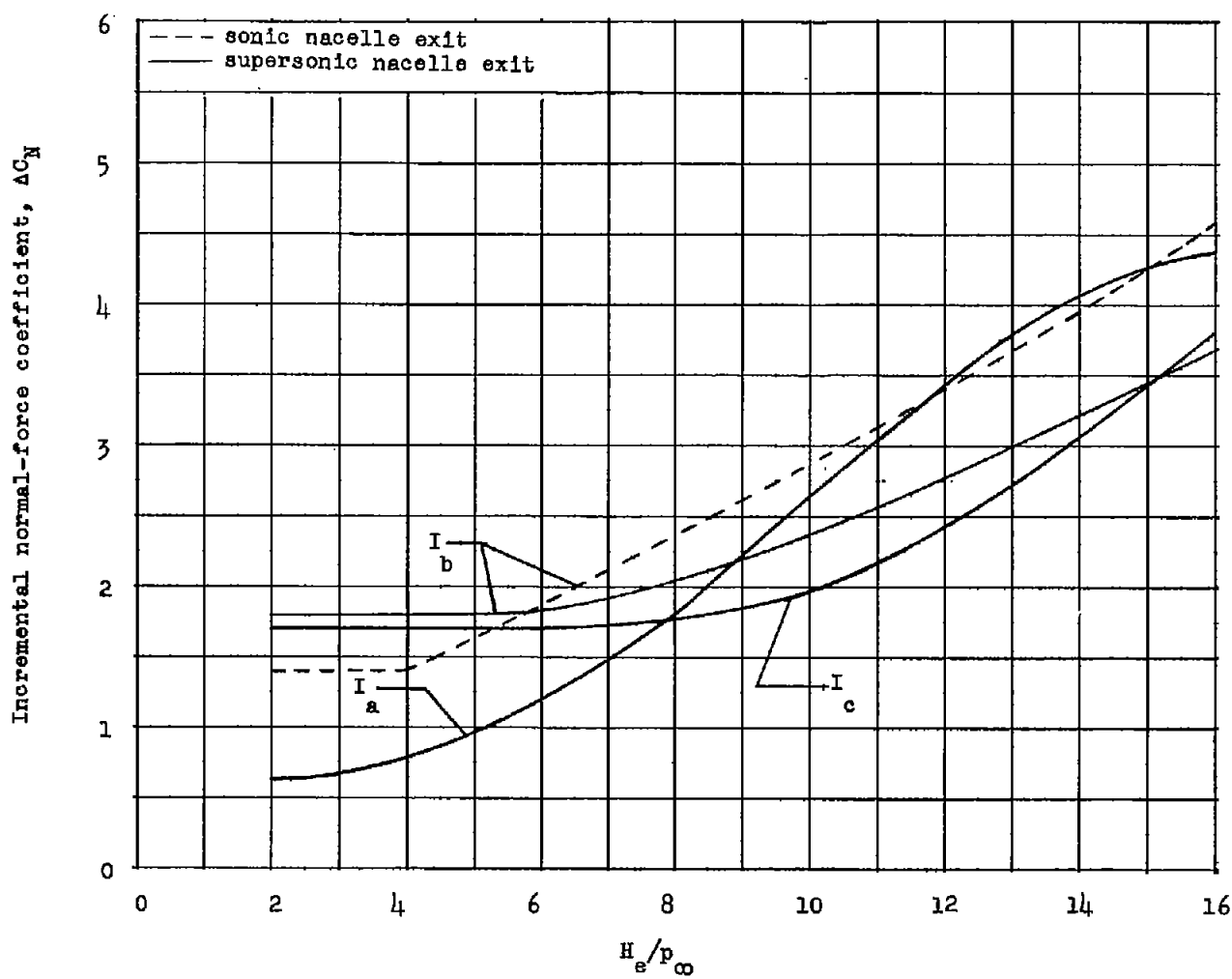


Figure 23.- Variation of incremental normal-force coefficient, based on  $A_T$ , with nacelle-exit total-pressure ratio for both the sonic and supersonic nacelle exits at test positions  $I_a$ ,  $I_b$ , and  $I_c$ .

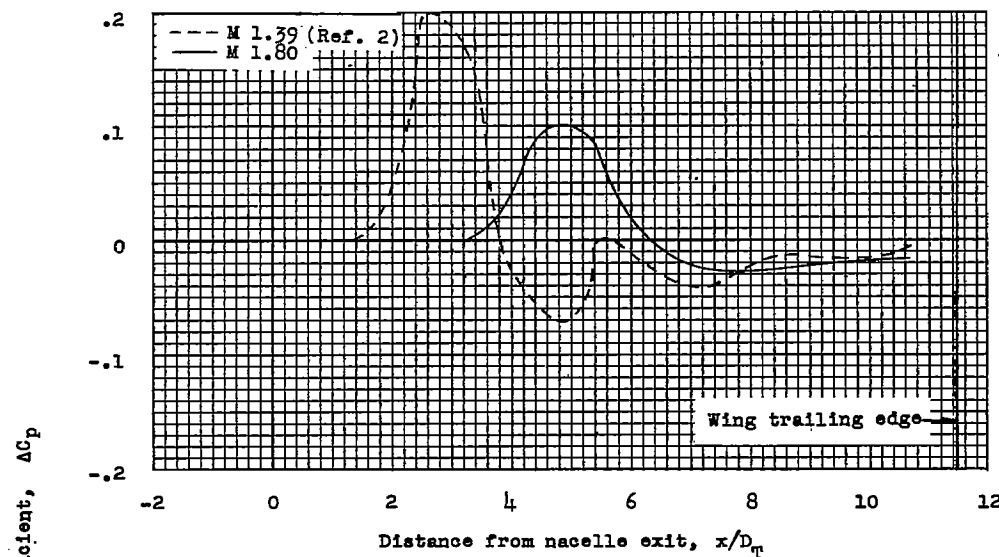
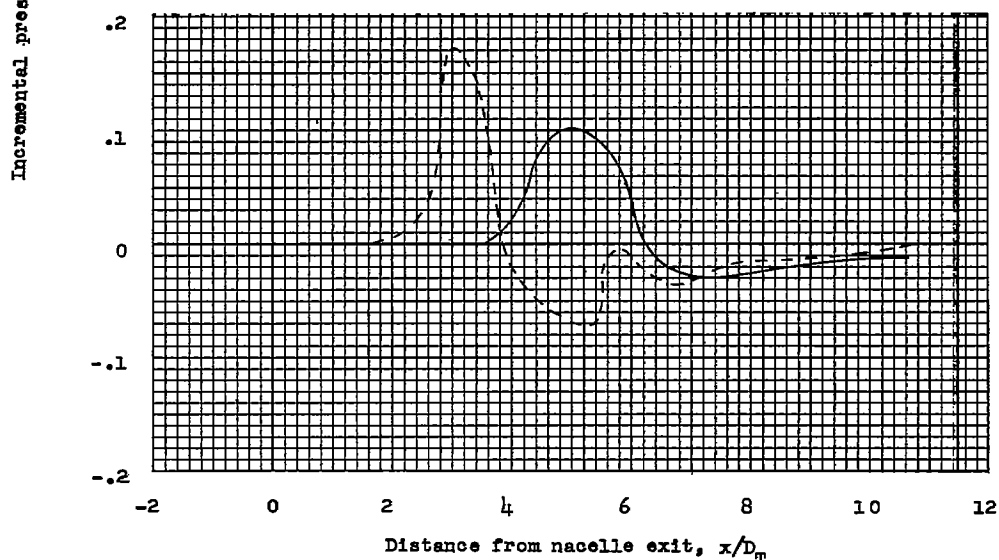
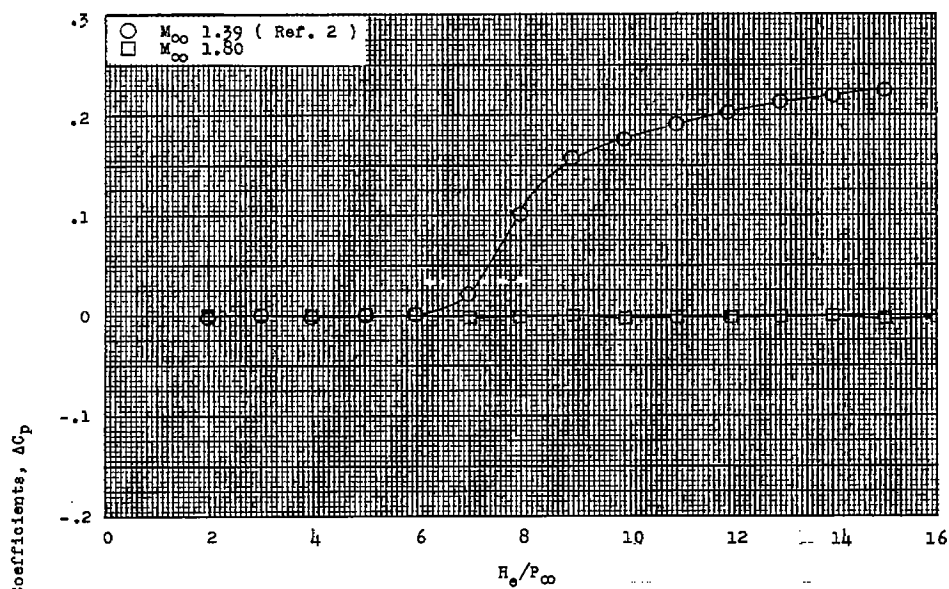
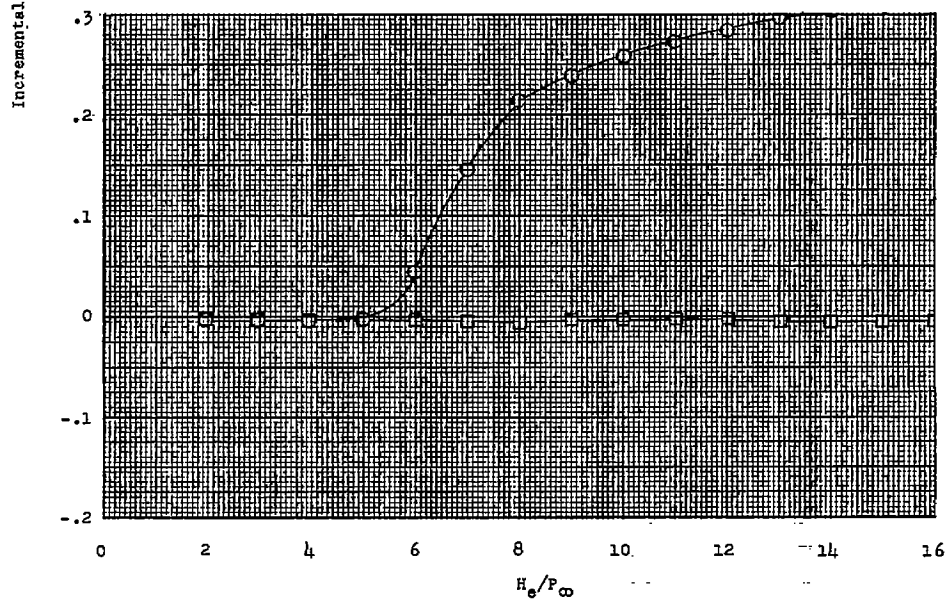
(a) Sonic nacelle exit.  $H_e/p_\infty = 7.$ (b) Supersonic nacelle exit.  $H_e/p_\infty = 7.$ 

Figure 24.- Chordwise variation of incremental pressure coefficients at test position  $I_b$  for both sonic and supersonic nacelle exits along the nacelle center line at free-stream Mach numbers of 1.39 and 1.80.



(a) Supersonic nacelle exit for orifice.  $x/D_T = 2.43$ ;  $y/D_T = 0$ .



(b) Sonic nacelle exit for orifice.  $x/D_T = 2.43$ ;  $y/D_T = 0$ .

Figure 25.- The variation of incremental pressure coefficients with nacelle-exit total-pressure ratio for free-stream Mach numbers 1.39 and 1.80 at test position  $I_b$  for supersonic and sonic nacelle exits.

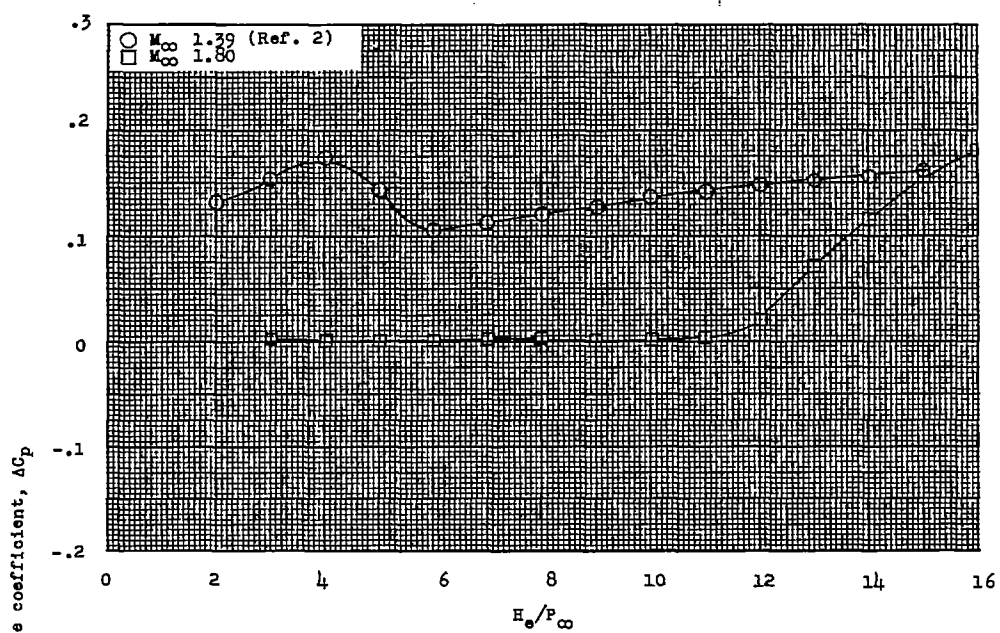
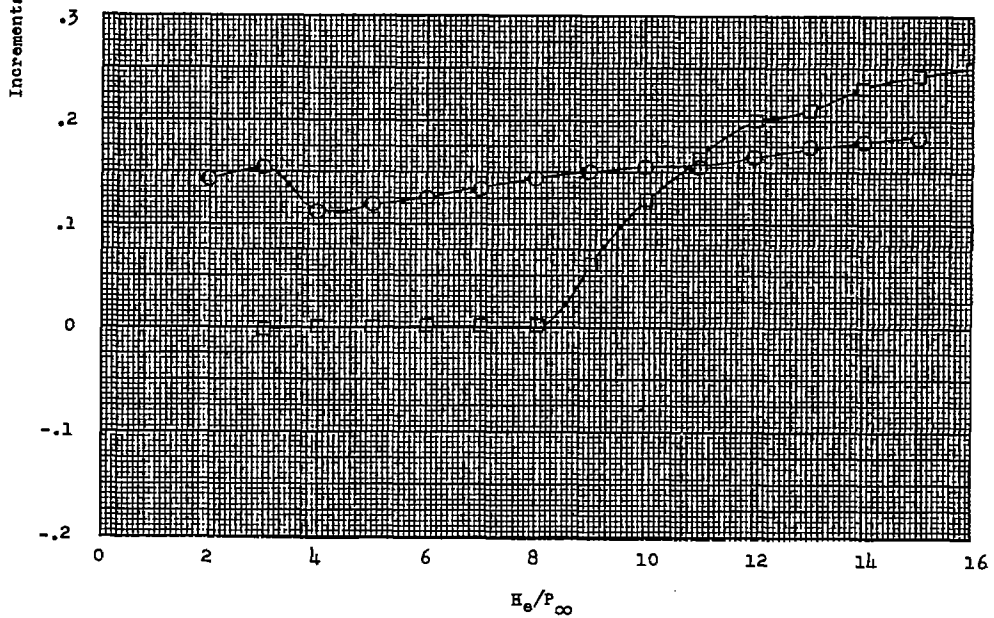
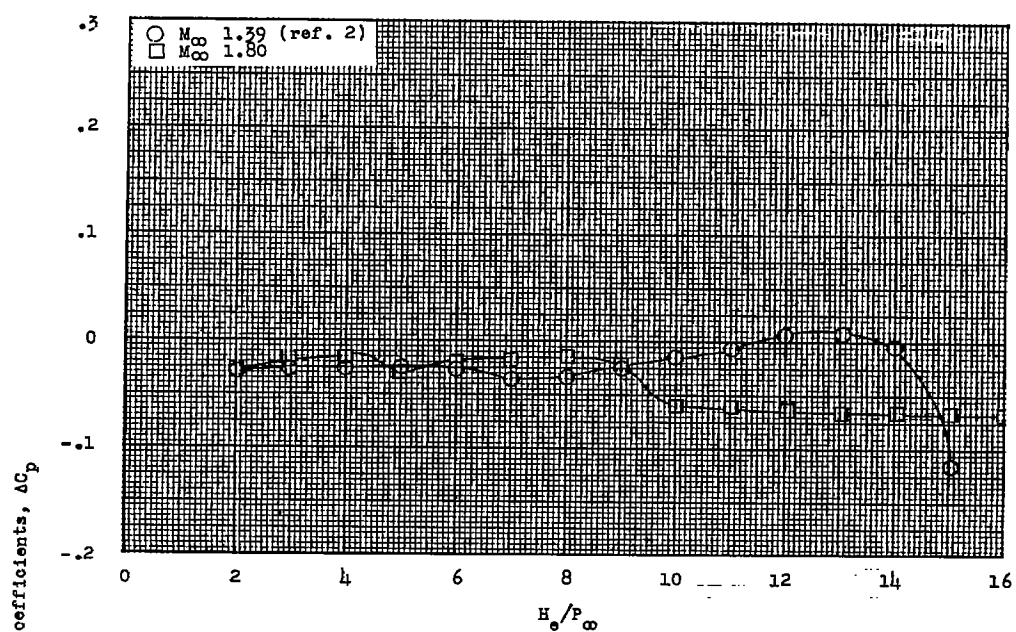
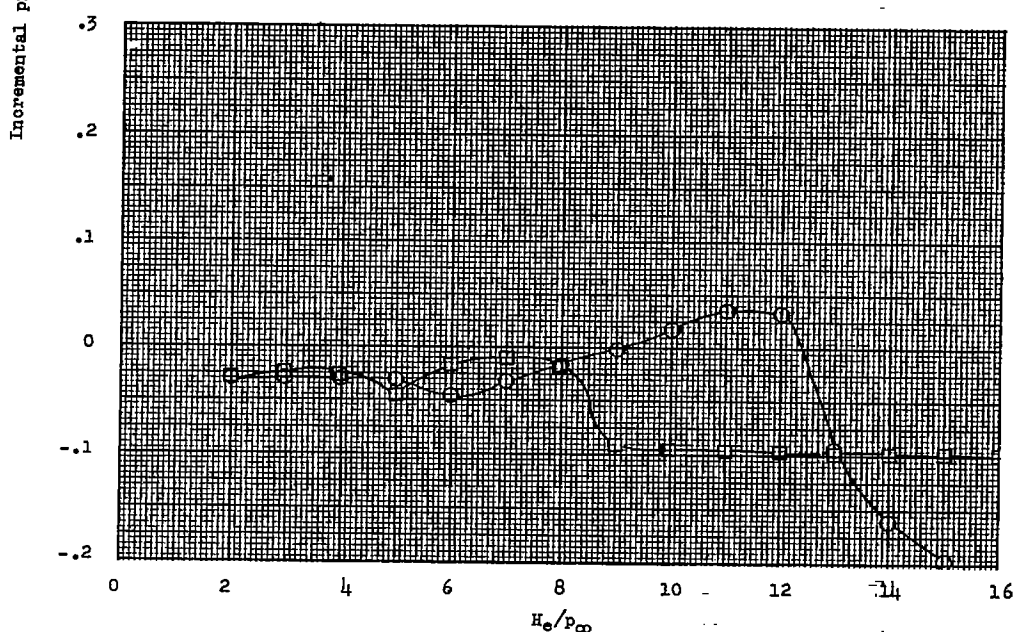
(c) Supersonic nacelle exit for orifice.  $x/D_T = 3.47$ ;  $y/D_T = 0$ .(d) Sonic nacelle exit for orifice.  $x/D_T = 3.47$ ;  $y/D_T = 0$ .

Figure 25.- Continued.

CONFIDENTIAL



(e) Supersonic nacelle exit for orifice.  $x/D_T = 6.59$ ;  $y/D_T = 0$ .



(f) Sonic nacelle exit for orifice.  $x/D_T = 6.59$ ;  $y/D_T = 0$ .

Figure 25.- Concluded.

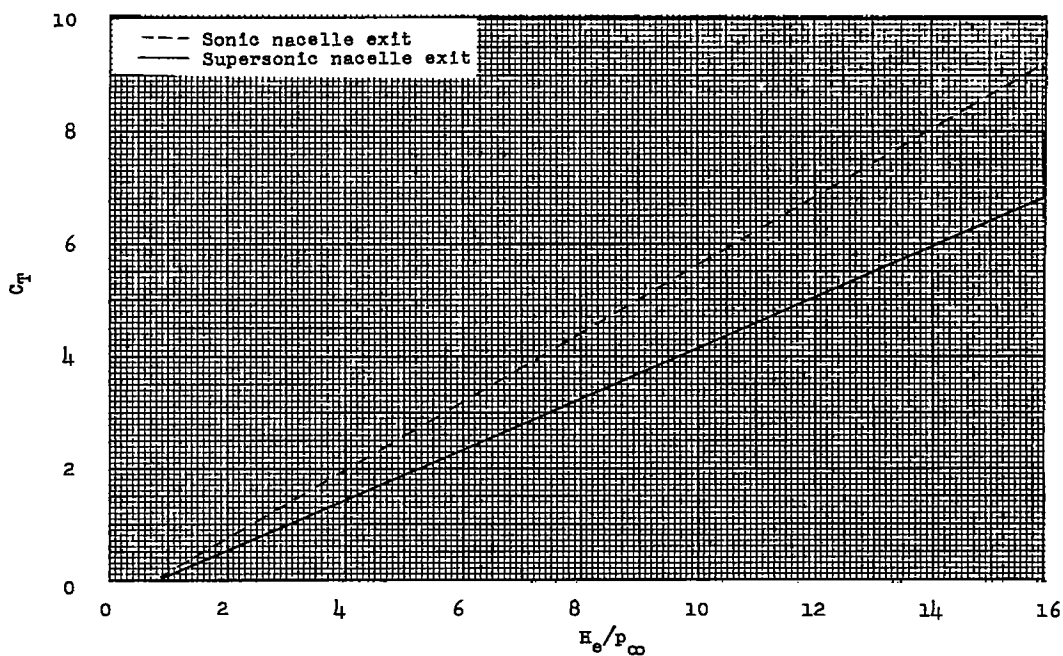


Figure 26.- Variation of gross-thrust coefficient with nacelle-exit total-pressure ratio for both sonic and supersonic nacelle exits based on  $A_e$ .

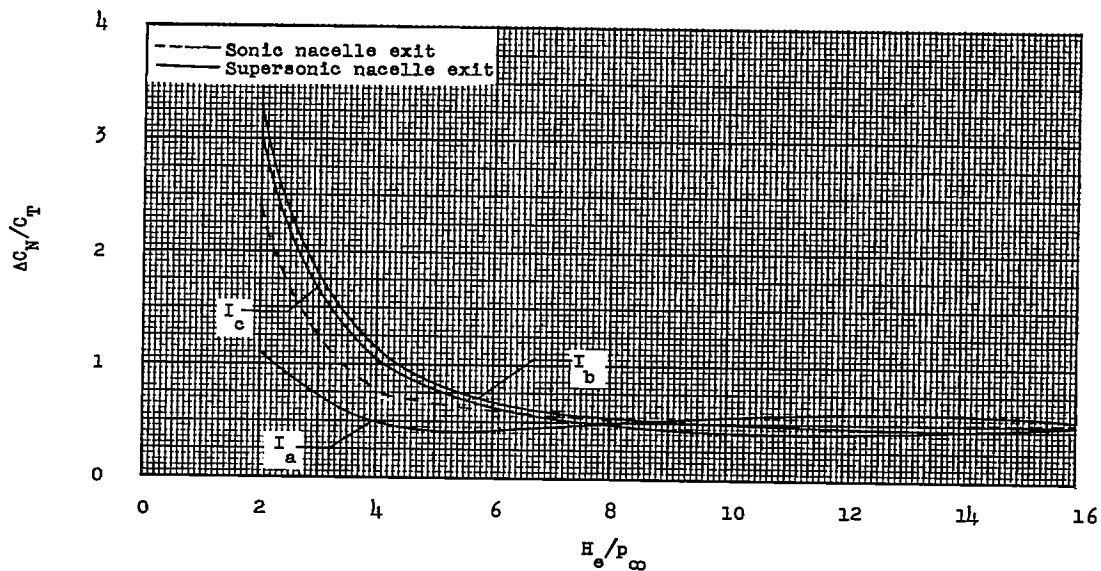
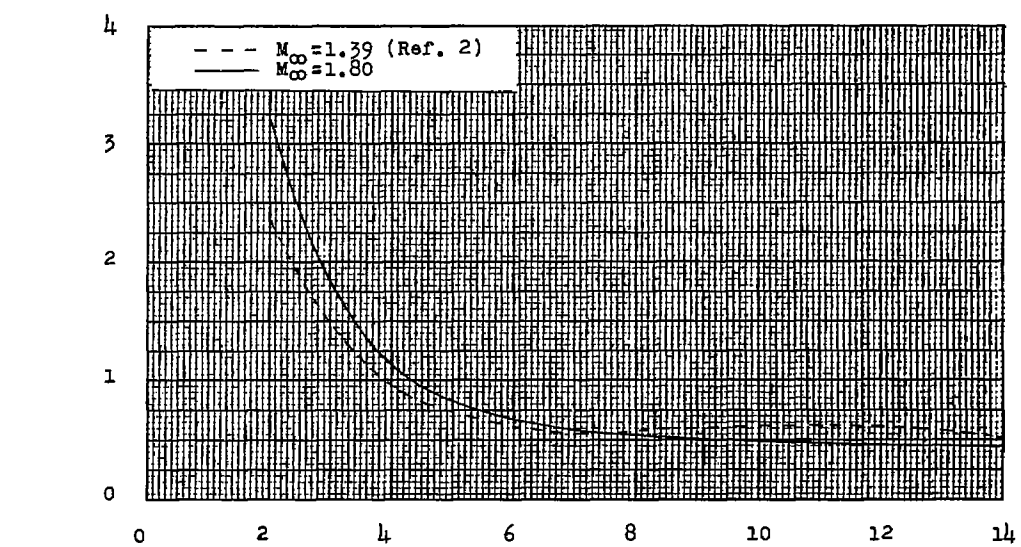
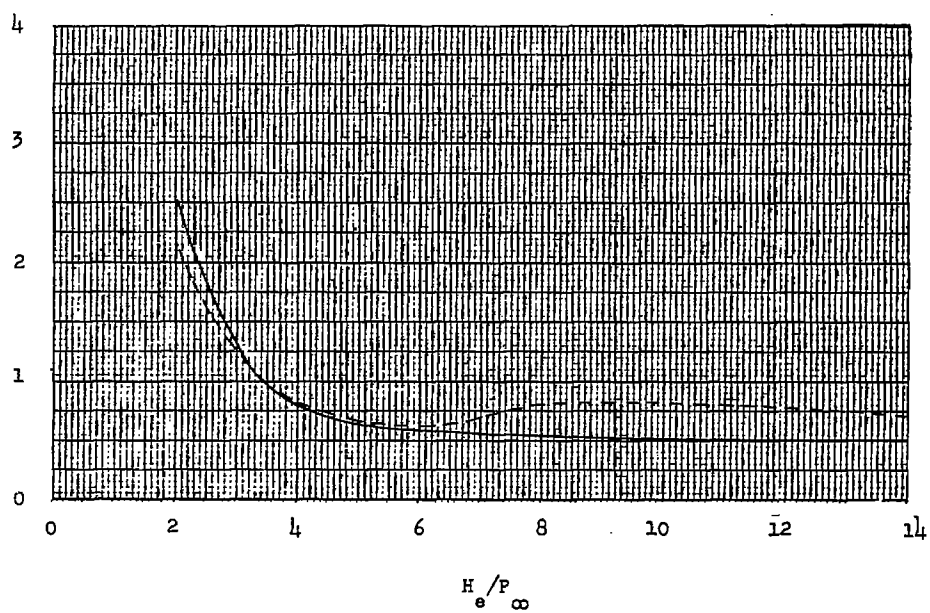


Figure 27.- Variation of incremental normal force to thrust-coefficient ratio with total-pressure ratio at test positions  $I_a$ ,  $I_b$ , and  $I_c$  for both sonic and supersonic nacelle exits.



(a) Supersonic nacelle exit.



(b) Sonic nacelle exit.

Figure 28.- Variation of incremental normal force to thrust ratio with nacelle-exit total-pressure ratios at position  $I_b$  for both sonic and supersonic nacelle exits at free-stream Mach numbers of 1.39 and 1.80.

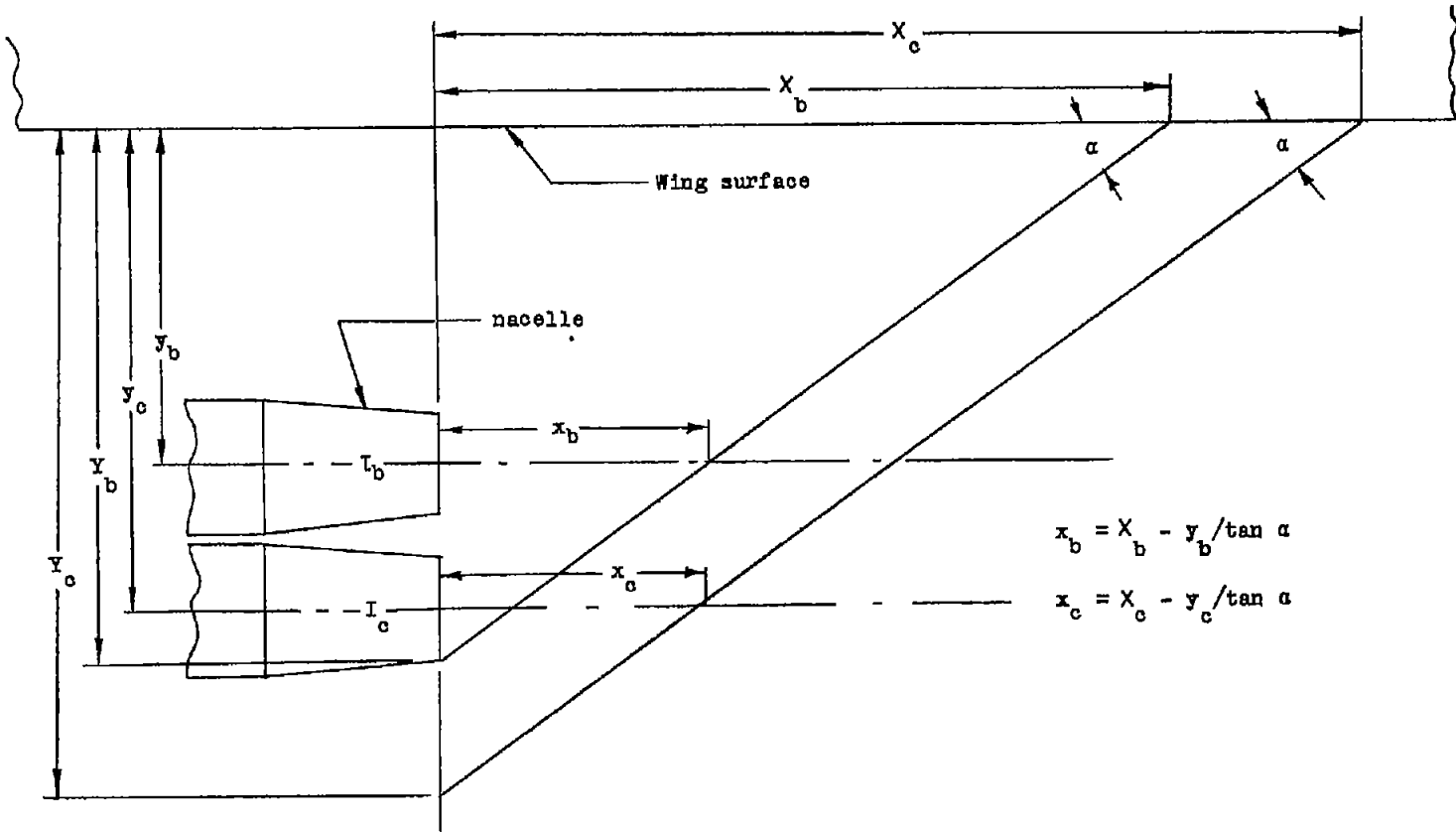


Figure 29.- Geometric layout of jet-shock-wave location.